AD-A152 064 A STUDY OF THE TIME DEPENDENCE IN FRACTURE PROCESSES RELATING TO SERVICE..(U) CALIFORNIA INST OF TECH PASADENA GRADUATE AERONAUTICAL LABS W G KNAUSS 1/3

UNCLASSIFIED 30 JUN 84 GALCIT-SM-84-10 AFOSR-TR-85-0239 F/G 11/4 NL

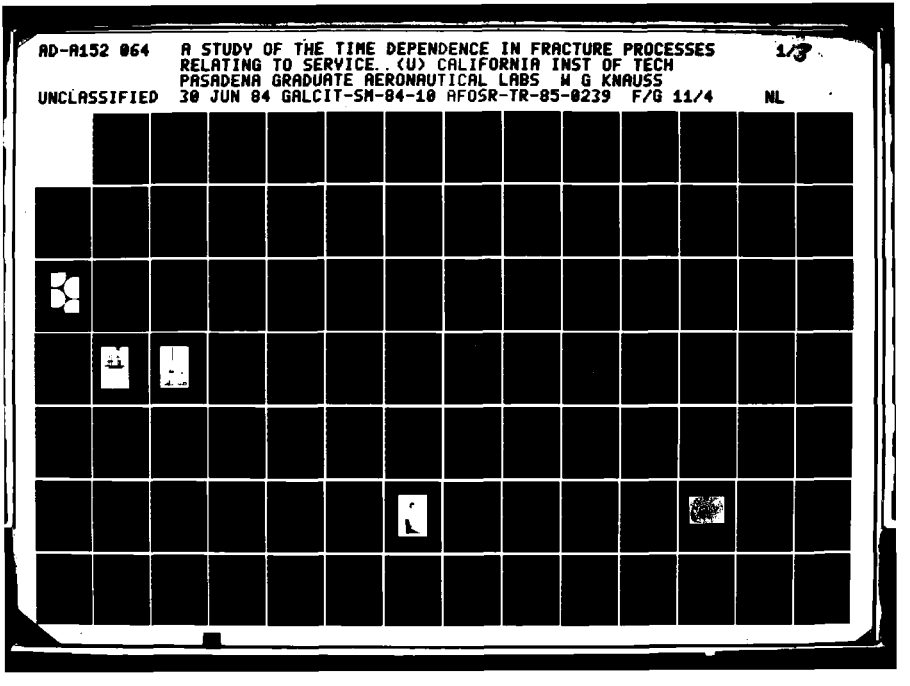

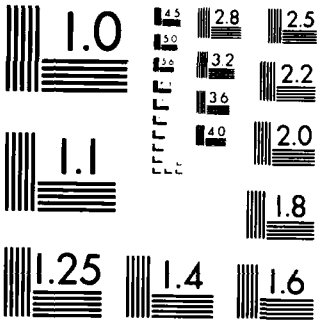

UNCLASSIFIED

SECURITY CLASSIFICATION OF THIS PAGE

(2)

AD-A152 064

REPORT DOCUMENTATION PAGE

1a. REPORT SECURITY CLASSIFICATION UNCLASSIFIED	1b. RESTRICTIVE MARKINGS
2a. SECURITY CLASSIFICATION AUTHORITY	3. DISTRIBUTION/AVAILABILITY OF REPORT Approved for Public Release; Distribution is Unlimited.
2b. DECLASSIFICATION/DOWNGRADING SCHEDULE	
4. PERFORMING ORGANIZATION REPORT NUMBER(S) California Institute of Technology, SM 84-10	5. MONITORING ORGANIZATION REPORT NUMBER(S) AFOSR-TR- 85-0239
6a. NAME OF PERFORMING ORGANIZATION California Inst. of Tech.	6b. OFFICE SYMBOL (If applicable)
7a. NAME OF MONITORING ORGANIZATION The Airforce Office of Scientific Research	
6c. ADDRESS (City, State and ZIP Code) 1201 E. California Blvd. Pasadena, CA 91125	7b. ADDRESS (City, State and ZIP Code) Bolling AFB, D.C. 20332-6448
8a. NAME OF FUNDING/SPONSORING ORGANIZATION AIR FORCE OFFICE OF SCIENTIFIC RESEARCH	8b. OFFICE SYMBOL (If applicable) NA
9. PROCUREMENT INSTRUMENT IDENTIFICATION NUMBER AFOSR 81-0127	
8c. ADDRESS (City, State and ZIP Code) Bolling AFB, D.C. 20332-6448	10. SOURCE OF FUNDING NOS

PROGRAM ELEMENT NO	PROJECT NO.	TASK NO.	WORK UNIT NO.
61102F	2307	B2	

11. TITLE (Include Security Classification)
A STUDY OF TIME DEPENDENCE IN FRACTURE PROCESSES RELATING TO SERVICE PREDICTION OF ADHESIVE JOINTS AND ADVANCED COMPOSITES , Unclassified

12. PERSONAL AUTHOR(S)
W.G. Knauss

13a. TYPE OF REPORT	13b. TIME COVERED	14. DATE OF REPORT (Yr., Mo., Day)	15. PAGE COUNT
Final	FROM 15AUG83 TO 30JUN84	June 30, 1984	

16. SUPPLEMENTARY NOTATION

17. COSATI CODES			18. SUBJECT TERMS (Continue on reverse if necessary and identify by block number)
FIELD	GROUP	SUB. GR	

19. ABSTRACT (Continue on reverse if necessary and identify by block number)

Please see the reverse side of this form.

DTIC FILE COPY

DTIC ELECTE MAR 03 1985

20. DISTRIBUTION/AVAILABILITY OF ABSTRACT	21. ABSTRACT SECURITY CLASSIFICATION
UNCLASSIFIED UNLIMITED ☒ SAME AS RPT ☐ DTIC USERS ☐	UNCLASSIFIED

22a. NAME OF RESPONSIBLE INDIVIDUAL	22b. TELEPHONE NUMBER (Include Area Code)	22c. OFFICE SYMBOL
DAVID A GLASGOW, Major, USAF	(202) 767-4937	AFOSR/NA

DD FORM 1473, 83 APR EDITION OF 1 JAN 73 IS OBSOLETE

UNCLASSIFIED

SECURITY CLASSIFICATION OF THIS PAGE

Problems related to fracture of bonded structures and composites were studied with emphasis on the time dependence of the failure process. Three subject areas in this area are identified:

a. Residual stresses due to changes in temperature through the glass transition range. It is found that determination of the creep compliance or of the relaxation modulus is the most important material property for accurate stress determination general experimental and analytical agreement prevails.

b. In temperature "accelerated" crack propagation tests along interfaces it is found that crack propagation stops upon raising the temperature. The reason for this "unexpected" behavior is that with raising the temperature the elimination of residual? stresses overcomes the reduction of viscosity so that crack arrest becomes possible.

c. Fatigue crack propagation is studied for a viscoelastic material. In contrast to metals the rate of crack growth per cycle is strongly affected by the frequency, declining with increasing frequency. However, the average velocity (cm/sec) per cycle increases with frequency. Thus it is more important to consider the time under stress than merely the number of cycles.

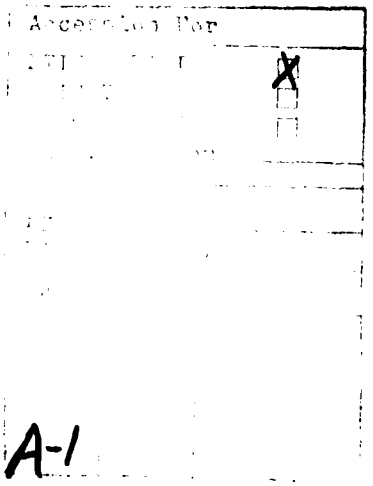

SM 84-10

Final Technical Report to

The Airforce Office of Scientific Research

on

A STUDY OF THE TIME DEPENDENCE IN FRACTURE PROCESSES RELATING TO SERVICE PREDICTION OF ADHESIVE JOINTS AND ADVANCED COMPOSITES

Grant No. AFOSR-81-0127

by

W.G. Knauss

June 30, 1984

Graduate Aeronautical Laboratories
California Institute of Technology
Pasadena, CA 91125

TABLE OF CONTENTS

1. PURPOSE AND OBJECTIVE OF PROGRAM

Polymers are increasing in prominence in the design of aerospace structures as exemplified by the use of epoxies in advanced composite materials and by adhesives for metal/metal and metal/composite joining. However, only in very rare instances do designers worry about the consequences of the "time dependent" properties which these materials exhibit. The reasons for this neglect are manyfold; however, primary amongst them is the general lack of familiarity with the consequences of viscoelastic material behavior on the one hand, and the misjudgement of long-term time dependent response as estimated from short term laboratory test, on the other. With regard to the latter point it is not uncommon to experience laboratory data that exhibit time- or rate-sensitivity which is lost in the data scatter, with the common conclusion that time- or rate-sensitivity is absent or not important. Such finding is, of course, justified only if the application of the polymer is likewise limited to short times comparable to those encountered in the laboratory test, but is not justified if applications involve time spans or frequencies several orders of magnitude different than those underlying the laboratory test.

From a structural point of view it may be undesirable to design structures for extended use with materials that possess strongly rate sensitive behavior. Nevertheless, in order to understand the limits of designs incorporating polymers one must be thoroughly familiar with the special problems derived from viscoelastic material response.

One might suggest that the limits of viscoelastic behavior can be readily ascertained by simple compliance or relaxation testing. For some deformation-limited designs that may be true. However, our recent discovery that elevated stress loads accelerate the deformation and relaxation processes (non-linearly

viscoelastic behavior) points out that standard material characterization is marginally adequate at best. In particular, these findings point out that because of the stress-induced acceleration of creep processes the fracture behavior of polymers will be affected significantly. Specifically, the high stresses at the tip of a crack induce time dependent phenomena that proceed much more rapidly there than those in the bulk of the material. As a consequence a material that might, by other criteria, appear to be nearly rigid and rate insensitive can indeed exhibit time dependent fracture response. Such apparent inconsistency is observed even with silicate glasses. It is thus clearly of engineering interest to develop and disseminate a better understanding of time dependent phenomena of failure in structural polymers.

It was with this desire and purpose in mind that we undertook the p.esent program, the primary intent being the development of analysis tools for the prediction of time dependent phenomena. Because the physical behavior of these materials is generally poorly understood - especially with regard to fracture - we felt that an experimental program with some analytic undergirding was an appropriate mode of operation.

Specifically, the program was designed to elucidate those physical phenomena that control the time dependence of the failure process. Such failure or fracture processes cover both the separation of a viscoelastic solid from an elastic substrate as well as the growth of cracks in rigid polymers. Both problems are germane to the failure of bonded joints and of advanced fiber reinforced composites.

2. SUMMARY OF TECHNICAL RESULTS

We feel that progress has been made on all fronts with one exception. We delineate the progress below, but comment first on the past that met with

unforseen difficulties.

Part of an earlier program on which the present effort was to build depended on servomechanical control by an 8 bit micro-processor. It turned out that the Northstar micro-processor, while only about four years old at the time a problem arose, was claimed to be too old to be worth repairing. The processor was finally repaired but too late to benefit the thesis research of the student who was to use it. The student had to change his research topic and has since completed his thesis (see Section 2.3 below).

We have learned an important point out of this misfortune, however. Because we were totally dependent on off-campus, i.e. outside technical service and analysis we were virtually totally subject to competition for repair in the general market place but with a relatively trivial problem that did not weigh heavily in the general competition. Future involvement with computer will entail a) more direct involvement in understanding and designing the system, plus b) working with systems for which expertise exists on campus. Thus assistance in trouble shooting, not to speak of cost sharing, will be of direct advantage to system maintenance.

We turn now to outlining briefly the three major areas of research accomplishments. These areas are delineated in two theses, one a Ph.D. thesis and the other a thesis for the degree of Aeronautical Engineer. The details are well represented in these documents, which are appended as part of this final report. The topics contained in the Ph.D thesis are

a. Analysis of residual stresses as a polymer is cooled through the glass trnsition temperture and

b. Effect of residual stresses on adhesive failure.

The third topic,

c. relates to the effect of viscoelastic material behavior on fatigue crack propagation. The latter topic is the subject of the Engineer's Thesis.

Topics a) and b) are subjects that were motivated by bonding problems relative to solar cell construction but are of a much more fundamental mature than energy engineering. Although that reserch was started under DOE sponsorship the problems considered are precisely those of structural adhesive use, in fact, are especially germane to fiber reinforced composite materials. That work was substantially done and completed under the present grant.

2.1 Residual Stresses in Polymers Cooled Through the Glass TransitionTemperature

In may aerospace structures polymers are formed together with non-polymers (metal, graphite fibers) while the polymer is in the semi-liquid or "soft" state. As the temperature drops material shrinkeage occurs which undergoes a transition at the glass temperature. While this is a qualitatively well-known fact the quantitative aspects were not at all explored. Because of the great sensitivity of the mechanical properties to the temperature around the glass transition this was always judged to be a very difficult problem. Nevertheless, it is a very important engineering problem because all polymer using structures involve that question. Specifically, if it turns out that these residual stresses are large enough to almost cause fracture without much additional loading it would be important to assess the residual strength.

The study revolved thus around the following question: Given the current knowledge and state of affairs in analyzing thermoviscoelastic behavior, and given material characterization techniques that considerably exceed in precision what is practice in industry and most engineering schools, how well can one predict the residual stresses and/or deformations in composite structures as the temperature passes through the glass transition range. One might call this a

careful sensitivity study.

The answer to this question is represented essentially graphically in Figures 24 through 27 in Appendix A (starting at page 56). These figures represent computed and interferometrically measured radii of curvature of sandwiches made of glass and Polyvinylacetate. It turns out, that the most influential parameter in this comparison is the creep or relaxation behavior (see Figure 5 in Appendix A). Although on a log-log plot such data may "look very good" it turns out that most of the deviation in the Figures 24-27 in Appendix A between theory and experiment results from the uncertainty (variability) of the time dependence of the material rheology. The data in Figure 5 was measured painstakingly - by normal engineering standards - and repeatedly on high purity PVAc.

The net result of this study is thus that if predictions of residual stresses need to be made to within even only 10-15 % accuracy such an estimation will be practically speaking impossible within the normal run of engineering practice and applications.

2.2 Effect of Residual Stresses on Adhesive Failure

One of the most important subjects in the assessment of durability of structures is the ability to either predict long term (10-30 years) failure or to possess accelerated test methods with the help of which one can determine experimentally whether a specific design will endure. The most common means of accelerating tests involving polymers is to test under elevated temperatures. When more than one material is involved such temperature changes induce thermal stresses which can, by themselves, cause fracture. Again, one of the most often used tests to assess adhesion is the peel test; it seemed appropriate, therefore, to examine the effect of temperature on peel rate.

At the same time one notes, that in the peel test there is rarely, if at all, mention made of the thickness of the peeled layer other than a mere recording, but not as a recognition that peel layer thickness would or could affect "peel strength."

While specimen-to-specimen variation renders fairly large data scatter the answer to the latter question is that there is a dependence of peel strength in terms of energy expended per unit of new interface surface. The experimental results, while not the best in data clarity, indicate a non-monotonic dependence, which makes sense, if one considers that the viscoelastic energy expenditure depends on the detail of the strain field in the vicinity of the disbond. For a thick specimen the strain rates are, on the average low because the local bend radius is large leading to "smaller" strains and strain rates, hence less dissipation. At the same time, physical observation shows that more volume is coming under strain the larger the thickness is, not only because of the increased thickness but because there is more material along the length of the peel layer under strain because the mean bend radius is larger. Moreover, the strain field tends to become more non-uniform as the thickness increases (see page 87 of Appendix A). The net effect allows then for a maximum of viscoelastic dissipation at some thickness of the peel layer.

In the second part of the peel study it was examined what the effect of residual thermal stresses was on the peel rate at different temperatures. It turns out that in a certain temperature range peel does not take place while under the same load. The explanation is found in the fact that below a certain temperature the thermally induced strain energy assists the fracture process. When the temperature rises to a given value the thermal and cure shrinkeage induced strain energy no longer assists fracture and the crack propagation process stops. This behavior is opposite to what one expects normally on purely

rheological grounds. Crack growth can then be promoted only by increasing the peel force.

2.3 Recent Results on the Validity of a Non-Linearly ViscoelasticRepresentation

One of the recurring topics in the failure or fracture of viscoelastic solids is the question of non-linearly viscoelastic material behavior. In particular it is the goal of materials behavior research to find that mathematical representation of experimentally accessible states of stress or strain histories which lend themselves to generalizations to less readily tested states.

Leaderman has suggested many years ago that a generalization of linearly viscoelastic behavior be achieved through a convolution of a material function, say the relaxation modulus with a non-linear function of strain instead of the strain itself. On the other hand, an equally acceptable representation in terms of the creep compliance would be the convolution of the creep compliance with a non-linear function of the (Cauchy) stress. The latter form is the one used in Schapery's "generalization" of the J-integral to include viscoelastic material behavior.

The particular form of material representation with a special form for the non-linear function of the strain was used by Bloch, Chang and Tschoegl [1] to generate excellent fit of experimental data. Let ε be the normal engineering strain and let the uniaxial extension ratio be $\lambda = 1 + \varepsilon$. Then, if n is some constant at a temperature T_o the stress can be represented by

$$\sigma(t) = \frac{2}{3n}\int_o^t E(t-u)\,\frac{d}{du}\{\lambda^n(u) - \lambda^{-\frac{n}{2}}(u)\}\,du \,. \qquad (1)$$

The corresponding fit to experimental data is shown in Figure 1; details as to how the single free parameter n is fitted by the data is recorded in the cited reference. Note that the data in Figure 1 is obtained from monotonic loading

histories, in particular from uniaxial constant strain rate tests.

In many situation it is of interest to deal with periodic deformation histories such as are encountered in fatigue-type problems. In such situations it is of paramount importance to be able to estimate the amount of energy dissipation in a material in order to assess the associated temperature rise. It was the intent, therefore, to estimate with the excellent material representation in mind the amount of energy dissipation per cycle for this material and to compare that estimation with that for the small strain behavior, i.e. for linearly viscoelastic behavior.

In order to compute the energy dissipation per cycle one calculates, for uniaxial deformation the loss per cycle

$$W_c = \int_o^T \sigma(t)\,\frac{d\lambda}{dt}\,dt = \int_o^T \sigma(t)\dot{\varepsilon}\,dt \qquad (2)$$

Suppose we consider only a cyclic tensile strain be letting

$$\varepsilon = \varepsilon_o\,(1 + \sin\omega t) \qquad (3)$$

Let the function in curly brackets be $F^*(u) = \lambda^n(u) - \lambda^{-\frac{n}{2}}(u)$ so that with (2)

$$F^*(u) = [\,1 + \varepsilon_o(1 + \sin\omega u)\,]^n - [\,1 + \varepsilon_o(1 + \sin\omega u)\,]^{-\frac{n}{2}} \qquad (4)$$

which has the Fourier series representation

$$F^*(u) = \sum_{n=1}^{\infty} \frac{a_n}{n\omega}\,\text{sinn}\omega u - \frac{b_n}{n\,\omega}\,\text{cosn}\,\omega n - b_o$$
$$= \frac{1}{n\,\omega}\sqrt{a_n^2 + b_n^2}\,\sin(n\,\omega u + \delta_n) \qquad (5)$$
$$\tan\delta_n = -\frac{b_n}{a_n}$$

Substitution of (5) into (1) yileds for steady state condition and by definition of the complex modulus $E^*(\omega) = E(\omega)e^{i\Delta(\text{omega})}$ and the Loss tangent $\tan\Delta$ (omega), the periodic stress is

PREFACE

Polymeric coatings are often applied in order to protect a substrate from the influences of the environment. If polymer films are to adhere for many years to such substrates it is necessary to understand how material and system parameters affect the process of separation between coating and substrate. The phenomena involved play a recurring role in all problems of separation at an interface between dissimilar materials.

The present work deals with the long time integrity of polymer coatings. The goal of this study is the long time prediction of the initiation and propagation of an interfacial crack, that can lead to the debonding of a protective layer. The immediate motivation for this study arose in the need for encapsulation of solar photovoltaic cells. These have become important as a possible alternative source of energy. However, the work presented here should be viewed in a more general manner because it applies to other coatings subject to similar environmental loading conditions. For example, the peeling of paint from its substrate falls into this category. Due to a changing atmosphere or possibly deficient manufacturing procedures the coating materials might no longer adhere perfectly, opening the path to further degradation of the adhesive bond. Problems of this kind occur in the encapsulation of solar cells and are exemplified in Figure 1 which illustrates a delamination in a solar cell array ; the coating has separated from its underlying substrate after lengthy exposure to environmental loading conditions. The appearance of such structural defects indicates the need to determine under what conditions the adhesive bond will continue to fail. The present study deals with two distinct aspects related to the long time integrity of a viscoelastic material layer bonded to an elastic, rigid substrate.

1. The first part concerns the magnitude of the stresses present in layered

erties of the adhesives needs to be carefully analyzed. This time dependence is also reflected in the energy required to create new surfaces as interfacial debonding proceeds ; the adhesive fracture energy is one of the dominant parameters in time dependent adhesive failure. In our investigation it is characterized through peel testing.

With the knowledge of the pertinent material properties as well as of the adhesive fracture energy, we then proceed to formulate a criterion for continuing interfacial crack propagation. The analysis is carried out for elastic solids, with the effect of viscoelastic behavior incorporated later on. Debond tests provide a way to check how well the theoretical predictions correspond to experimental debond results.

ABSTRACT

An important source of interface fracture contributing to adhesive failure in a bimaterial sandwich, consisting of a rigid substrate and a viscoelastic encapsulant material, arises from residual stresses. The encapsulant is often deposited on the substrate above its glass transition temperature region but used below this temperature range. In order to determine the magnitude of the residual stresses a viscoelastic stress analysis of a bimaterial sandwich is carried out, taking into account the time-dependent material properties of the polymeric layer and the environmental "loading" conditions. The theoretical analysis is paralleled by an experimental examination of the time-dependent out-of-plane deformation of thin, circular sandwiches.

Polyvinyl acetate was chosen as a model material exhibiting significant viscoelastic effects under room test conditions. Therefore the pertinent physical and mechanical properties of PVA_c are determined ; these include the thermal coefficient of expansion, the shear creep compliance and the relaxation modulus. In the experimental work BK-7 glass is taken as the "rigid" substrate. The measurements connected to the stress analysis are monitored with laser interferometry (Newton's rings). A comparison between theory and experiment completes the viscoelastic stress analysis.

In the second part of this study time dependent adhesive failure of rubbery materials is investigated. Polymeric materials are being used increasingly for a wide variety of applications. Some of these materials are applied as protective layers to isolate their substrates from a hostile environment. Others achieve remarkable structural bond strengths thereby displacing the traditional mechanical fasteners like bolts and rivets. If one wants to investigate the long time integrity of a layer assembly the time dependence of the material prop-

This thesis is dedicated to my parents in recognition of their love and support throughout all these years.

ACKNOWLEDGEMENTS

At the end of my graduate studies it gives me great pleasure to thank Dr. Knauss for providing me with the opportunity to do this work. His support, trust and patience during the course of my graduate work were indispensable.

I would also like to thank Dr. Babcock and Dr. Tschoegl for their guidance during my stay at Caltech. I am very grateful to my undergraduate advisors Dr. De Meester and Dr. Aernoudt of the K.U. Leuven who helped me choose Caltech as my second alma mater.

This work was performed under sponsorship of the Department of Energy through the Large Scale Solar Array Project at the Jet Propulson Laboratory of the California Institute of Techonolgy (Research Order 49-767-1D002-0-3460) and under sponsorship of the Air Force Office of Scientific Research (Grant Number AFOSR-81-0127). Their support is gratefully acknowledged.

I wish to express my sincere gratitude to my friends and colleagues at Caltech for cultivating a stimulating and congenial athmosphere and for many helpful discussions. Special thanks go to my roommates Jim Gibbons, Walter De Logi, Per Reinhall and their families, whose help and encouragement made life in Pasadena more enjoyable.

I much appreciate the help and advice of all members of the Aeronautics Machine and Electronics Shops. I also want to thank Mrs. B. Wood and Mr. H. Hamaguchi for their help in the preparation of figures for the thesis. Last, but certainly not least, I am deeply indebted to Ms. Marta Nyiri for her incomparable help in typing this thesis quickly, accurately and always cheerfully.

Finally I owe much gratitude to Sylvia whose dedicated emotional support helped to stabilize an at times turbulent environment.

To my Parents.

SM 82-16

AN ENGINEERING ANALYSIS OF POLYMER FILM ADHESION TO RIGID SUBSTRATES

Thesis by

Luc J. Heymans

In partial fulfillment of the requirements

for the degree of

Doctor of Philosophy

California Institute of Technology

Pasadena, California

(1983)

Submitted November 3, 1982

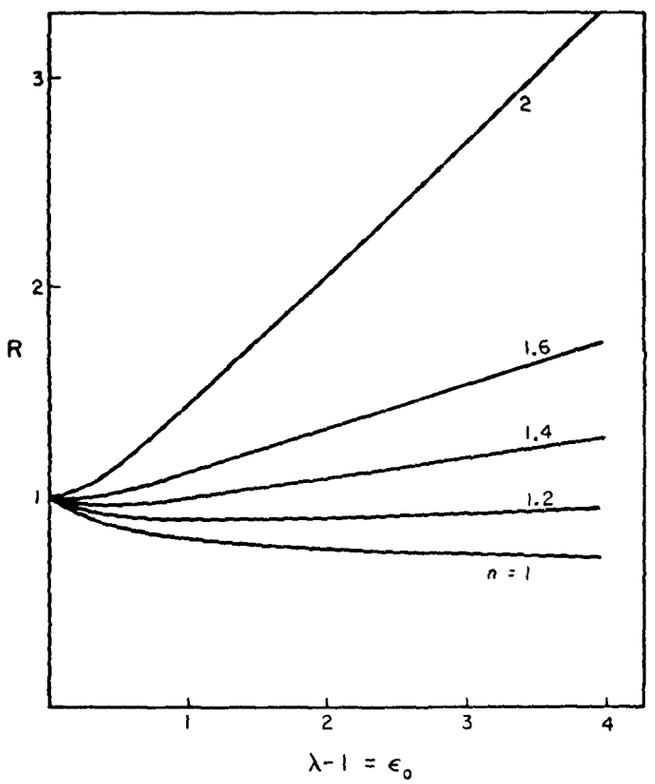

Fig. 2 Work per cycle expended for non-linearly viscoelastic body normalized by that for linearly viscoelastic body as a function of unaxial strain.

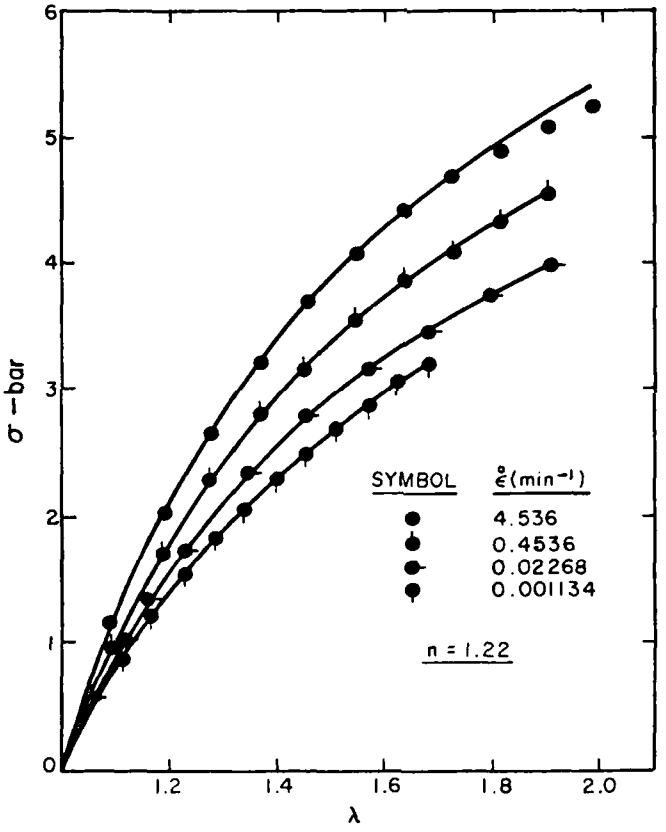

Fig. 1 Response of plasticized SBR (silicone oil) at 23 °C to a ramp of strain at various rates of extension.

The following papers appeared during the period of this grant:

1. K.M. Liechti and W.G. Knauss, "Crack Propagation at Material Interfaces: II. Experiments on Mode Interaction," *Experimental Mechanics*, Vol. 22, No. 10, pp. 383-391, October 1982. J. Romanko, K.M. Liechti, and W.G. Knauss, "Life Prediction Methodology for Adhesively Bonded Joints," Symposium on Adhesive Joints, September 12-17, 1982, Kansas City, MO.

2. W.G. Knauss, "The Effect of Viscoelastic Material Behavior on Fatigue Crack Propagation," American Chemical Society, Rubber Division, May 9-11, 1984, Indianapolis, Indiana.

2.4 Effect of Viscoelastic Behavior on Fatigue

It is a commonly acceptedfact that crack growth rates (da/dn) under fatigue type loading does not depend on test frequency (in metals). As a result one can accumulate fatigue data quickly at high frequencies. In viscoelastic materials, we have calculated[1] that under cyclic loading cracks should propagate more rapidly on a per unit time basis the higher the frequency. That prediction is verified in the following sense: Crack growth per cycle decreases as the frequency increases. Yet the decrease is such that when one considers the average crack *speed (per cycle) that latter quantity increases with frequency. Thus* it is found that it is essentially the time under load which controls crack growth and not the deformations per unit cycle as in metals. These results are summarized in Figures 4.8 and 4.12 in Appendix B.

3. EDUCATIONAL BENEFITS

This program has produced or materially aided two advanced degrees one Ph.D. and one Professional Engineer's Degree. Dr. Luc Heymans now works for the Eastman Kodak Compay in Rochester, N.Y., and Engr. Samuel Chang is employed by American Telecom in Anaheim, CA. Furthermore the following students have contributed to the program and have derived educational benefits from it: Mile Moser and Sotirios Natsiavas.

4. COUPLING ACTIVITIES

Under this grant the above mentioned degree students produced thesis which are included here as Appendices A and B. These theses will be written into three publications according to the outlines in Section 2.1-2.3.

---

1. W.G. Knauss and H. Dietmann, "Crack Propagation Under Variable Load Histories in Linearly Viscoelastic Solids," *Int. J. Engng Sci.*, Vol 8, pp. 643-656 (1970).

the linearly viscoelastic solid which has the same relaxation modulus. It is of interest to note that for the material represented in the measurements in Bloch, Chang and Tschoegl's work, i.e. when $n \approx 1.2$ the energy dissipated by the non-linear body is about 90 % of that for the linearly viscoelastic one, and in a way, that is rather insensitive to the level of the maximum strain (in the range examined).

This result would seem to be of considerable interest inasmuch as it would represent the first estimate of the effect of non-linearly viscoelastic material behavior on hysteresis. There is, however, one serious catch to this result which questions the validity of the representation in equation (1) and thus questions also the validity of Schapery's non-linear J-integral extension. The latter statement derives from the fact that Schapery uses the same type of representation.

Noting that integrals of the type

$$\int_0^{2\pi\omega} \sin n\omega t \sin m\omega t \, dt = \begin{cases} 0 & n \neq m \\ \pi/2n = m \end{cases}$$

are involved in evaluating (2) we recognize that in the evaluation of (2) with the use of (7) only the fundamental frequency in the stress expression contributes to the dissipation integral. Specifically, all the terms in the series representation for the stress higher than the fundamental mode ***do not contribute to dissipation.*** That result, being entirely a consequence of the mathematical representation of the stress, is highly suspect in its physical correctness. In fact, each term in the series representation contains a term that involves a phase shift due to the loss tangent. Yet, those terms do not contribute to the loss. We can only conclude that, inspite of the excellent representation for montonic load histories, that even this non-linear formulation of only the unieaxial stress-strain behavior is not universally valid.

$$\sigma(t) = \frac{2}{3n} \sum_{m=1}^{\infty} E(m\omega) \frac{\sqrt{a_m^2 + b_m^2}}{m\omega} \sin[\, m\omega t + \delta_m + \Delta(m\omega)\,] \qquad (5)$$

It turns out for all the parameters considered below b_o is very small and may be taken to be zero, and b_1 is identically zero. We have thus, more explicitly,

$$\sigma = \frac{2}{3n} E(\omega) \frac{a_1}{\omega} \sin[\, \omega t + \Delta(\omega)\,]$$

$$+ \frac{2}{3n} \sum_{m=2}^{\infty} E(m\omega) \frac{\sqrt{a_m^2 + b_m^2}}{m\omega} \sin[\, m\omega t + \Delta_m + \Delta(m\omega)\,] \qquad (7)$$

Substitution of (7) into (2) yields then the energy dissipated per cycle for the non-linearly viscoelastic material. This computation has been carried out for a range of parameters "n" as well as for a range of extension rations.

One finds for the energy dissipated per cycle W_c

$$W_c = \frac{2\pi}{3} \left(\frac{a_1}{\omega}\right) \varepsilon_o E''(\omega) \qquad (E'' = \text{imaginary part of the dynamic modulus})$$

One can show that

$$a_m = \{(1 + \varepsilon_o)^{n-1} + \frac{1}{2}(1 + \varepsilon_o)^{-\frac{n+2}{2}}\} \varepsilon_o A_m \omega$$

with A_n a sequence of numbers, the first of which, A_1, does not vary much from unity in magnitude. In considering the limit $\varepsilon_o \to 0$ one finds for the dissipation at infinitesimal strain per cycle W_{lim}

$$W_{Lim} = \pi \varepsilon_o^2 E''(\omega) .$$

So that the ratio for "non-linear" to "linear" histories is

$$R \equiv \frac{W_c}{W_{lin}} = \frac{2}{3}\{(1 + \varepsilon_o)^{n-1} + \frac{1}{2}(1 + \varepsilon_o)^{-\frac{n+2}{2}}\} A_1$$

The results are presented in Figure 2. Here I have defined as "R" the ratio of the energy dissipated by the non-linearly viscoelastic solid to that dissipated by

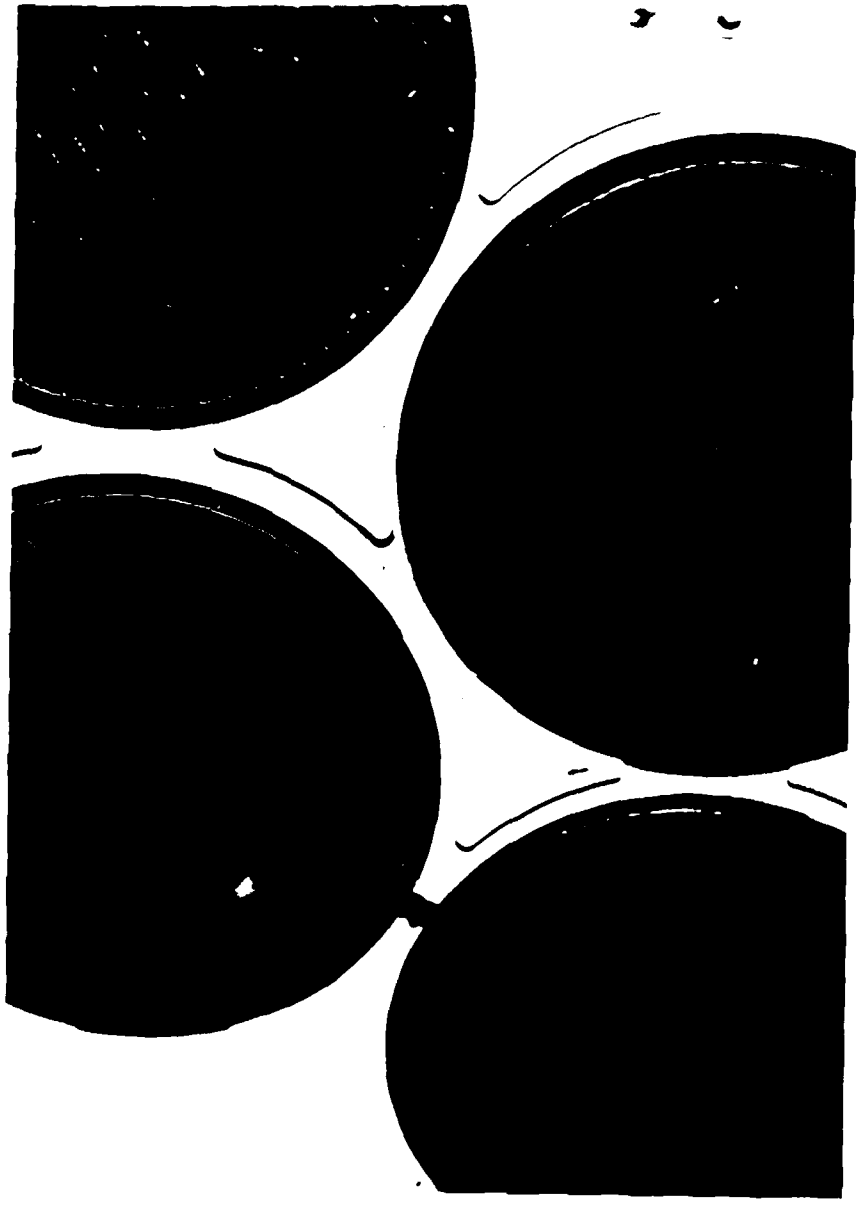

Figure 1. Interfacial failure between solar cells.

structures involving viscoelastic encapsulant materials. Some polymers or encapsulant materials are likely to be deposited on their substrates at higher temperatures followed by a cooldown to the working temperature range. The first part of this work focuses therefore on an assessment of how well we are presently able to predict such stresses. At this stage interfacial fracture is not considered. For purposes of predicting long time stability of an adhesive bond it may become necessary to compute and determine the magnitude of these residual stresses. In particular, if the temperature at which the coating is bonded to its substrate lies above the glass transition temperature of the viscoelastic material a cooling through the glass transition range may not be avoidable. This cooling is accompanied by relaxational behavior as well as by changes in the thermal expansion characteristics of polymeric materials. The resulting thermal stresses or strains induced by the mismatch in thermal expansion between adherend and substrate are then important. For most encapsulant materials adhering to a rigid sublayer the difference between thermal expansion coefficients typically varies around 5 x 10^{-4}/°C ; a cool down of 100°C (180°F) may readily introduce several percent strain and cannot thus be disregarded unequivocally. With very rigid substrates the thermally stored energy will not be disposed of through bending. Hence more driving force remains available for interfacial fracture.

2. The second type of problem under study here concerns the separation of a rubbery material from its substrate, using a fracture mechanics approach. The behavior of rubbery materials differs markedly from the one exhibited by the materials studied in the first part of this work ; there the cooldown from higher temperatures through the glass transition region makes the polymeric materials behave increasingly like a hard or even brittle material. The investigation of debonding of such rigid or semi-rigid polymers is very difficult ; as a precursor

to such studies it seems prudent to deal first with debonding of rubbery materials which allow more reasonable assumptions in the stress analysis of the failure or crack propagation process. In the study of the debonding of rubbery materials the viscoelastic character of the coating or encapsulating material can be accounted for more readily. Especially the high stresses and strains around an interfacial crack tip generate the need to incorporate the relevant viscoelastic phenomena in any fracture analysis for adhesive bonds. The former are difficult to determine accurately and one may have to be satisfied with reasonable estimates for their amplitude.

Besides material properties and the evaluation of stresses and strains, other parameters involved in time dependent adhesive failure need investigation. One of these parameters arises from the need to quantify the surface energy associated with the creation of new surfaces. For crack growth in viscoelastic elastomers it is possible to define fracture progression in terms of a rate dependent fracture energy. Such a formulation is possible as long as there is no significant creep or relaxation in the body far from the crack tip so that an elastically stored energy can be defined, and viscous dissipation due to crack propagation is confined to a small region in the crack tip vicinity.[1] For rubbery adhesives there is an analogous function for interface separation that needs to be determined in order to assess the failure rate of bond interfaces. Inasmuch as an elastic stress analysis is conducted, the time dependent failure process can be described solely through this material function of the adhesive and adherend. In the kind of vanishingly small interfacial crack growth rates the problem reduces to one of purely elastic fracture mechanics. In the second portion of this thesis, which deals with the fracture analysis, we are thus concerned with a quasi-elastic energy consideration in which the forces driving the interfacial

1. H.K. Müller and W.G. Knauss, The Fracture Energy and Some Mechanical Properties of a Polyurethane Elastomer, Trans. Soc. Rheol., 15 (1971) pp. 217-233.

fracture process are derived from temperature changes as well as residual stresses induced by cure shrinkage of the elastomer. Additional steady state stresses can be induced through volume changes caused by the outgassing of low molecular weight components of the polymer or by ingression of water or organic solvents.

The sources of forces driving interface fracture derive from a variety of environmental conditions, mainly diurnal and seasonal changes to which protective polymer films may be exposed. The cyclic loading pattern of these forces gives rise to a fatigue type load history for the adhesive bond. Small values of the amplitude of the temperature differential, whether between day and night or between seasonal averages can contribute to sizeable strains. In an analogous manner possible material sensitivity to humidity changes the integrity of the bond interface. This combined effect of temperature and moisture, in addition to the cumulative fatigue damage over longer periods of time, significantly affects the lifespan of an encapsulated solid.

Interfacial failure is not a new problem. It has been investigated from a variety of viewpoints most of which are connected with surface chemistry or surface physics. In that connection it is useful for later reference to recall here the relative size scales associated with the technical problem that motivates this work. They include the in-plane dimensions and sizes of the various layers in the composite structure. Where the panel containing the solar cells is on the order of meters (or yards), the thicknesses of the protective coatings are several orders of magnitude smaller. For later reference we note that :

1. A silicon cell typically measures 1 to 2 mm in thickness.

2. Protective layers are thinner, namely on the order of 10^{-1} to 10^{-4} mm.

3. The interphase or transition between dissimilar solids is about 10^{-6} mm.

It is also appropriate to record here the time scales of interest. If an interfacial crack propagates at a rate as low as 1×10^{-7} centimeter per minute, such a debond rate would produce a separation on the order of 1 centimeter after 20 years, which is a typical projected lifespan for an encapsulated solar cell. On the other end of the time spectrum one has to consider the material relaxation time of the encapsulant. In order to exclude viscoelastic phenomena, the glass transition temperature range has to remain sufficiently far below the operating temperatures if one wants to deal with rubbery materials. At the crack tip however material relaxation and viscous dissipation demand a more careful analysis. From these considerations the importance of the size and time scales appears more clearly.

Summarizing, it is useful to keep in mind that the two problems under study in this engineering analysis of polymer film adhesion are necessarily interrelated through the common viscoelastic phenomena occurring in both cases. Nevertheless the present investigation into the debonding of rubbery materials is limited to the formulation of a crack propagation criterion using an energy approach.

TABLE OF CONTENTS

PART 1 - VISCOELASTIC STRESS ANALYSIS OF A BIMATERIAL SANDWICH

PART 2 - TIME DEPENDENT ADHESIVE FAILURE

Part 1 - VISCOELASTIC STRESS ANALYSIS OF A BIMATERIAL SANDWICH

1. INTRODUCTION

We consider now the stress analysis for a viscoelastic layer bonded to a thin substrate and cooled through its glass transition temperature range. It is our intention to quantify the residual stresses in the adhesive bond through theoretical calculations as well as experimental measurements. The validity of the assumptions made in the theoretical analysis can thus be checked against the experimental results. At the same time, the determination of the accuracy of the experimental techniques, in particular of the physical property determination is a corollary purpose.

It is clear that this stress analysis requires a "careful" material characterization. The need to include the viscoelastic character of the polymer points the choice towards materials exhibiting their glass transition within easy experimental reach, i.e. close to ambient temperatures. For this reason polyvinyl acetate (PVA_c), an uncrosslinked amorphous polymer and of narrow molecular distribution is chosen as the model material, since it possesses a glass transition temperature zone around 30 °C.

Since the bulk modulus does not change by far as much as the shear modulus throughout the transition region, it is proposed for engineering purposes that a constant value is a reasonable approximation. This assumption is a part of the present check on our ability to predict thermoviscoelastic stresses in the bimaterial sandwich. The same assumption however does not hold with respect to the relaxation modulus or creep compliance in shear. These material properties need to be determined accurately over a wide time interval. Even though the shear relaxation modulus is used later on in the stress analysis, the creep compliance is measured because a torsion apparatus measuring the latter was available. The relaxation modulus could thus be calculated from the creep

data.

The temperature dependence of the relaxation mechanisms in amorphous polymers is well known [1]. Because of the great sensitivity of the material behavior to temperature variations the temperature control during the measurement of the viscoelastic material properties must be very fine in order to avoid disproportionately sizeable changes in the time scale of the material response. In a similar manner the sensitivity of the polymer to moisture [2] makes it necessary to keep humidity levels under control so as not to introduce any stray effects into the measurements.

Because stresses are introduced in the bimaterial sandwich by thermally induced volume changes the pertinent expansion characteristics need to be determined, in a range including the glass transition. Volume changes result from thermal loading histories or curing of the polymeric material. In order to avoid grappling with thermal transients the thickness of the specimens was chosen to be so small so as to ensure a uniform temperature throughout the sample at all times.

Next we review several analytical treatments of problems related to the current interest. Several decades ago work on bimaterial laminates concentrated on bimetallic strips. Timoshenko [3] reported on his investigation in connection with bimetal strip thermostats using a general theory for bending deformation of a bimetal strip, submitted to uniform heating.

An early analysis of problems related to failure in bonded joints was carried out by Goland and Reissner [4]. In their investigation of cemented lap joints, they obtained explicit solutions for the stresses for two limiting cases, i.e., the case of a very thin cement layer, and the case where the joint flexibility is mainly due to that of the cement layer. More recently the growing interest in

adhesive bonding for automotive and aerospace applications has triggered an extensive research effort. The advent of the finite element method opened up new ways to analyze adhesive joints. It is however beyond the scope of this study to include a broad review of the work related to the knowledge of the stress distribution in different kinds of adhesive joints. For this the reader is referred to a paper by Kinloch [5]. That author also compiled an elaborate review of surface and interfacial phenomena relevant to the adhesive joining of materials [6]. In the following we limit ourselves to review research efforts more closely related to the topic of this investigation.

Durelli and coworkers [7,8,9] conducted an extensive study of stresses and strains in rectangular strips of epoxy material, bonded on one face to a rigid plate and then shrunk. Conducted by means of photoelasticity techniques, they included slabs with different edge geometries in their investigation. In their work on interfacial crack propagation Mulville and Vaishnav [10] determined via photoelastic techniques the magnitude of the residual stresses due to casting and curing of an epoxy bonded to aluminum. These stresses were found to contribute up to 20 percent of the strain required for crack initiation at the interface. Weitsman [11] calculated approximately residual thermal stresses that develop within the resin of a fiber reinforced composite laminate. Comparisons with linear elasticity indicate that viscoelastic relaxation may reduce the residual stresses by about 20 percent. He also presented an elastic analysis of the stresses in adhesive joints due to moisture and temperature using variational principles [12]. It is observed that the significant stresses at the interface are essentially confined to the neighborhood of the outer edge.

Weitsman has also analyzed the effect of moisture sorption on the mechanical behavior of viscoelastic adhesive layers [13] ; for steady ambient humidity the viscoelastic stresses are smaller than their elastic counterparts In their work

Abbott and Bumpton [14] concluded that the physical properties of a polyurethane adhesive polymer are affected by exposure to moist environments particularly at higher temperatures. Sargent and Ashbee [15] carried out an optical interference investigation of swelling due to water uptake by adhesives. They found that the swelling in their specimens was strongly inhomogeneous, resulting in the presence of both compressive and tensile stresses normal to the bond.

In this part of this thesis we consider a model specimen which consists of only two layers of dissimilar materials with free edges (PVA_c and BK-7 glass). The material characterization is delineated in Chapter 2. Next the calculation of stresses and strains in a bimaterial specimen emphasizing the time dependent material properties of the adhesive is developed in Chapter 3. The fundamental field equations for isothermally varying temperature fields in viscoelastic materials have been stated by Muki and Sternberg [16], and by Morland and Lee [17]; these equations are used to formulate the model presented here. The final step in this analysis consists in the experimental examination, which parallels the model. the measurements consist of the time-dependent out-of-plane deformations of thin sandwiches composed of glass and PVA_c through the use of optical interferometry; that work is presented in Chapter 4.

2. VISCOELASTIC MATERIAL CHARACTERIZATION

This chapter is concerned with the determination of mechanical and physical properties of polyvinyl acetate pertinent to the stress analysis.[1] Section 2.1 studies the thermal expansion behavior of PVA_c leading to the measurement of its temperature dependent thermal coefficient of expansion. In Section 2.2 the creep behavior of polyvinyl acetate is investigated and the shear relaxation modulus is then calculated numerically via the appropriate relations between the material parameters.

2.1 Thermal Expansion Behavior

The thermal expansion characteristics of polyvinyl acetate were determined using a glass dilatometer containing mercury as the confining liquid [18,19].[2] This expansion contains a reversible component on which other changes in volume due to variations in moisture content, to curing and outgassing of low molecular weight components are superimposed. The method used here excludes these spurious factors.

Polymers display significant changes in their mechanical and physical properties in the glass transition range ; these include the coefficient of thermal expansion, the heat capacity and the compressibility. Outside the glass transition region the relation between volume change and temperature remains nearly linear ; the intersection of the extension of these linear portions from below and above the transition domain determines the position of the glass-transition temperature T_g. The value of T_g will vary slightly with the rate of cooling or heating.

1. The average weight molecular weight of polyvinyl acetate was indicated by the manufacturer (Polysciences Inc., Warrington, PA) to be 500,000.

2. In the early stages of the material characterization it was attempted to use a KD-38 Fotonic Sensor (Mechanical Technology Inc.) to record the expansion of a PVA_c sample. This non-contact optical displacement detector forms an application of a fiber optics principle. Due to non-linear and non-repeatable response to temperature changes in the sensor, its further use was discontinued and a mercury dilatometer was constructed subsequently.

The algorithm of Hopkins and Hamming [29] is used to determine the relaxation modulus of PVA_c with the master creep curve of Figure 7 as input for the calculations. The results are presented in Figure 8.

It should be noted however that algorithms available for numerically inverting viscoelastic functions are usually illustrated by generating creep functions from relaxation data, i.e. the converse procedure of the one attempted here. These calculations, like the one illustrating the procedure in [29], are successful because errors in calculating the creep function do not propagate and amplify in subsequent stages of the computation. We document this assertion by considering the recursion formula used in reference [29] ; values of the creep compliance at successive time intervals are calculated using the expression

$$\varphi(t_{n+1/2}) = \frac{t_{n+1} - \sum_{i=0}^{n-1} \varphi(t_{i+1/2}) \left[f(t_{n+1} - t_i) - f(t_{n+1} - t_{i+1}) \right]}{f(t_{n+1} - t_n)} \qquad (6)$$

In equation (6) $\varphi(t)$ refers to normalized values of the creep function, and

$$f(t) = \int_0^t \psi(\tau)\, d\tau \qquad (7)$$

in which $\psi(t)$ represents normalized values of the shear modulus. In order to study potential sources of error propagation we look at the coefficient of $\varphi(t_{n-1/2})$ in the expression for $\varphi(t_{n+1/2})$. This coefficient, after application of the mean value theorem, is :

$$\left[\frac{\psi(t_{n+1} - \vartheta_1)}{\psi(t_{n+1} - \vartheta_2)} \right] \left[\frac{t_n - t_{n-1}}{t_{n+1} - t_n} \right] \qquad (8)$$

where t_i and ϑ_i are values of time, such that $t_n > \vartheta_1 > t_{n-1}$ and $t_{n+1} > \vartheta_2 > t_n$, and where t_i correspond to equidistant time intervals on the logarithmic scale such that $t_{n-1} < t_n < t_{n+1}$. Hence each bracket has an absolute value less than unity so that the potential error in $\psi(t_{n-1/2})$ is multiplied by a number less than

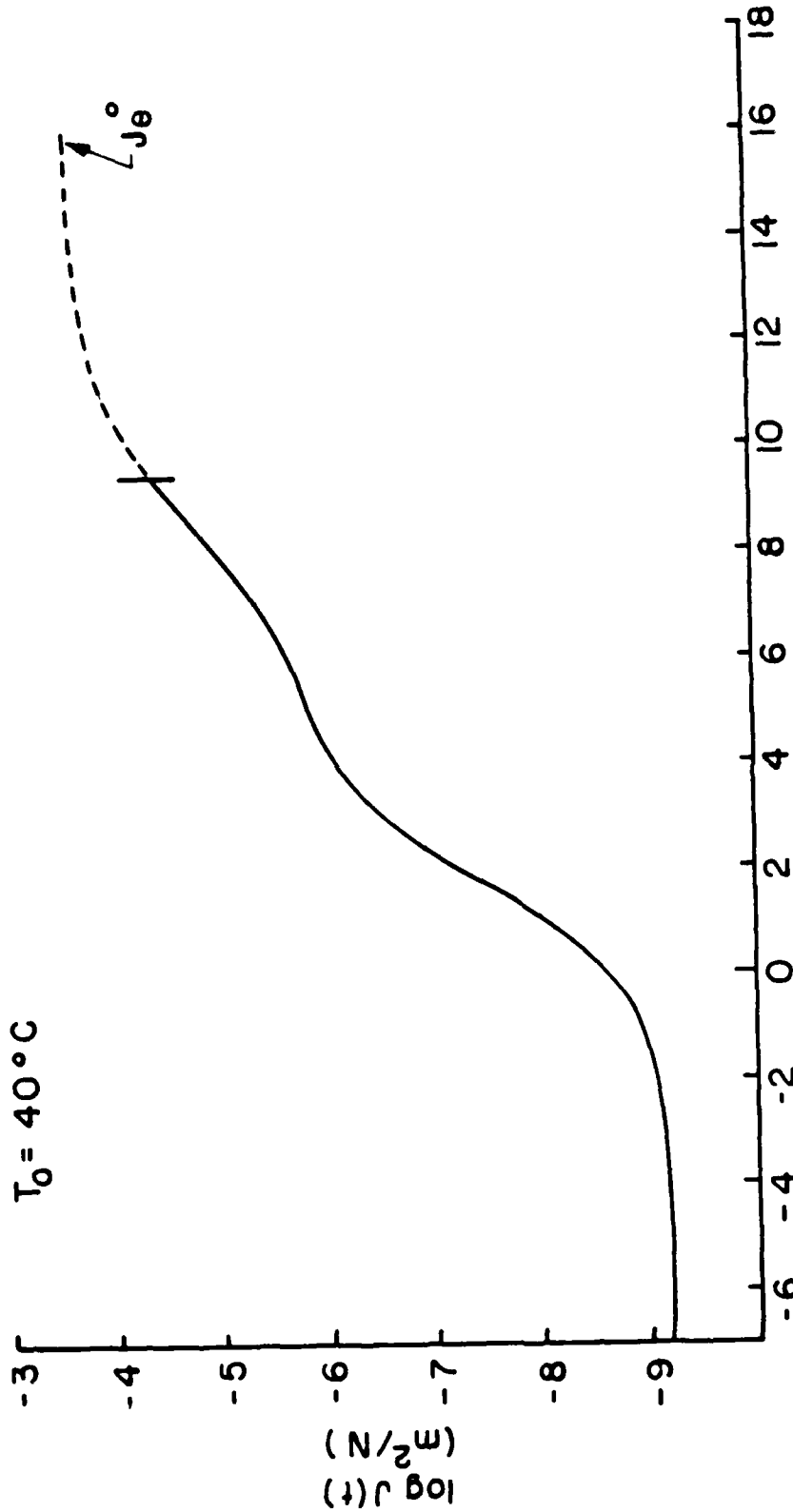

Figure 7. Master creep curve for dry PVA_c at 40 °C.

$$\log a_T = - \frac{C_1 (T-T_r)}{C_2 + (T-T_r)} \qquad (4)$$

The constants C_1 and C_2 in equation (4) are found to be

$$C_1 = 9.49$$
$$C_2 = 36.12 \qquad \text{for } T > T_g \quad \text{and} \quad T_r = 40.$$

These values seem acceptable in light of the data presented by Ferry [27].

As indicated before, our results complement initial results obtained by Knauss and Kenner [2]. Comparison of their data as well as the present ones with those by Plazek indicate a slight shift for these results toward shorter time. Residual moisture present in the PVA_c seems the most reasonable explanation for this difference.

Plazek's data [25] are used to estimate the steady state compliance[6] J_e^o : the limiting value is taken to be $\log J_e^o = -3.60$ (in m^2/N). Figure 7 shows the master curve for the recoverable creep compliance of PVA_c at 40 °C, including the long time values from reference [25] ; the dashed line beyond log t = 9.50 indicates this extrapolation.

2.2.2 Relaxation Modulus of Polyvinyl Acetate As the final step in the viscoelastic characterization of the model polymer, the shear relaxation modulus $\mu(t)$ is calculated from the experimental data for J(t). The creep compliance and the relaxation modulus are connected by the relations [27],

$$\int_0^t J(t-\xi)\mu(\xi)d\xi = t$$

or (5)

$$\int_0^t \mu(t-\xi)J(\xi)d\xi = t$$

6. The steady state compliance is defined as .

$$\lim_{t \to \infty} [\, J(t) - t/\eta \,] = J_e^o .$$

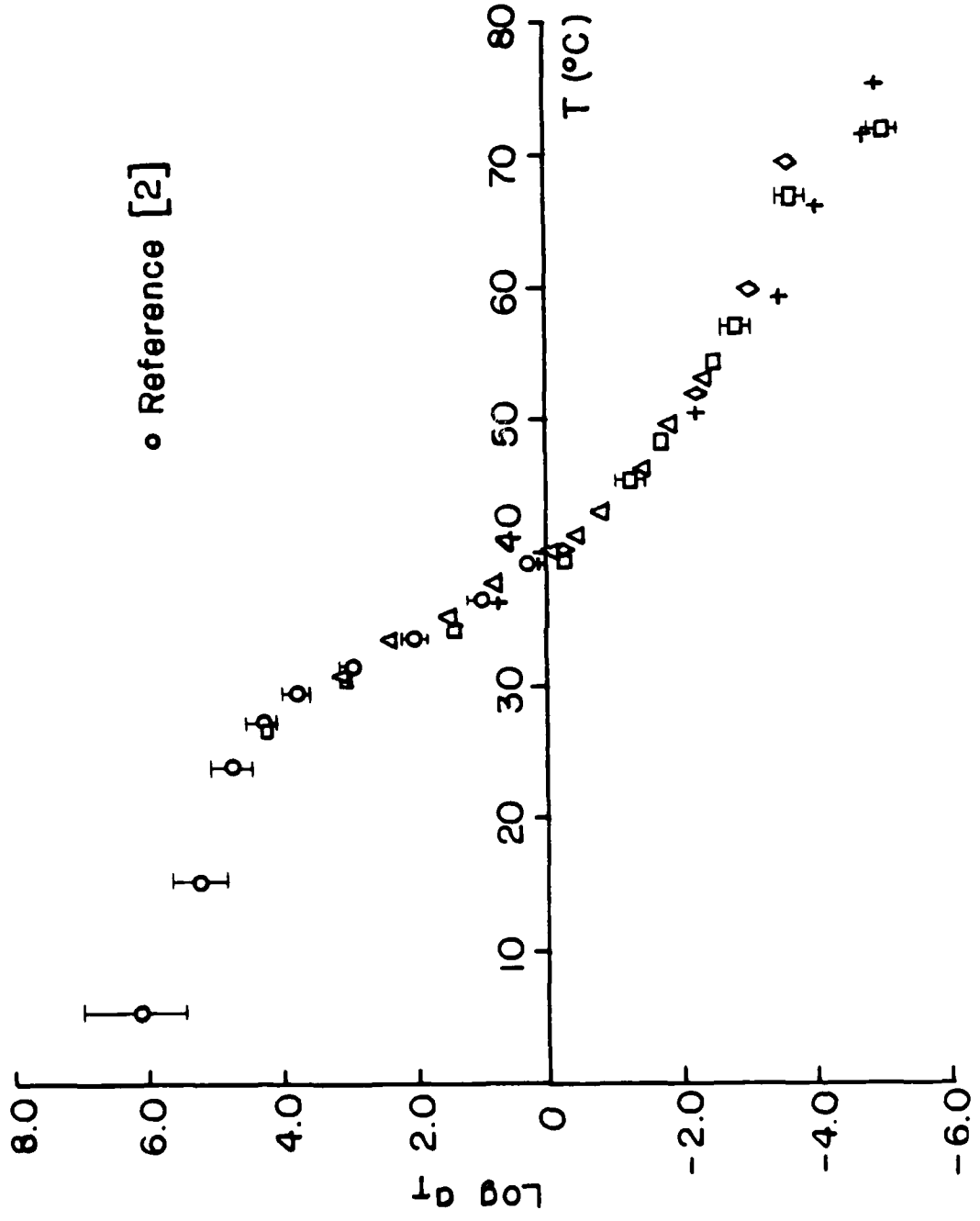

Figure 6. Log shift factor versus temperature of the master creep curve of Figure 5.

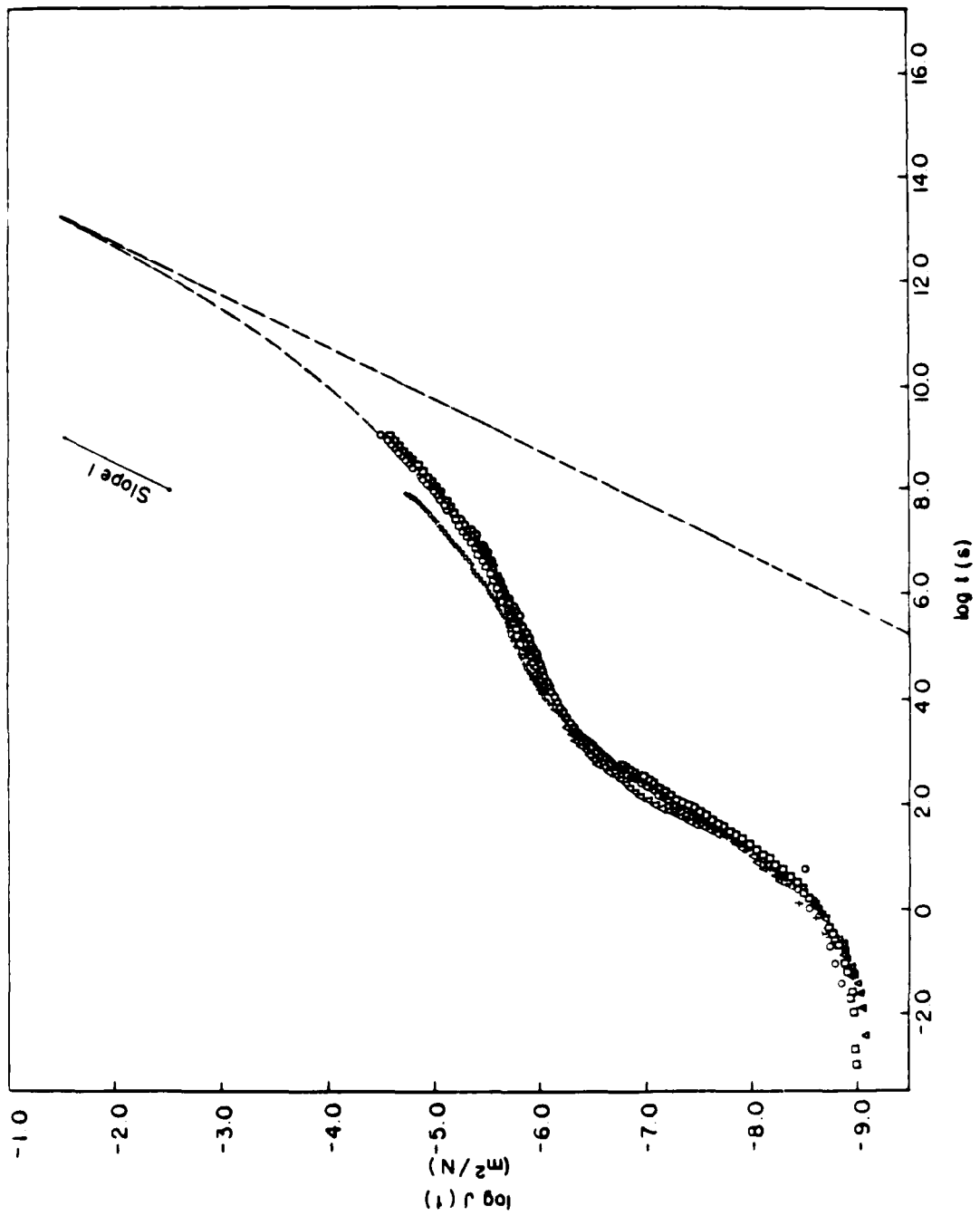

Figure 5. Master creep curve for dry PVA_c at 40° C.

heating degrades the material, it becomes nearly impossible to obtain experimental data in this temperature domain in a "finite" time interval. Therefore the upper temperature data are given a "natural" extension towards a slope equal to unity. This procedure allows an estimate of the viscous contribution in the temperature range covered by the measurements.

Subsequently horizontal shifting is attempted relative to the data for 24 °C, obtained by Knauss and Kenner [2]. A smooth composite curve is obtained from the individual curves, as shown in Figure 5, where the results for the four test runs involving several specimens are presented. The above mentioned "natural" extension is indicated in dashed line segments, namely beyond log t = 9.50. It is also found that the viscous contribution in the range of test temperatures is essentially negligible[5].

It is apparent from the quality of the master curve that PCA_c can be considered to behave like a thermorheologically simple material whose temperature dependence can be described by a shift factor $a_{T_o}(T)$, such that

$$J(T,t) = (T_o/T)\, J\left\{T_o,[t/a_{T_o}(T)]\right\}. \qquad (3)$$

This time-temperature shift factor a_T is shown in Figure 6 for dry PVA_c, including error bars representing the uncertainty in shifting the individual curves of Figure 4. The different symbols correspond to the various test runs, including the results of reference [2]. One should note a marked change in slope in the glass transition temperature range. For temperatures above T_g the shift factor a_T can be represented by the WLF equation [1], namely

5. Recovery experiments, associated with one of the four test runs, had failed to yield satisfactory results for the value of the viscosity. The recovery times turned out to be extremely long in the temperature range under consideration. Another approach for determining the value of η_1, suggested by Ninomiya [28], also fell short in producing useful results ; this was due to a poorly defined extrapolation of $(dJ(t)/dt)$ versus $1/t$.

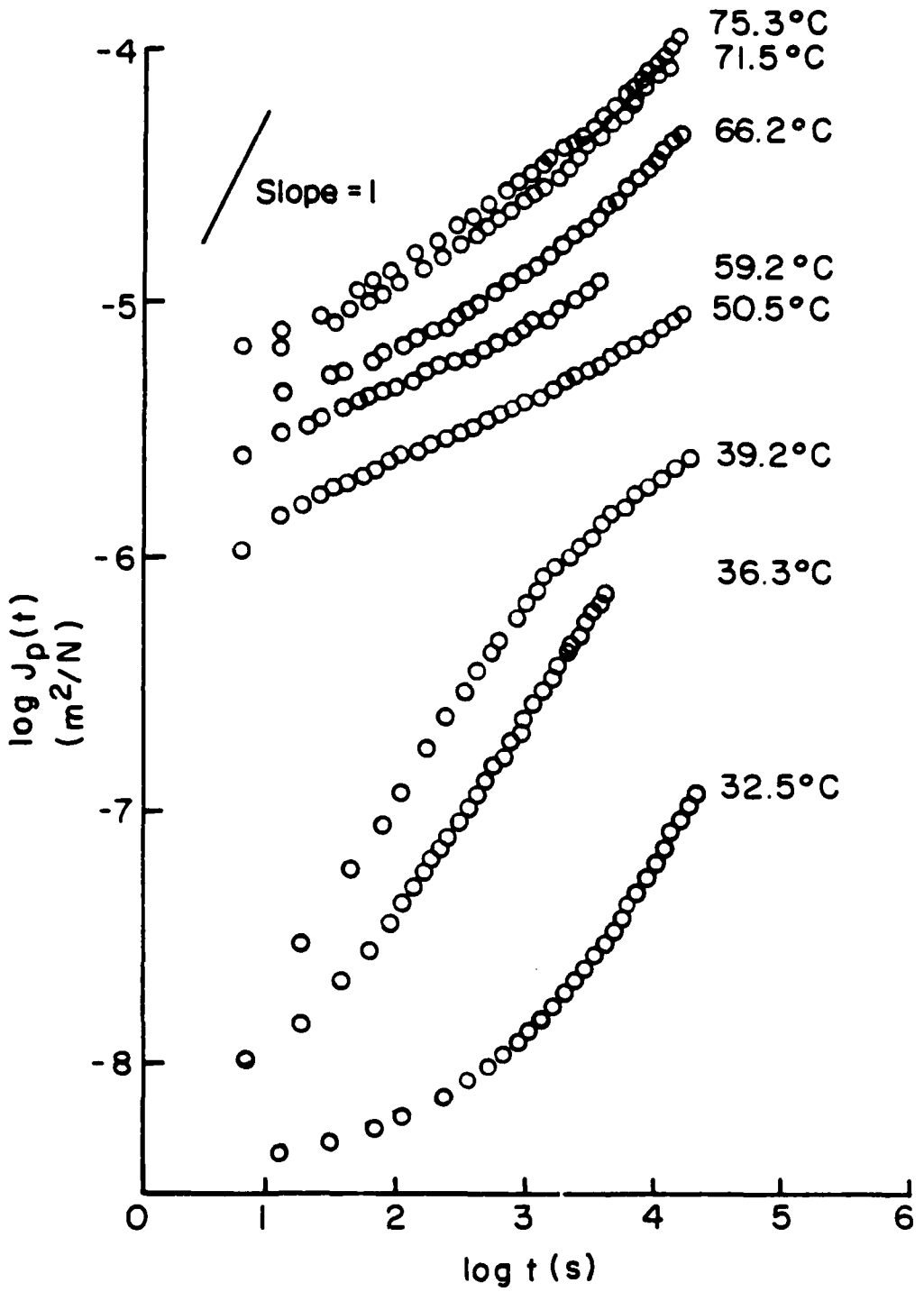

Figure 4. Creep curves for dry PVA_c at various temperatures.

the geometry of the specimens was changed significantly with respect to the one used in reference [2]. Short cylindrical PVA_c-samples are glued with an Eastman 910 adhesive to aluminum holders. The dimensions of the cylindrical PVA_c specimens range from 7.94 to 17.72 mm in diameter, and from 5.0 to 5.96 mm in length. For these composite specimens the amount of strain in the metal parts is negligible compared to the strain in the polymeric central part.

Figure 4 displays the recorded creep compliance for dry[4] PVA_c as a function of time with the temperature as a parameter, for one of the four test runs. The error level for these curves is evaluated to be approximately 2 %. From these data a master creep curve for PVA_c is generated. At first the curves are shifted vertically by an adjustment factor T/T_o, where T_o is taken to be 40 °C ; hence the temperature dependence of the rubberlike nature of the response is accounted for [27]. This shift is included in Figure 4 where $J_p(t)$ represents the vertically shifted creep compliance. In order for subsequent horizontal shifting to be successful, the importance of the long time viscous contribution needs to be determined.

According to the theory of linear viscoelasticity the creep compliance of an amorphous uncrosslinked polymer can be described by,

$$J(t) = J_g + J_d(t) + \frac{t}{\eta} \qquad (2)$$

where J_g, $J_d(t)$ and η are the glassy compliance, the delayed creep compliance and the viscosity, respectively. In the long time, high temperature domain J(t) is largely determined by the viscous contribution t / η, indicated by a linear portion in a plot displaying log J(t) versus log t with a slope equal to unity. Because it takes an inordinate amount of test time to reach this 45° slope and long time

4. *The term "dry" refers to the in vacuum storage of the specimens. This does not exclude some possible residual moisture which could not be extracted from the samples in our laboratory.*

contraction of the polymeric samples does not yield repeatable values for T_g. The values of the cubical thermal coefficient of expansion are found to be 2.50×10^{-4}/°C in the glassy domain and 5.98×10^{-4}/°C above T_g. The error for these data was calculated to be about 3 %. The test results from different runs, indicated by distinct symbols in Figure 3, proved to be very repeatable. The numerical data for this particular type of PVA_c are in good agreement with results previously obtained for PVA_c by Kovacs [23].

2.2 Shear Creep Behavior

In order to complete the necessary material characterization of the model material PVA_c, its shear creep compliance is determined. The testing was carried out on a creep torsiometer, as outlined in reference [24]. These authors also report creep data for PVA_c in the temperature region around the glass transition temperature [2].[3] These initial results are here extended in the upper temperature region, so as to account also for the possible viscous flow contribution of this uncrosslinked polymer. This latter determination is necessary to assess the residual stresses due to cooldown from the melt.

2.2.1 Experimental Results and Analysis The creep compliance J(t) can be derived from the experimentally measured twist angle $\vartheta(t)$ as a function of time, through the relation for torsion of circular cross-sections, given by

$$J(t) = \frac{\pi d^4 \vartheta(t)}{32LT} \qquad (1)$$

where d, L and T are the specimen diameter, specimen gauge length and applied torque respectively. The derivation of equation (1) is trivial and is found in Appendix 1. In order to guarantee the accuracy of the measurements at higher temperatures and due to the limitations of the torsiometer described in [24],

3. Complementary work on PVA_c has been reported by Plazek [25,26] in a broader temperature range.

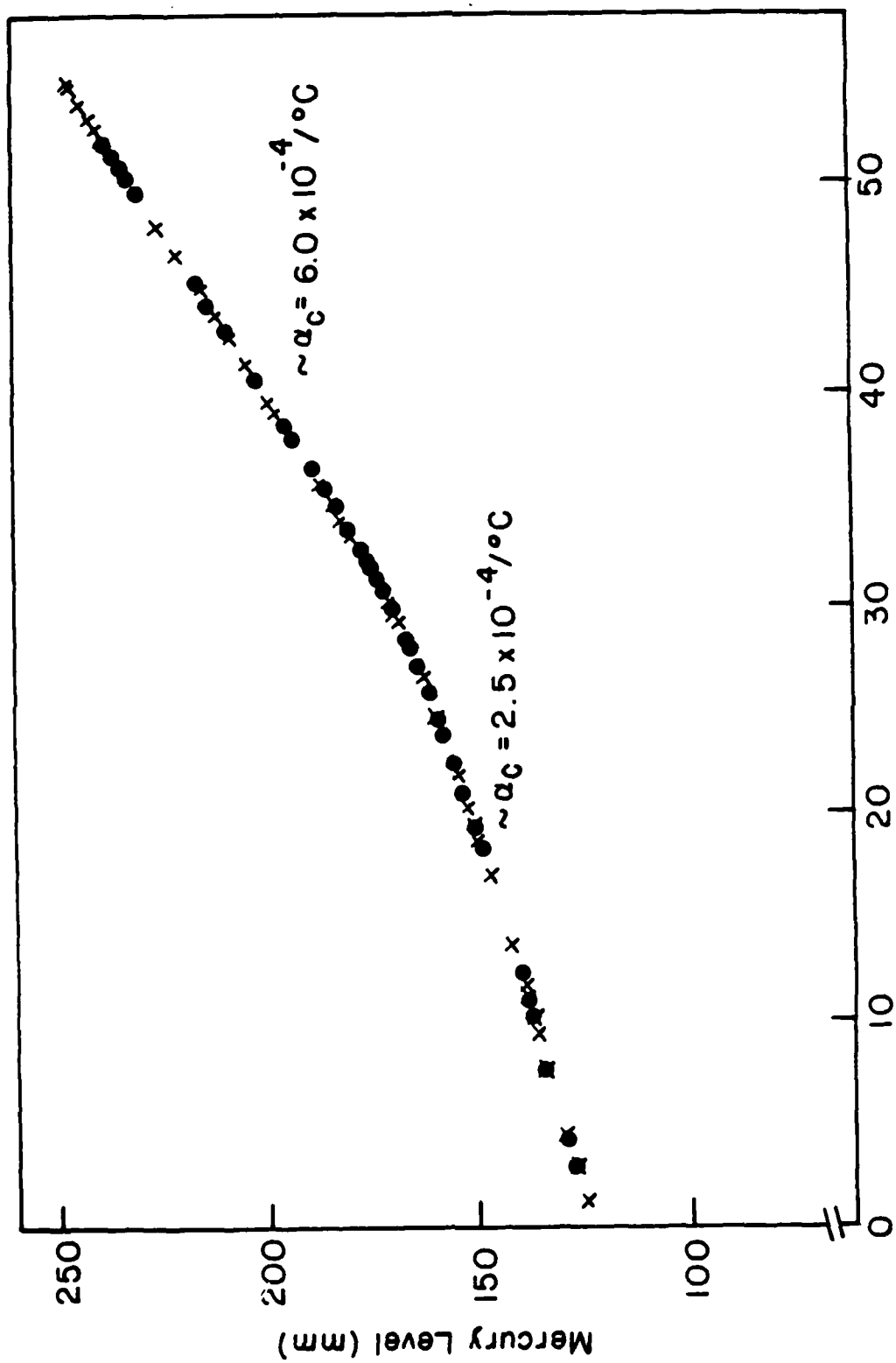

Figure 3. Thermal expansion characteristics for dry PVA_c.

tubing through which liquid nitrogen can flow for cooling purposes ; a thermocouple monitors the temperature of the specimen environment. The uniformity of the temperature throughout the bath is maintained by two continuously moving propellers. Specimen volume changes result in changes in mercury level, in the capillary, which are read using the ruling on the capillary.

For accurate results a calibration is necessary to account for both the non-uniformity of the capillary bore and the intrinsic thermal expansivity of the apparatus. The former calibration was made prior to making a U-bend in the capillary. With a stop-cock affixed at the lower end of the capillary, mercury was drawn by a vacuum into the capillary. The mercury level was then lowered in small increments by opening the stop-cock ; the corresponding volume of the capillary was determined by weighing the removed mercury with a Mettler HL32 analytical balance with a readibility range of 0.1 mg, and then using standard tabulated data for the density of mercury. The average volume of the tube per height increment was found to be 0.00013 ml/mm ; any nominal volume above reference level computed using this average can thus be corrected.

The calibration for thermal expansion effects involves measuring the apparent volume change with temperature while the specimen chamber is completely filled with mercury. The change in volume with temperature of a volume of mercury equal to the nominal specimen volume, yields the volume change that has to be subtracted from the recorded data when a specimen is present.

2.1.2 Experimental Results The data of the dilatometric measurements are presented in Figure 3. The thermal expansion characteristics for dry PVA_c display the change of mercury level in the capillary versus the temperature for a cooling rate of approximately 4 °C per hour from which the glass transition temperature T_g is determined at 29.0 °C. At faster cooling rates the non-equilibrium

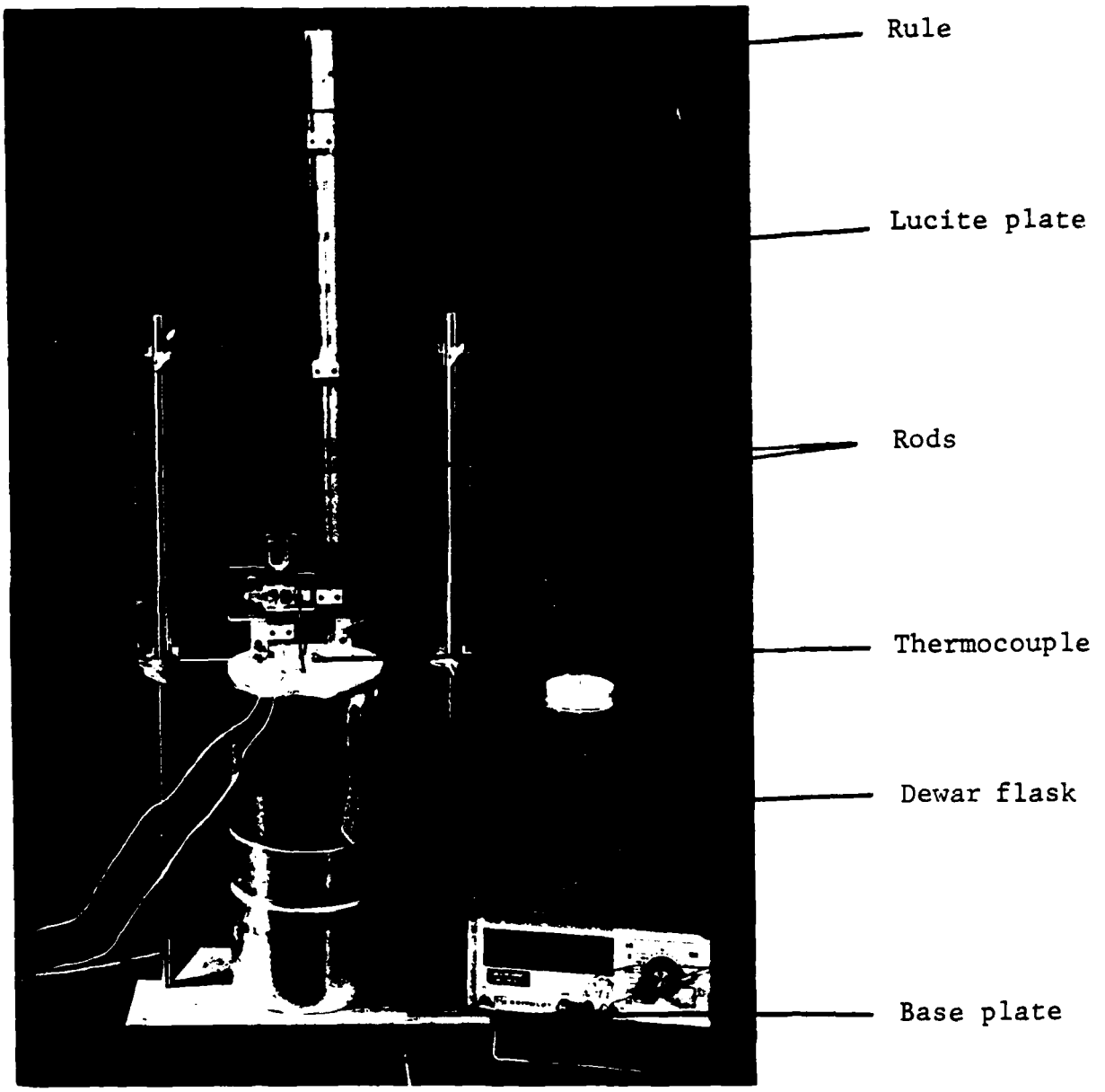

Figure 2. Dilatometer in Dewar with ancillary apparatus.

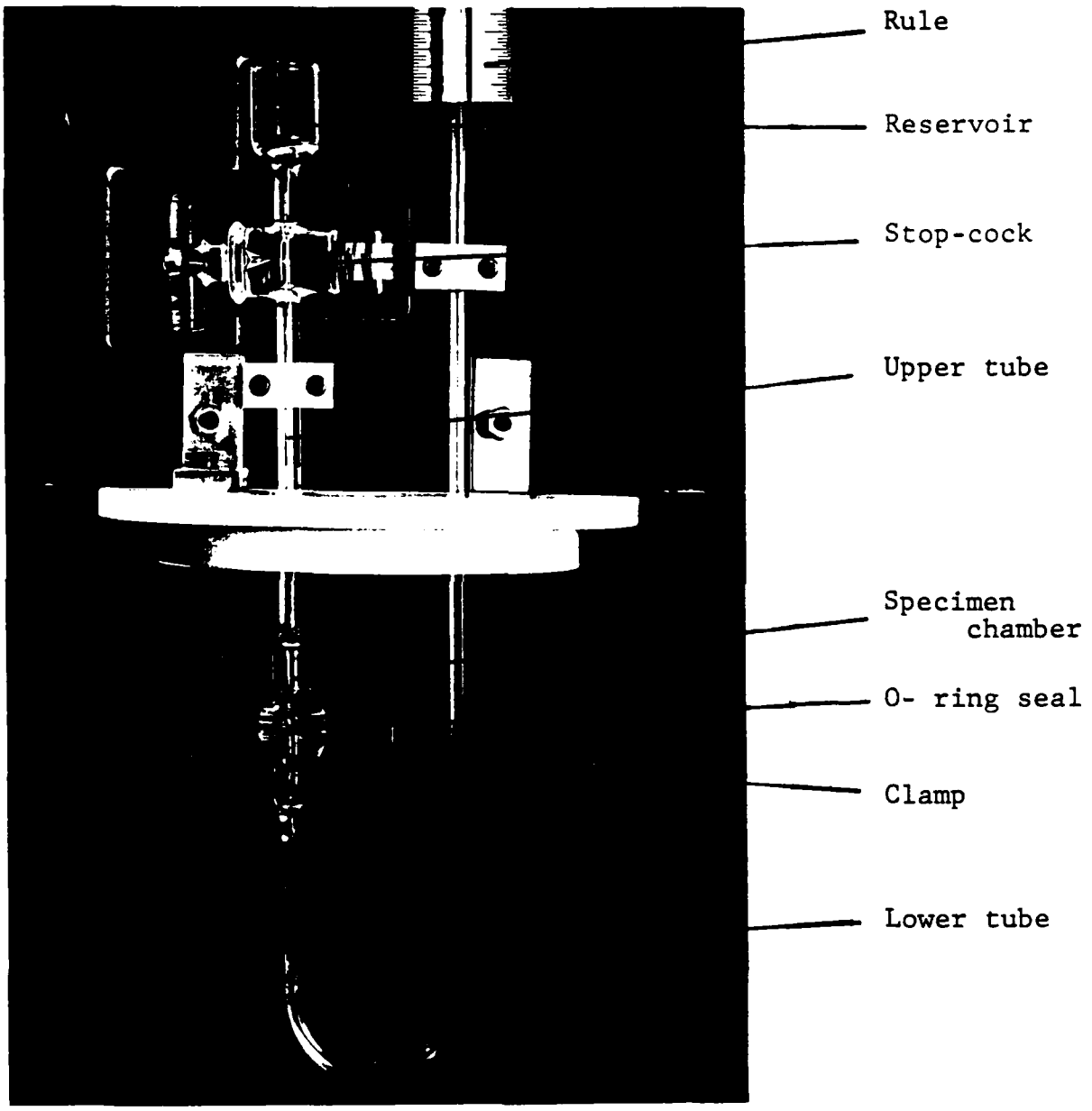

Figure 1. Dilatometer.

An extensive phenomenological study of the glass transition in amorphous polymers and in particular in PVA_c has been carried out by Kovacs [20]. Other glass dilatometry measurements yielding very satisfactory results include the findings of Rush [21,22]. Both these authors follow the method of quenching the dilatometer from a reference temperature into baths at some other temperature. From the equilibrium volumes at the bath temperature the thermal expansion data are then calculated.

2.1.1 Specimen Preparation and Experimental Method The polyvinyl acetate obtained from the manufacturer in the form of clear spherical beads, is molded at a temperature of 125 °C in a steel mold. The details of the preparation are reported in reference [2]. Cylindrical specimens about 35 mm long and 6.35 mm in diameter, are used in the dilatometric measurements.

The design of the apparatus was guided to a large extent by the description outlined by Bekkedahl [18]. The essential parts of the dilatometer are shown in Figure 1. A specimen chamber is formed from the laterally expanded ends of two Pyrex glass tubes which are clamped together via an O-ring seal. The upper tube proceeds to a stopcock and subsequently terminates at a reservoir. The lower tube, a capillary of nominally 0.5 mm inside diameter, undergoes a U-bend and then ascends vertically for approximately 700 mm along a rule with a least count of 0.5 mm. These components are supported on a lucite plate, as shown in Figure 2.

The specimen is placed in the specimen chamber and the chamber clamp secured. The remaining volume of the dilatometer is filled with mercury from the reservoir via the stop-cock, which is then closed to exclude any air bubbles. The specimen chamber is submerged in a silicone bath contained in a Dewar flask. The latter contains an inductance heating element and a coiled copper

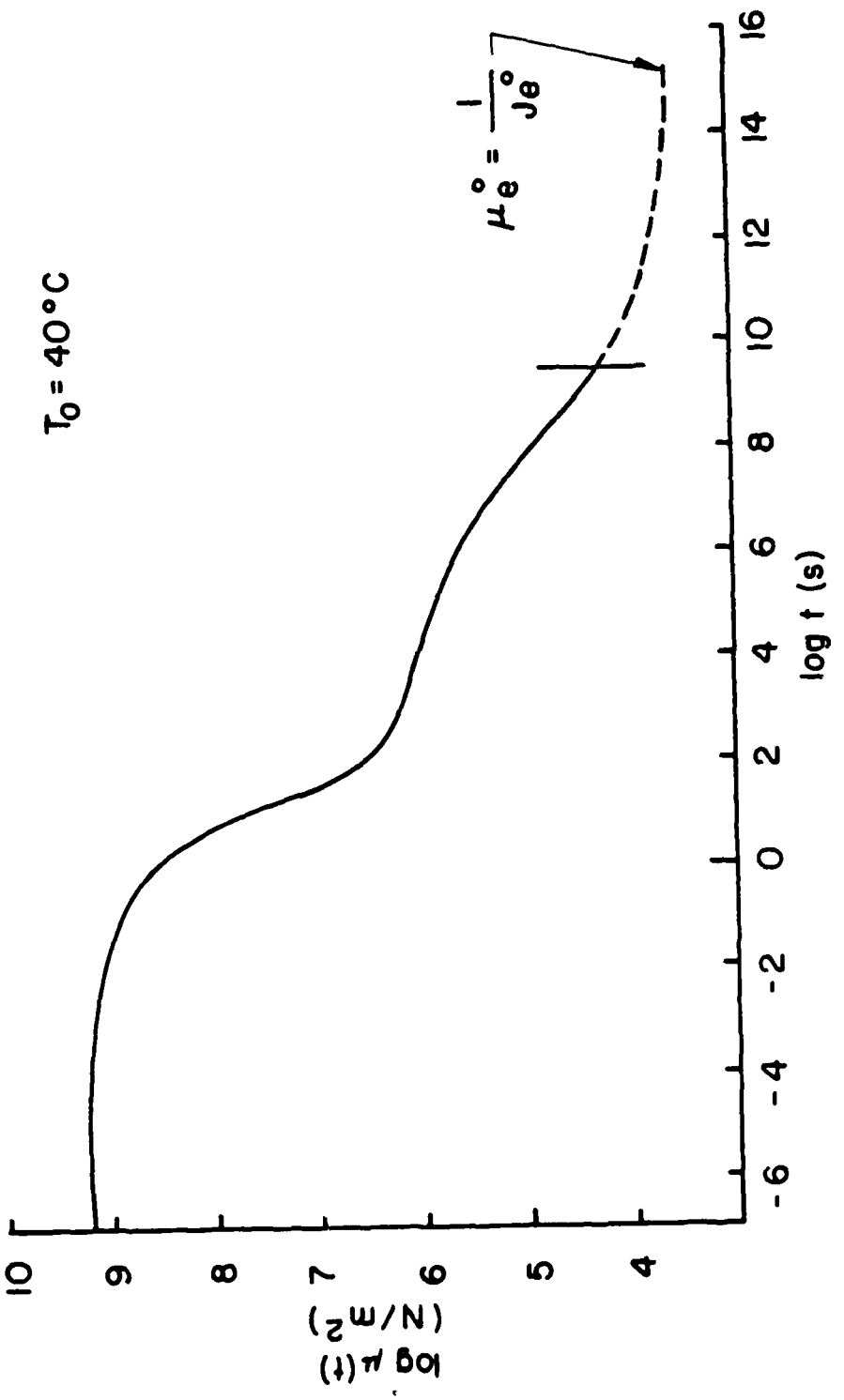

Figure 8. Master relaxation curve for dry PVA_c at 40 °C.

unity in size if the input function $\psi(t)$ is a monotonically decreasing function. Hence the effect of the error dies out.

In the present case, where it is attempted to generate the shear modulus from creep data, the error propagation becomes unstable because the input function is a monotonically *increasing* function and because of the steep slope of the master creep curve of PVA_c in the transition range. This consideration becomes apparent by evaluating the ratio between the first pair of brackets in expression (8). With the creep compliance as input function, the product of the first term is no longer less than unity. Nevertheless using time intervals whose amplitude was chosen on the basis of [29] it was tried to invert the creep compliance. In the single precision mode the error growth was unstable ; therefore the computations were executed in double precision. The error oscillations did not completely die out, but a solution throughout the whole time spectrum was nevertheless obtained. Consequently an essentially trial and error inversion procedure was finally developed. The domain where the inital solution for $\mu(t)$ did not appear smooth is approximated by a smooth curve. Then as a check, the numerically obtained shear relaxation modulus was itself again inverted to insure that the experimentally measured creep compliance was recovered. In these calculations the choice of the time intervals seemed the critical factor : with an appropriate choice of this parameter, very few iterations were necessary. At long time values, i.e. beyond log t = 9.50, the data are extended in accord with the procedure used earlier for the creep data.

3. VISCOELASTIC STRESS ANALYSIS

Having obtained the pertinent material properties for the viscoelastic material we proceed to the stress analysis of a bimaterial specimen, composed of an elastic stiff substrate and an attached viscoelastic layer. The theoretical results obtained next will be compared with experimental results in Chapter 4. Section 3.1 outlines the relations derived to compute the stresses as a function of time. The second part of this chapter, namely Section 3.2, presents the numerical results of the modelling.

3.1 Formulation of the Problem

It is assumed that a perfect bond exists between the two dissimilar materials involved. Furthermore we consider only slow thermal changes such that the sample does not experience a temperature gradient through its thickness nor incurs any non-equilibrium volume changes. The analysis allows only for small deformations.

The geometry of the specimen is shown in Figure 9. The viscoelastic material is modelled by a thermorheologically simple material ; its mechanical properties include the shear relaxation modulus $\mu(t)$ and its temperature dependent shift factor $a_{T_0}(T)$, the bulk modulus K_0, taken to be a constant, and the thermal coefficient of expansion $\alpha(T)$. The latter is assumed to be simply a function of the temperature, i.e. no explicit time or temperature rate dependence is allowed [30]. Comparison with experimental results later will examine the validity of this assumption. The mechanical behavior of the adhering substrate is characterized by corresponding elastic and physical parameters.

Let a displacement field be defined for both material domains as :

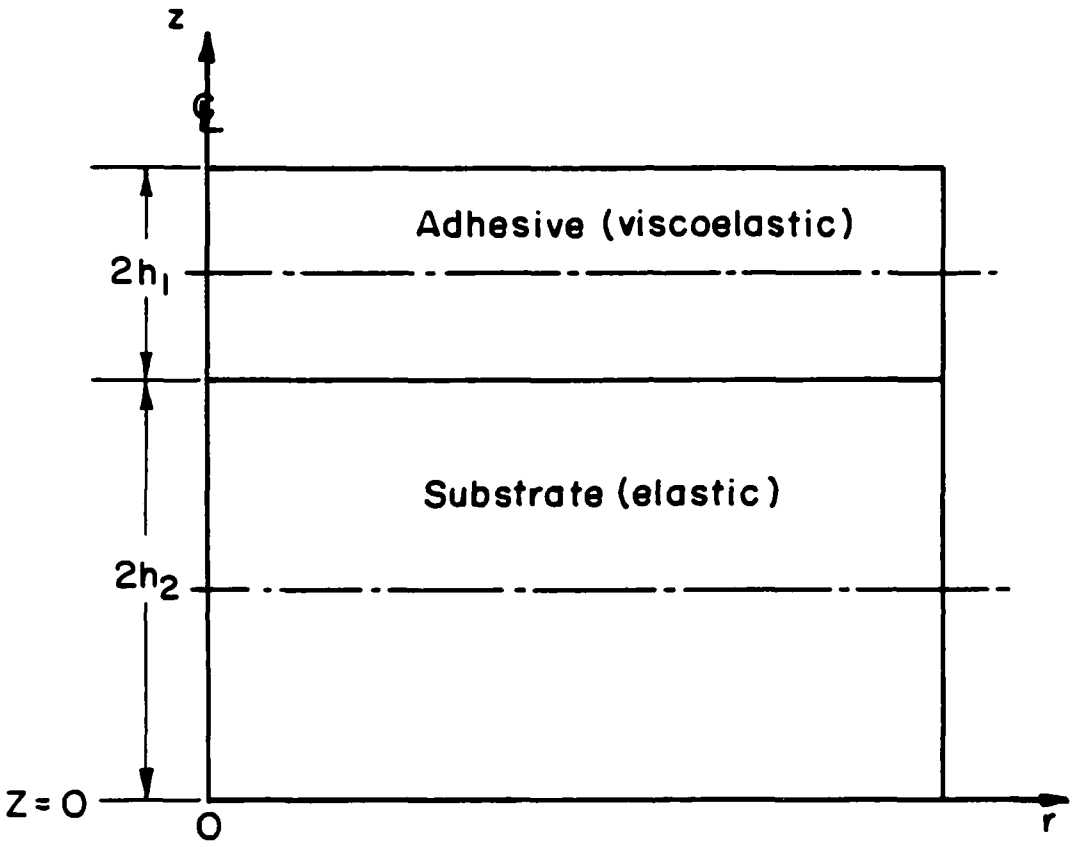

Figure 9. Geometry of the bimaterial specimen.

$$u = \varepsilon_o r - z\frac{\partial w}{\partial r}$$

$$v = 0 \tag{9}$$

$$w = w(r)$$

where u, v, and w are the displacements in the r, ϑ and z-direction respectively ; the coordinates are defined in Figure 9 and ε_o is the radial strain of the bottom fiber of the bimaterial element. Let the curvature be given by :

$$\frac{1}{R} = \frac{\partial^2 w}{\partial r^2} \tag{10}$$

where w(r) denotes a spherical deflection, whose magnitude is supposed to be small enough to have equation (10) hold near r = 0. Our immediate purpose here is to calculate the strain ε_o as well as the curvature $\frac{\partial^2 w}{\partial r^2}$ occurring as a result of a changing temperature.

The stress in the z-direction is zero so that the only non-vanishing stresses are $\sigma_r = \sigma_\vartheta \simeq \sigma$, while $\sigma_z \simeq 0$. Furthermore all shear strains vanish (except near an edge). Under non-isothermal conditions :

$$\sigma_{kk} = 3K_o \left\{ \varepsilon_{kk} - 3\alpha\vartheta \right\} \quad \dagger \tag{11}$$

where ϑ indicates the temperature difference with respect to the reference temperature. Also,

$$S_{ij} = 2\mu \ * \ de_{ij} \quad \ddagger \tag{12}$$

where S_{ij}, e_{ij} are deviator stresses and strains, respectively. For the present

† Repeated indices denote the summation convention.

‡ The star notation (*) refers to Stieltjes convolution ; equation (12) should read in full as :

$$S_{ij} = 2\int_{-\infty}^{t} \mu(t-\xi)d\varepsilon_{ij}(\xi) .$$

geometry, we have :

$$\sigma_{kk} = \sigma_r + \sigma_\vartheta = 2\sigma_r$$

$$S_r = \frac{1}{3}\sigma_r$$

$$e_r = \varepsilon_r - \frac{1}{3}\left(\frac{2\sigma_r}{3K} + 3\alpha\vartheta\right). \tag{13}$$

Hence equation (12) becomes:

$$\sigma_r(z,t) = 6\mu(t) \ * \ \left\{ d\left[\varepsilon_r(t) - \frac{2\sigma_r(z,t)}{9K_o} - \alpha(T(t))\,\vartheta(t) \right] \right\} \tag{14}$$

or

$$\sigma_r(z,t) + \frac{4\mu(t)}{3K_o} * d\sigma_r(z,t) = 6\mu(t) * d[\varepsilon_r(t) - \alpha(T(t))\,\vartheta(t)]. \tag{15}$$

If the temperature varies during the stress history one has, upon applying instantaneous temperature reduction [16],

$$d\xi' = \frac{d\xi}{a_T} \tag{16}$$

or

$$\xi' = \int_o^\xi \frac{d\zeta}{a_T[T(\zeta)]} \tag{17a}$$

and

$$t' = \int_o^t \frac{d\zeta}{a_T[T(\zeta)]} . \tag{17b}$$

Thus equation (15) can be written as,

$$\sigma_r(z,t) + \frac{4}{3K_o}\int_o^t \mu(t'-\xi')\frac{\partial\sigma_r(z,\xi)}{\partial\xi}d\xi = 6\int_o^t \mu(t'-\xi')\frac{\partial[\varepsilon_r(\xi) - \alpha(T(\xi))\,\vartheta(\xi)]}{\partial\xi}\partial\xi \tag{18}$$

Because by assumption the temperature T does not depend on z (nor on r and ϑ) and since the temperature reduced time t' is a function of t, any explicit

reference to real time t can be eliminated in favor of t'. Thus,

$$\begin{aligned} \sigma_r(z,t) &= \hat{\sigma}_r(z,t') \\ \varepsilon_r(z,t) &= \hat{\varepsilon}_r(z,t') \\ \Omega(t) &= \hat{\Omega}(t') \end{aligned} \tag{19}$$

where $\Omega(t) = \alpha(T(t))\,\vartheta(t)$. In the t'-domain, equation (18) becomes now,

$$\hat{\sigma}_r(z,t') + \frac{4}{3K_o}\int_o^{t'} \mu(t'-\xi')\frac{\partial \hat{\sigma}_r(z,t')}{\partial \xi'}\,d\xi' = 6\int_o^{t'} \mu(t'-\xi')\frac{\partial[\hat{\varepsilon}_r(z,t') - \hat{\Omega}(\xi')]}{\partial \xi'}\,d\xi' \,. \tag{20}$$

So far use has been made only of the stress-strain behavior of the viscoelastic material. In order to satisfy equilibrium conditions equation (20) is transformed into the Laplace domain where the independent variable t' is being transformed into s. Hence

$$\hat{\bar{\sigma}}_r(z,s) + \frac{4}{3K_o}\bar{\mu}(s)\;\hat{\bar{\sigma}}_r(z,s)\;s = 6\bar{\mu}(s)\;[\hat{\bar{\varepsilon}}_r(z,s) - \hat{\Omega}(s)]\;s \tag{21}$$

from which

$$\hat{\bar{\sigma}}_r(z,s) = 18K_o\,\frac{\bar{\mu}(s)\;[\hat{\bar{\varepsilon}}_r(z,s) - \hat{\bar{\Omega}}(s)]\;s}{3K_o + 4\bar{\mu}(s)\;s}\,. \tag{22}$$

A new modulus P(t) is now defined such that

$$[3K_o + 4\bar{\mu}(s)\;s]\;\;s\;\;\hat{\bar{P}}(s) = 1 \tag{23}$$

which is the transform of the relation

$$\int_o^{t'} [3K_o + 4\mu(t'-u)]\,\hat{P}(u)du = t'. \tag{24}$$

Combining equations (23) with (22) results in :

$$\hat{\bar{\sigma}}_r(z,s) = 18K_o\,[\bar{\mu}(s)\;\;\hat{\bar{P}}(s)\;\;s]\left\{[\hat{\bar{\varepsilon}}_r(z,s) - \hat{\bar{\Omega}}(s)]\,s\right\} \tag{25}$$

and consequently

$$\hat{\sigma}_{r_1}(z,t') = 18K_o \left\{ \mu(t') \ast d\hat{P}_1(t') \ast d\left[\hat{\varepsilon}_r(z,t') - \hat{\Omega}(t')\right] \right\} \tag{26}$$

where the subscript 1 refers to the range of the viscoelastic material in which this expression for the σ_r stress is valid.

In a similar fashion the stress in the elastically behaving substrate can be computed. The elastic constitutive equations equivalent to equations (11) and (12) are :

$$\sigma_{kk} = 3K\left[\varepsilon_{kk} - 3\alpha\vartheta\right] \tag{27a}$$

$$S_{ij} = 2\mu e_{ij}. \tag{27b}$$

Hence,

$$\sigma_r(z,t) = 6\mu\left[\varepsilon_r(t) - \frac{2\sigma_r(z,t)}{9K} - \alpha(T(t))\,\vartheta(t)\right] \tag{28}$$

or

$$\sigma_r(z,t) = 6\mu\left[1 + \frac{4\mu}{3K}\right]^{-1}\left[\varepsilon_r(t) - \alpha(T(t))\,\vartheta(t)\right]. \tag{29}$$

Using the appropriate relations between the elastic moduli, and substituting the expression for the strain, namely

$$\varepsilon_r(t) = \varepsilon_o(t) - z\frac{\partial^2 w}{\partial r^2}(t) \tag{30}$$

into equation (29) yields analogously to equation (26),

$$\sigma_{r_2}(z,t) = \frac{E_2}{1-\nu_2}\left[\varepsilon_o(t) - z\frac{\partial^2 w}{\partial r^2}(t) - \alpha_2(T(t))\,\vartheta(t)\right] \tag{31}$$

where the subscript 2 refers to the range of the elastic substrate.

Next, equilibrium of forces and moments can be considered. This amounts to the requirements :

$$\int_{0}^{2(h_1 + h_2)} \hat{\sigma}_r(z,t')dz = 0 \qquad (32a)$$

and

$$\int_{0}^{2(h_1 + h_2)} z\,\hat{\sigma}_r(z,t')dz = 0 \qquad (32b)$$

Executing the indicated integration over the thickness of the bimaterial specimen yields the following pair of equations :

$$\left[18K_o h_1 \mu_1(t') \ast d\hat{P}_1(t') \ast d\hat{\varepsilon}_o(t') + \frac{E_2}{1-\nu_2} h_2\, \hat{\varepsilon}_o(t')\right]$$

$$-\left[18K_o(h_1^2 + 2h_1h_2)\mu_1(t') \ast d\hat{P}_1(t') \ast d\frac{\partial^2\hat{w}}{\partial r^2}(t') + \frac{E_2}{1-\nu_2} h_2^2\, \frac{\partial^2\hat{w}}{\partial r^2}(t')\right]$$

$$= 18K_o h_1 \mu_1(t') \ast d\hat{P}_1(t') \ast d\hat{\Omega}_1(t') + \frac{E_2}{1-\nu_2} h_2\, \alpha_2\, \hat{\vartheta}(t') \qquad (33a)$$

and,

$$\left[18K_o(h_1^2 + 2h_1h_2)\mu_1(t') \ast d\hat{P}_1(t') \ast d\hat{\varepsilon}_o(t') + \frac{E_2}{1-\nu_2} h_2^2 \hat{\varepsilon}_o(t')\right]$$

$$-\left[24K_o(h_1^3 + 3h_1^2h_2 + 3h_1h_2^2)\mu_1(t') \ast d\hat{P}_1(t') \ast d\frac{\partial^2\hat{w}}{\partial r^2}(t')\right.$$

$$\left. + \frac{E_2}{1-\nu_2} \cdot \frac{4}{3} h_2^3\, \frac{\partial^2\hat{w}}{\partial r^2}(t')\right]$$

$$= 18K_o(h_1^2 + 2h_1h_2)\mu_1(t') \ast d\hat{P}_1(t') \ast d\hat{\Omega}_1(t') + \frac{E_2}{1-\nu_2} h_2^2 \alpha_2\, \hat{\vartheta}(t') . \qquad (33b)$$

This system of two equations (33a) and (33b), in two unknowns $\hat{\varepsilon}_o(t')$ and $\frac{\partial^2\hat{w}}{\partial r^2}(t')$, yields solutions in the temperature reduced time domain. They are related to their counterparts in real time through expressions similar to equations (19), namely,

$$\hat{\varepsilon}_o(t') = \varepsilon_o(t) \tag{34a}$$

$$\frac{\partial^2 \hat{w}}{\partial r^2}(t') = \frac{\partial^2 w}{\partial r^2}(t). \tag{34b}$$

Through relations (17) the solution in the real time domain t can be computed.

In the limit of two linearly elastic solids the analysis simplifies. Those limit computations are outlined in Appendix 2. In temperature domains far removed from the glass transition temperature range the viscoelastic coating acts essentially like a purely elastic medium. Hence the glassy and long time properties of polyvinyl acetate can be used to calculate the elastic asymptotes, characterizing the behavior of the bimaterial layer in the corresponding temperature domains.

3.2 Numerical Results

Two cases are considered ; the first concerns the heating of a bimaterial sample from temperatures well below the glass transition of the polymer up to the temperature region where the viscoelastic material essentially acts like a rubbery solid. The second case deals with the cooling of a similar specimen between the same extreme temperature domains, this time however starting in the melt region. For each of the two examples three graphs are presented below. The first displays the graphical representation of the relation between the real time t and the temperature reduced time t' as given by equation (17). The next two figures represent the solutions of equations (33) for the radial strain in the bottom fiber of the specimen $\varepsilon_L(t)$, where

$$\varepsilon_L = \varepsilon_o(t) - \alpha_2(T - T_o) \tag{35}$$

and the radius of curvature $\frac{\partial w^2}{\partial r^2}(t)$. It should be noted that the radial strain of the specimen is referred to the bottom fiber (z=0) and not to the neutral axis or

plane of the bimaterial layer assembly ; this formulation was preferred because the location of the neutral axis or plane changes continuously - though not much - due to the varying material properties as a function of time throughout the thermal loading history.

Some mechanical and physical properties of polyvinyl acetate still need to be defined. From the glassy shear modulus μ_0 and a Poisson's ratio $\nu = 0.41$ [32], the bulk modulus, taken to be a constant, equals $K_0 = 8.28 \times 10^9$ N/m^2. This value of K_0 combined with the experimental rubbery shear modulus μ_∞ yields $\nu = 0.50$ in the rubbery limit. The properties of BK-7 glass included in these two sample calculations are [31] :

$$\alpha = 7.1 \times 10^{-6}/°C$$

$$E = 8.1 \times 10^9 \text{ N/m}^2$$

$$\nu = 0.208.$$

In both cases the temperature changes with a constant rate of $\pm$ 0.050 °C/min. Finally the thicknesses are $h_1 = 0.5$ mm for the polymer, $h_2 = 0.3$ mm for the glass substrate respectively.

3.2.1 Numerical Evaluation Procedure The solution of the system of equations (33) is carried out in several steps listed below :

1. First the relation between the real time t and the temperature reduced time scale t' is computed.

2. Subsequently the system of two equations (33) is solved in the t' domain. This computation involves determining the various material properties at the successive time steps at which the convolution integrals need to be evaluated.

3. The final step consists in solving a system of equations using Cramer's rule ; the solution in the real time domain t is then obtained through equations (17) and (34).

3.2.2 Heating Case The results pertinent to the heating case are shown in Figures 10,11 and 12. The relation between t and t' yields a monotonically increasing function resulting in an unambiguous one to one correspondence between the two time scales involved. Hence the solution of equations (33) can be readily reduced to real time, once it is known on the temperature reduced time scale t'. The solutions $\varepsilon_L(t)$ and $\frac{\partial^2 w}{\partial r^2}(t)$ exhibit a very similar qualitative behavior and can thus be discussed concurrently.

(1) At the onset of the heating at T = - 25 °C (T_g = 29 °C) the bimaterial specimen acts essentially like a sandwich with two elastic media. For purposes of comparison the elastic asymptotes, computed using equations (A2.2) and (A2.3), are also drawn in Figures 11 and 12 ; in these the polymer is characterized by its glassy properties.

(2) Approaching the glass transition region one first notices a slight increase in the strain and the curvature over the values predicted by the glassy elastic analysis ; this feature reflects the increase in the coefficient of thermal expansion of PVA_c before the material relaxation occurs.

(3) A few degrees (5 to 7) above the glass transition temperature (T_g = 29 °C) relaxation the polymer becomes the dominant phenomenon causing a sharp reversal in the slopes of both curves.

(4) Once the glass transition range has been crossed the specimen gradually starts acting again like a purely elastic bimaterial layer with the polymer now behaving in a rubberlike fashion. Eventually the solutions to converge to the elastic asymptotes calculated using the results outlined in Appendix 2. This correspondence is quite rapidly achieved for the axial strain $\varepsilon_L(t)$; for the curvature $\frac{\partial^2 w}{\partial r^2}(t)$ the convergence takes a little longer.

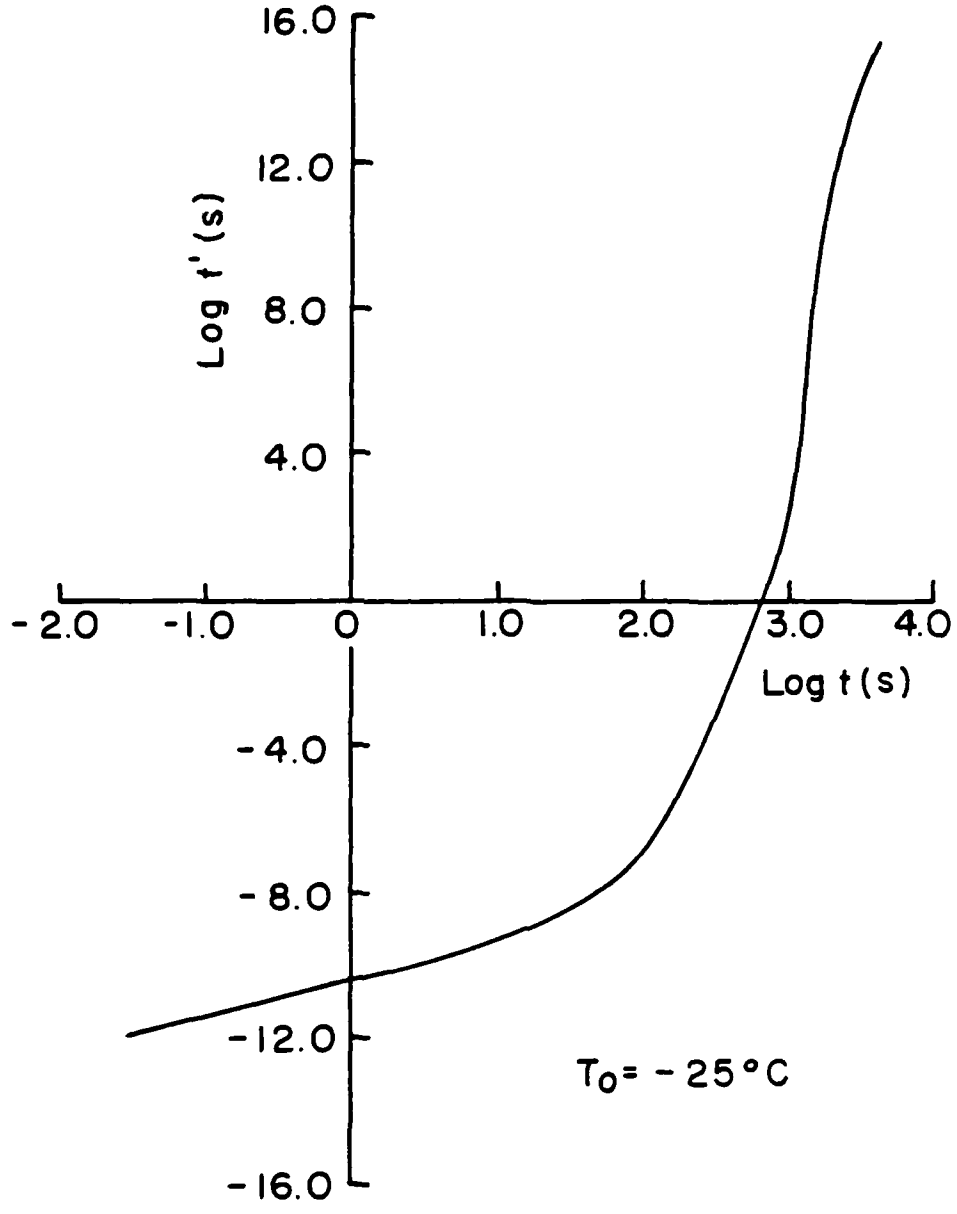

Figure 10. Relation between t and t' in the heating case.

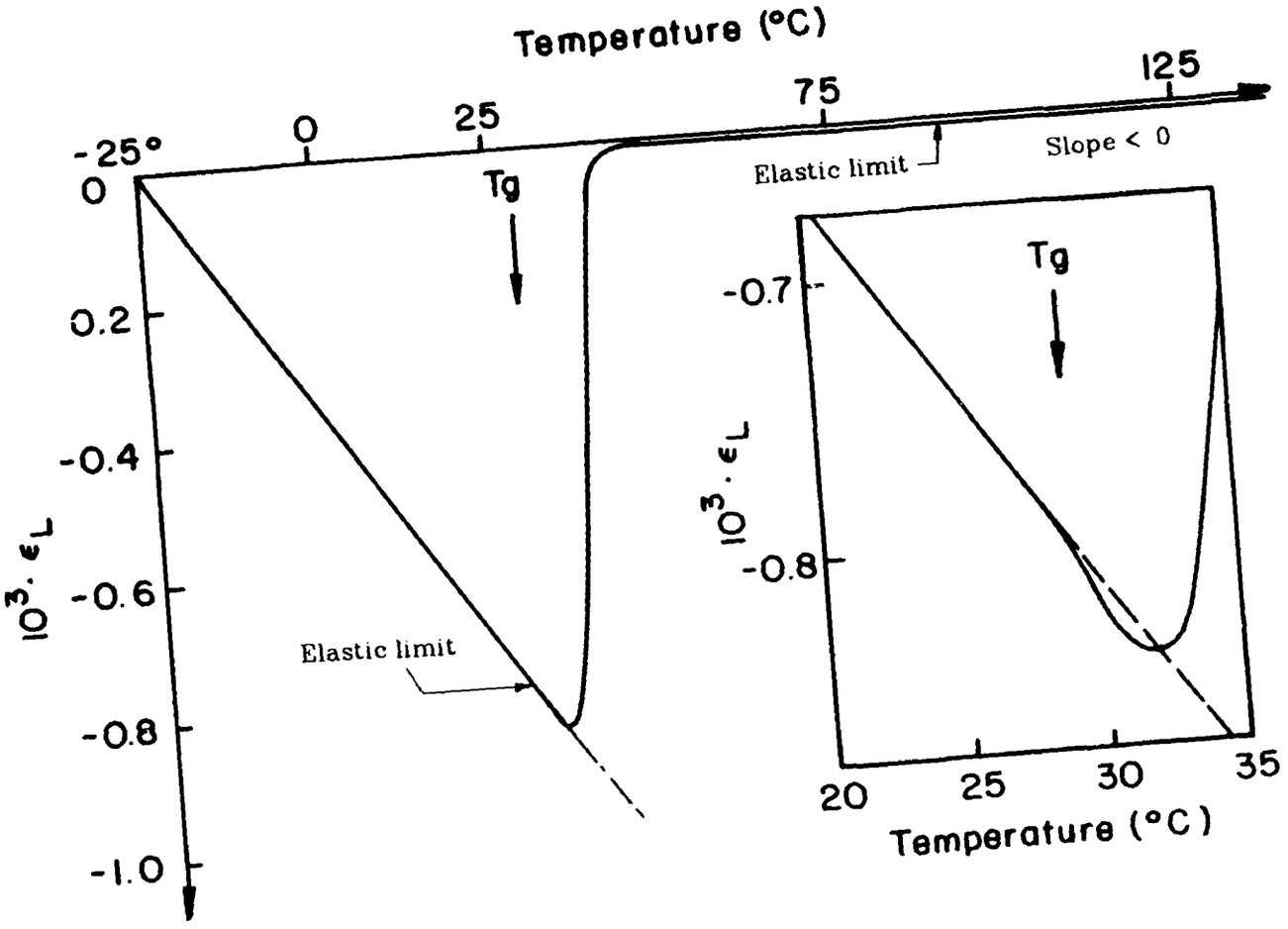

Figure 11. Axial strain ε_L of the bottom fiber as a function of time (heating).

ceeding through the glass transition region of PVA_c to higher temperatures
il the radius of curvature seems to reach a limit value, i.e. the fringe spacing
erved on the TV monitor appears to remain unchanging. Some examples of
uced experimental data are shown in Figures 20 and 22 which display the
ius of curvature R, calculated from the observed fringe patterns, as a func-
ı of time and temperature. The calculations leading to the displayed values
R are performed using a least square fit. Figures 21 and 23 display the
responding curvature 1/R. The initial values of R and 1/R are "negative" in
ord with our definition of the "sign" of the displayed curvature.

It should be pointed out at this time that the magnitude of R or 1/R in Figures 20 through 27 represent averaged "instantaneous" values for the ius of curvature or for the curvature at the corresponding time. One would ect that with continuously and slowly varying temperature the curvature inges also correspondingly slowly and continuously. Surprisingly this was not case, but in a certain temperature range the curvature would increase or crease steadily with a superposed cyclic excursion about the slowly changing an.

In each of the test runs corresponding to Figures 20 through 23, a nificant change in R or 1/R can be observed when the glass transition zone is ssed. The samples are eventually heated up to 65 °C or 58 °C respectively ; at se temperatures the recorded fringe pattern no longer seems to vary as a ction of the prescribed temperature history.

After the polymer relaxes at these high temperatures from 6.5 to 10 irs the samples are cooled down to room temperature conditions. It turns : that the radius of curvature does not drop its magnitude substantially with creasing temperature. When approaching the glass transition zone from

recorded with two Chromel-Alumel thermocouples. One of them is fixed in the chamber right above the sample ; the other one is embedded in a bimaterial specimen, made out of BK-7 glass and Solithane 113, and mounted right next to the glass - PVA_c specimen being tested. This procedure allowed monitoring the temperature in the chamber and in a specimen similar to the one being studied simultaneously ; the difference in reading between the two thermocouples averaged 1 °C ; consequently the output from the embedded thermocouple is taken as the indicator of the temperature in the neighborhood of the tested specimen unless specified otherwise. The moisture content inside the environmental chamber is measured by the wet bulb method. In addition, dry air is continuously pumped into the chamber to prevent moisture from building up.

4.3 Experimental Results

One series of experiments involves samples composed of a 0.25 mm (0.010") thick glass slide and a polymer layer about 0.50 mm (0.025") thick. The other specimens consist of a 0.50 mm (0.020") thick glass slide and a 0.35 mm (0.014") polymer coating.

At this point we need to specify the "sign" of the initial curvature of the specimen at the beginning of an experiment. We define a curvature to be "positive" if has its center on the positive z-axis as defined in Figure 9. It was verified experimentally that the pristine glass slides and the bimaterial specimens actually display a "negative" curvature at room temperature ; this observation explains the shape of the sample shown in Figure 18. The "sign" of curvature can be checked by considering the reflected parallel light beam coming off the surface under investigation. If we can locate a focal point, the specimen displays a "positive" curvature with respect to the incoming light beam.

Bimaterial specimens are heated starting from ambient conditions,

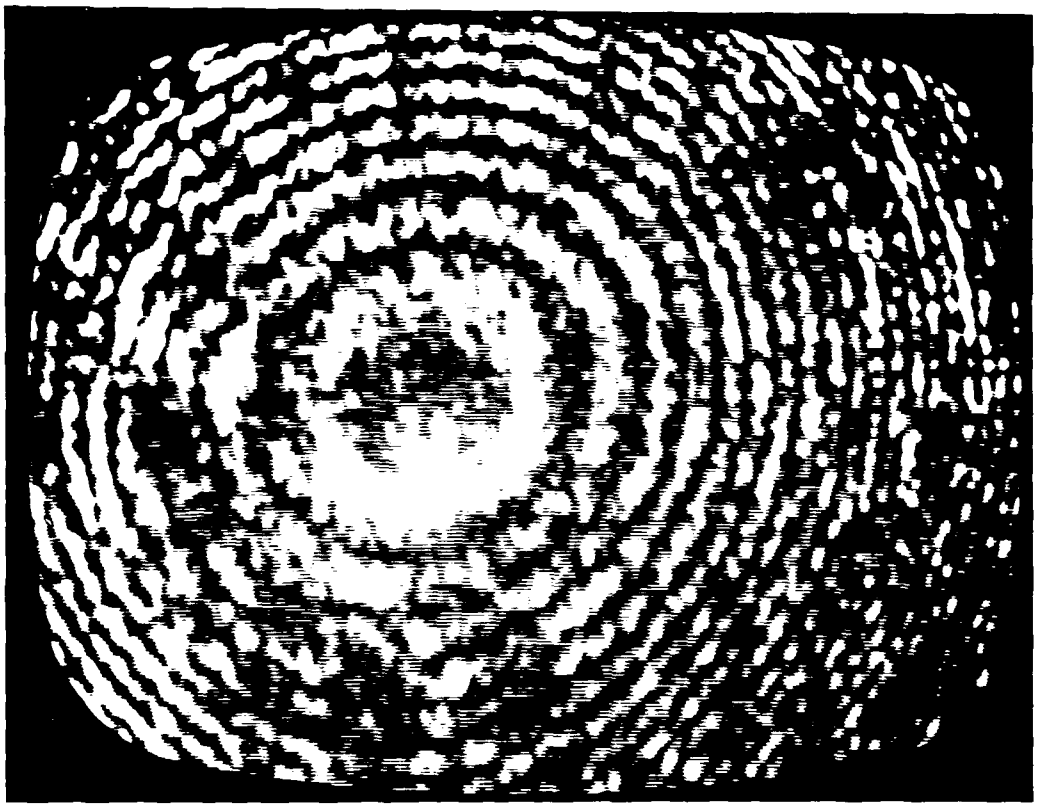

Figure 19. Circular interference fringes (Newton's rings).

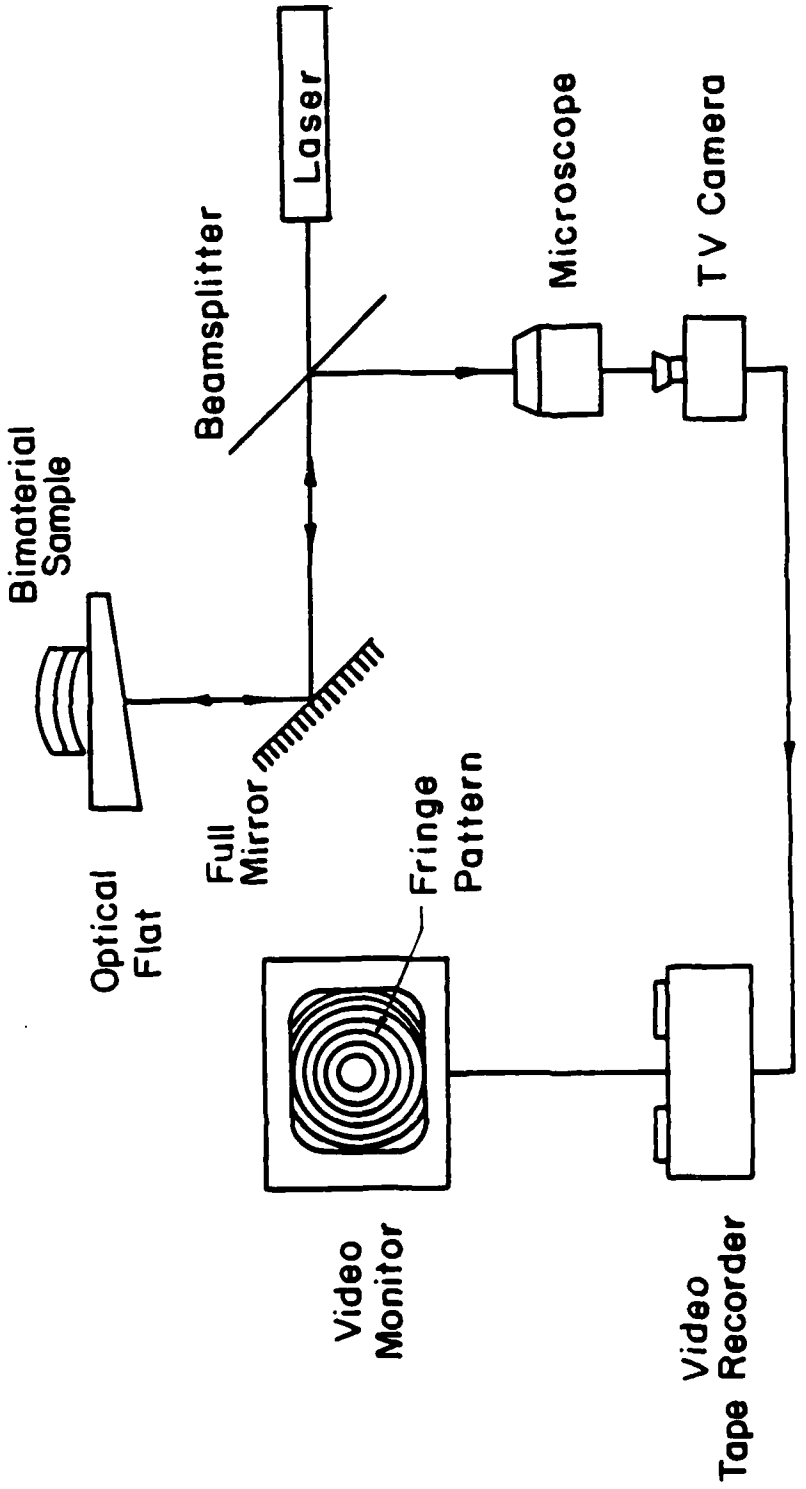

Figure 18. Measurement system for observing Newton's rings.

rings are then given by :

$$r = \sqrt{m \lambda R} \qquad m = 0,1,2,... \tag{38}$$

A remaining point of interest concerns the intensity of the central spot, corresponding to the point of contact between the convex surface and the reference plane. It is known that a relative phase change of π occurs under reflection at the air-to-glass surface [33] . If there were no such phase changes, the rays reflected from the two surfaces in contact should be in the same phase and produce a bright spot a the center. Hence when the contact is perfect, the central spot in the reflected light is black.

4.2.2 Experimental Setup A schematic of the experimental setup is shown in Figure 18. The curved bimaterial sample rests on an optically flat surface. This wedge shaped support is made out of BK-7 glass and has a wedge angle of 10° which feature prevents interference with reflections from the front surface of the wedge. The monochromatic light beam of a He-Ne laser (λ = 6328 Å) is directed towards the specimen through a beam-splitter, which also collects the resulting interference pattern from the reflected beam. The Newton's rings are observed through a Nikon Microscope SMZ-10 connected to a Hitachi CCTV Camera (Model HV-16SU) throughout the experiment. The recorded data can be viewed continuously on a Conrad TV Monitor while they are also stored on magnetic tape on a Sanyo Video Tape Recorder for later reference. An example of a recorded fringe pattern is shown in Figure 19.

The specimen and its support are enclosed in an environmental chamber, the temperature of which can be controlled to ± 0.5 °C. Nearly constant heating rates could be imposed fairly readily ; cooling to temperatures below ambient conditions in a steady fashion posed more difficulties due to problems in regulating the flow of nitrogen to the chamber. The temperature is

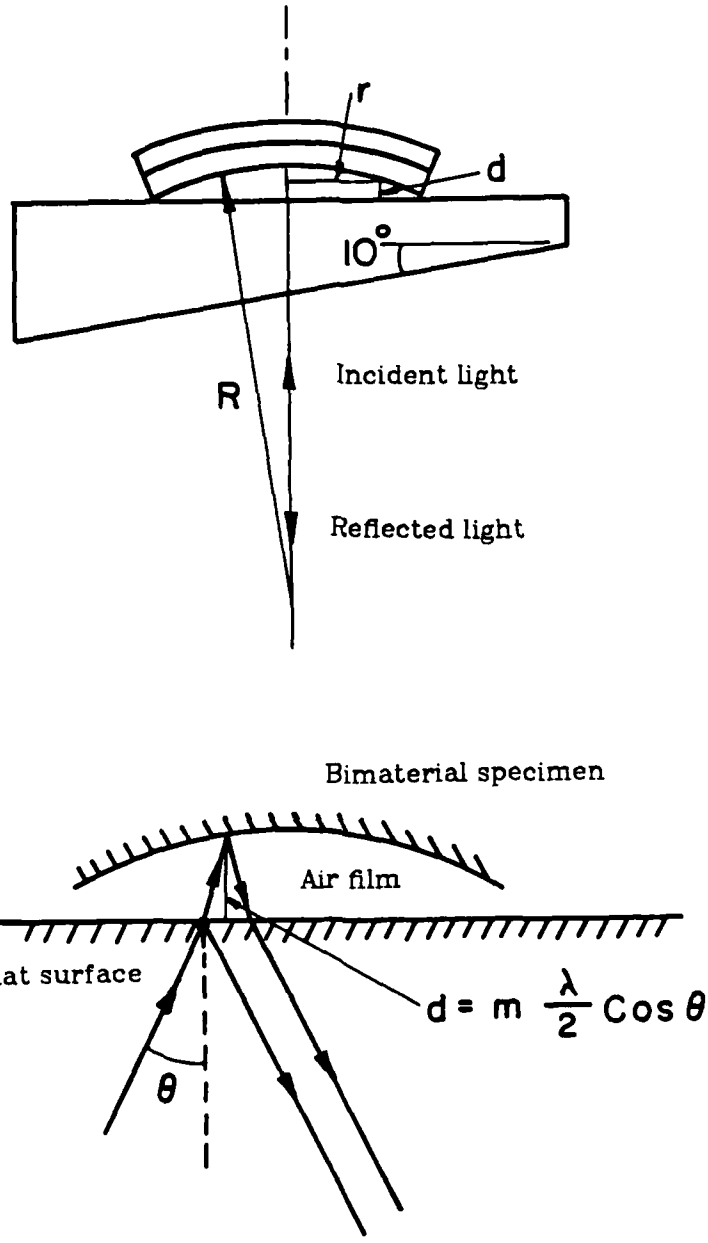

Figure 17. Interference method.

squeeze out any excess polymer material. After another 20 minutes the press is deactivated and the specimen is allowed to cool in its mold under ambient conditions for several hours.

Due to this cooldown residual thermal stresses are introduced in the bimaterial sample. Hence at room temperature the composite specimen displays a curvature. Apart from that the glass slides themselves display an initial curvature, which amplitude must be accounted for in the data reduction.

4.2 Experimental Method

4.2.1 Interference Method The optical method used to measure the out-of-plane displacement of the bimaterial specimen, is based on interference of light waves (Newton's rings). A schematic of the optical setup used in the interference method is shown in Figure 17. The reflected light contains a set of fringes, resulting from either constructive (bright fringes) or destructive (dark fringes) interference ; for the geometry shown in the schematic the condition for a minimum intensity is :

$$d = m \frac{\lambda}{2} \cos \vartheta \tag{36}$$

where m = 0,1,2,... denotes the order of the dark fringes ; λ and ϑ are the wavelength of the used light and the incident angle respectively. For normal incidence each consecutive dark fringe corresponds to a change in the out-of-plane displacement equal to half a wavelength of the incident light. At a given fringe of order m, counted from the center fringe, the air film thickness along that fringe is given by :

$$d = m \frac{\lambda}{2} \qquad m = 0,1,2,3,... \tag{37}$$

If the fringes are produced in the air film between a spherical surface and an optically flat surface, the resulting fringes will be circular. The radii of the dark

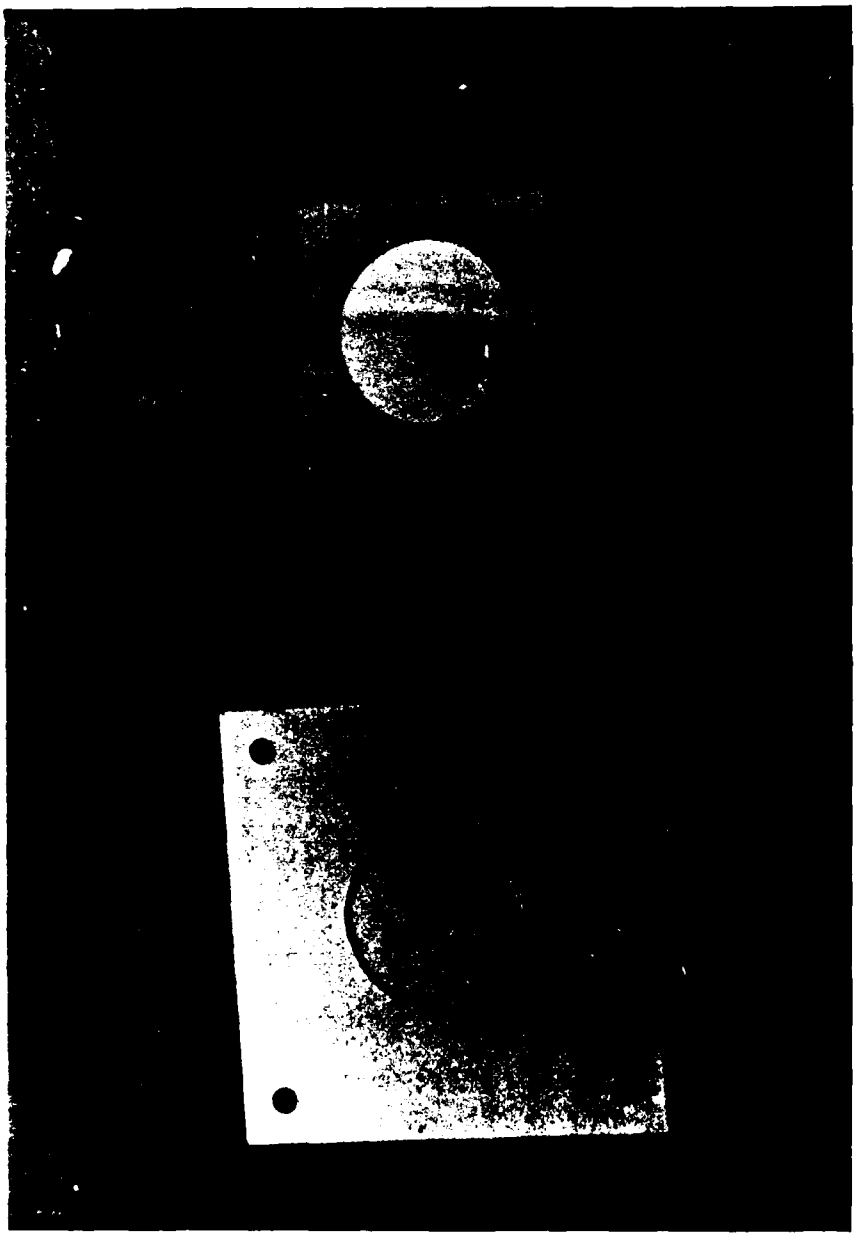

Figure 16. Bimaterial specimen and film deposition fixture.

4. EXPERIMENTAL EXAMINATION OF TIME DEPENDENT DEFORMATION

This last chapter of Part 1 concerns measurements related to the verification or examination of the viscoelastic stress analysis of the bimaterial specimen consisting of a glass slide and a PVA_c layer. Section 4.1. describes the preparation of the specimens. In Section 4.2 the experimental method is outlined ; in the subsequent sections the results are presented, as well as a comparison between the experimental data and the theoretical calculations of the previous chapter.

4.1 Test Materials and Specimen Preparation

In view of our desire to measure deformations optically it is preferable to work with glass adherends, although that is a not a necessary requirement. However, a clear adherend allows direct examination of the interface integrity. Circular slides of BK-7 glass were then used having a diameter of 25.4 mm (1.0") and are either 0.25 mm (0.010") or 0.50 mm (0 020") thick.

A bimaterial specimen and the polymer film deposition fixture are shown in Figure 16. In the latter the thickness of the film is controlled by metal spacers. In order to prevent the polymer from sticking to the spacers, the glass slides are enclosed by a Teflon ring of the same thickness as the spacers. In addition the top and bottom sides of the mold are sprayed with KRAXO 1711 Release Agent (Contour Chemical Company) to avoid potential adhesion problems when removing the specimen from the mold. The PVA_c[7] grains obtained as such from the manufacturer, are poured on to glass slide, before the top plate of the mold is secured. With the mold still not entirely closed, it is placed between the two plates of a hot press at about 150 °C. After heating for about 20 minutes, enough pressure is applied to close the film deposition fixture and to

7. The average weight molecular weight of polyvinyl acetate was indicated by the manufacturer (Polysciences Inc., Warrington, PA) to be 500.000.

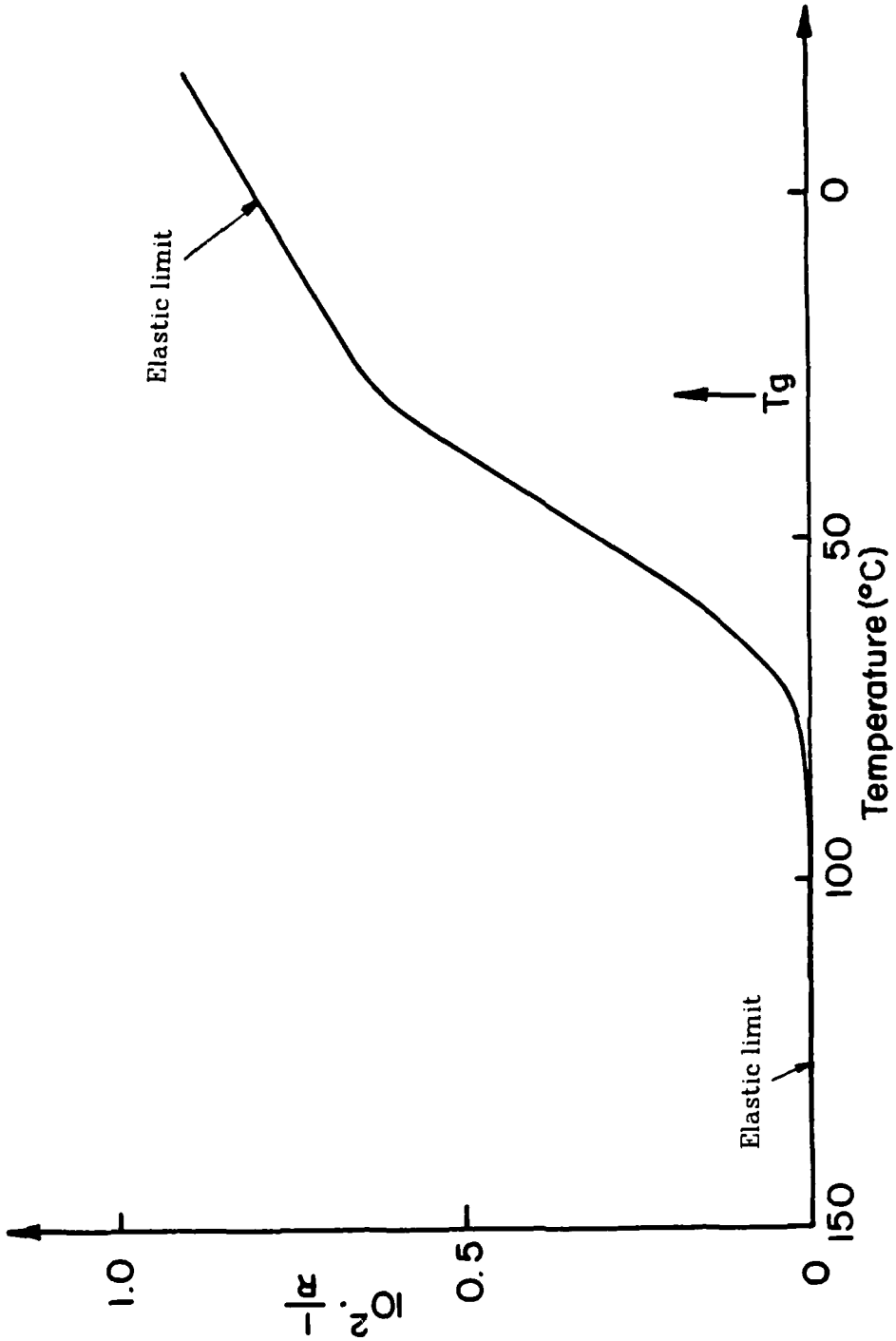

Figure 15. Curvature $1/R$ as a function of time (cooling).

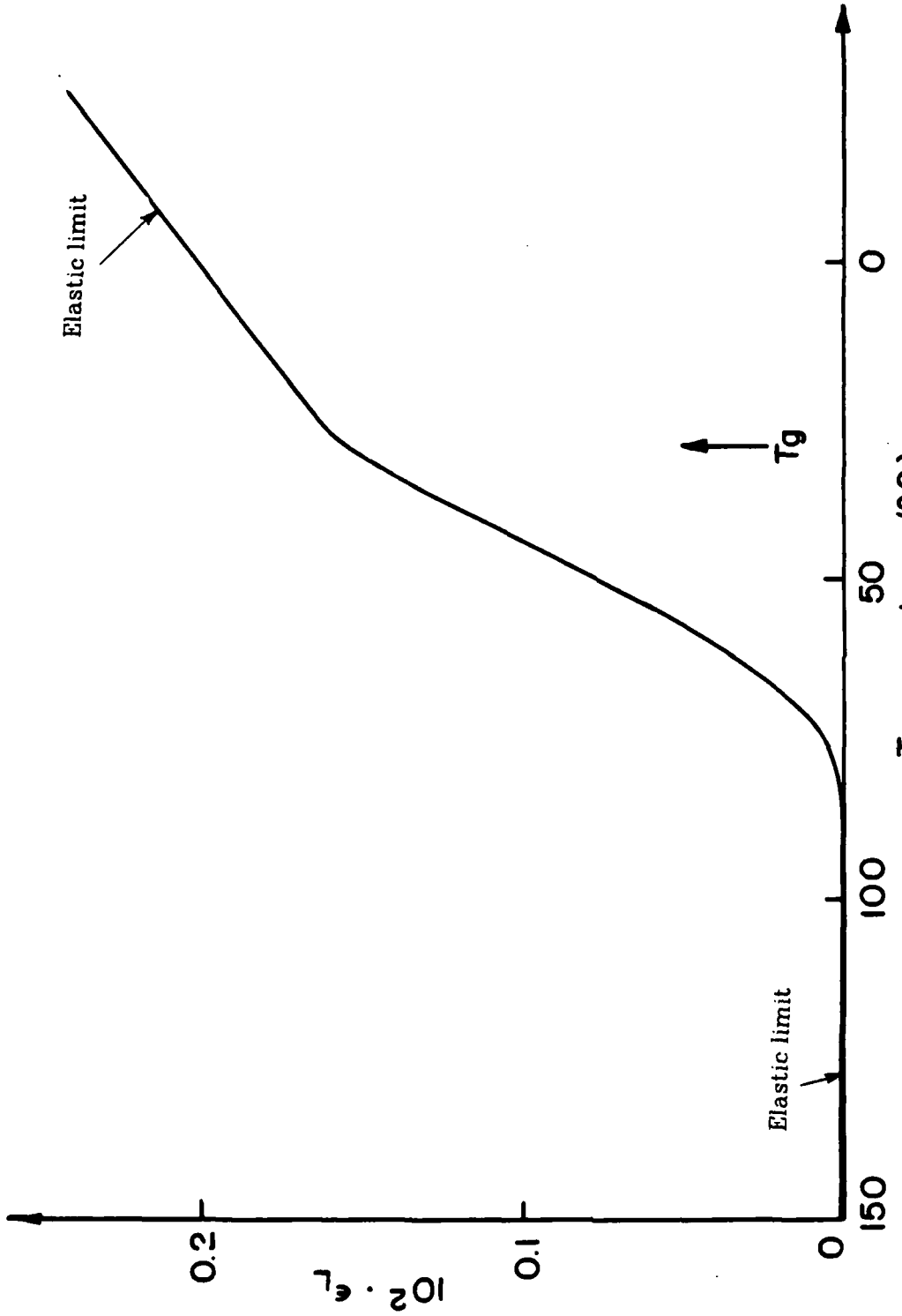

Figure 14. Axial strain ε_L of the bottom fiber as a function of time (cooling).

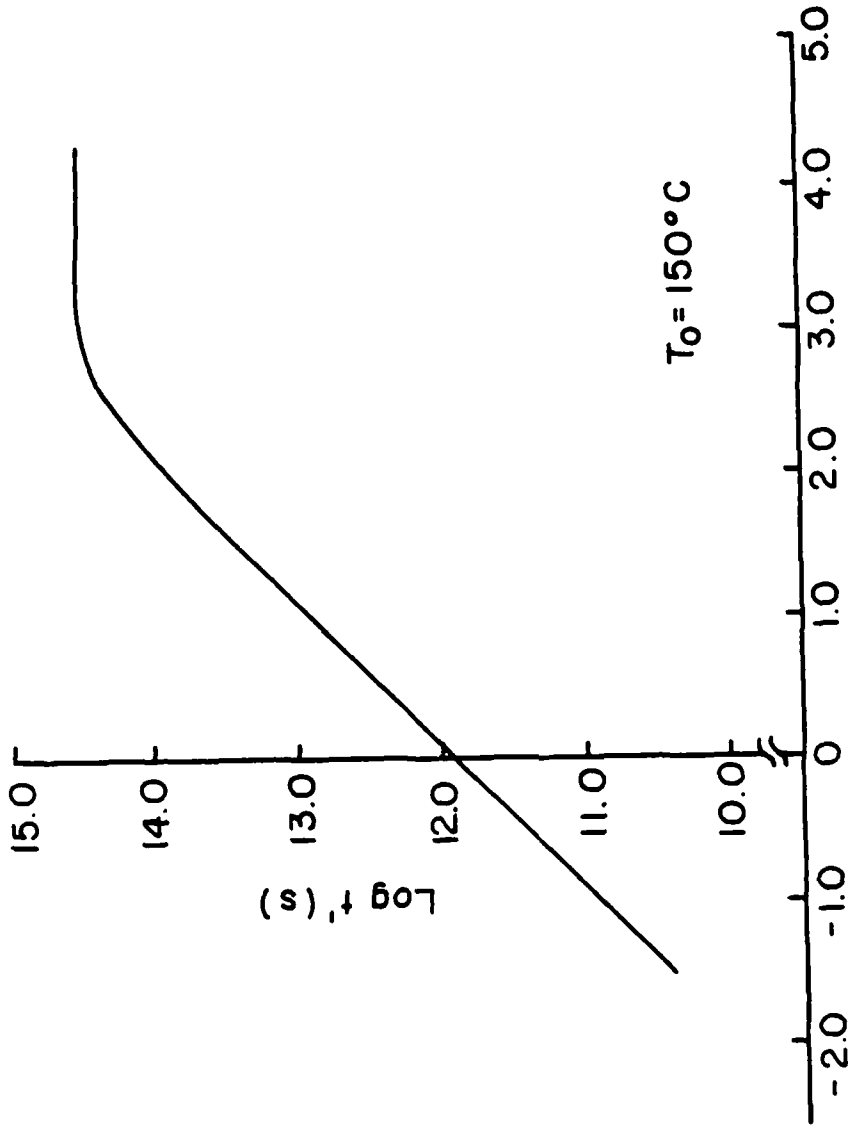

Figure 13. Relation between t and t' in the cooling case.

3.2.3 Cooling Case Figures 13,14 and 15 portray the results from the case of a cooldown from a temperature T = 150 °C towards the glassy region of the viscoelastic layer. The relation between the two different time scales t and t', indicated in Figure 13, shows a noticeable convergence to an almost constant value of t', corresponding to higher values of t and low temperatures. This particular behavior clearly exemplifies the "freezing-in" of the temperature reduced time t'. In order to ensure the one-to-one reciprocity between t and t', the calculation of expressions (17) has to be carried out in the double precision mode ; even then a rescaling of the values of t' close to the asymptotic limit of t' remains necessary in order to have a readily applicable correspondence between t and t' available. As in the previous example, the solutions $\varepsilon_L(t)$ and $\frac{\partial^2 w}{\partial r^2}(t)$ behave very similarly.

(1) During the initial cooling in the rubbery region, the bimaterial specimen acts like an elastic composite specimen ; the behavior matches the elastic asymptotes as indicated in Figures 14 and 15.

(2) Upon nearing the glass transition zone from above the freezing-in of the material properties starts far above T_g, in this case around 75 °C. This constitutes a rather surprising result, as it occurs about 45 °C above T_g for this particular cooling rate.

(3) After passing through the glass transition zone of PVA_c around 29 °C, the rate of increase in $\varepsilon_o(t)$ and $\frac{\partial^2 w}{\partial r^2}$ slows down to converge to the elastic limits, signaling glassy behavior of the polyvinyl acetate layer.

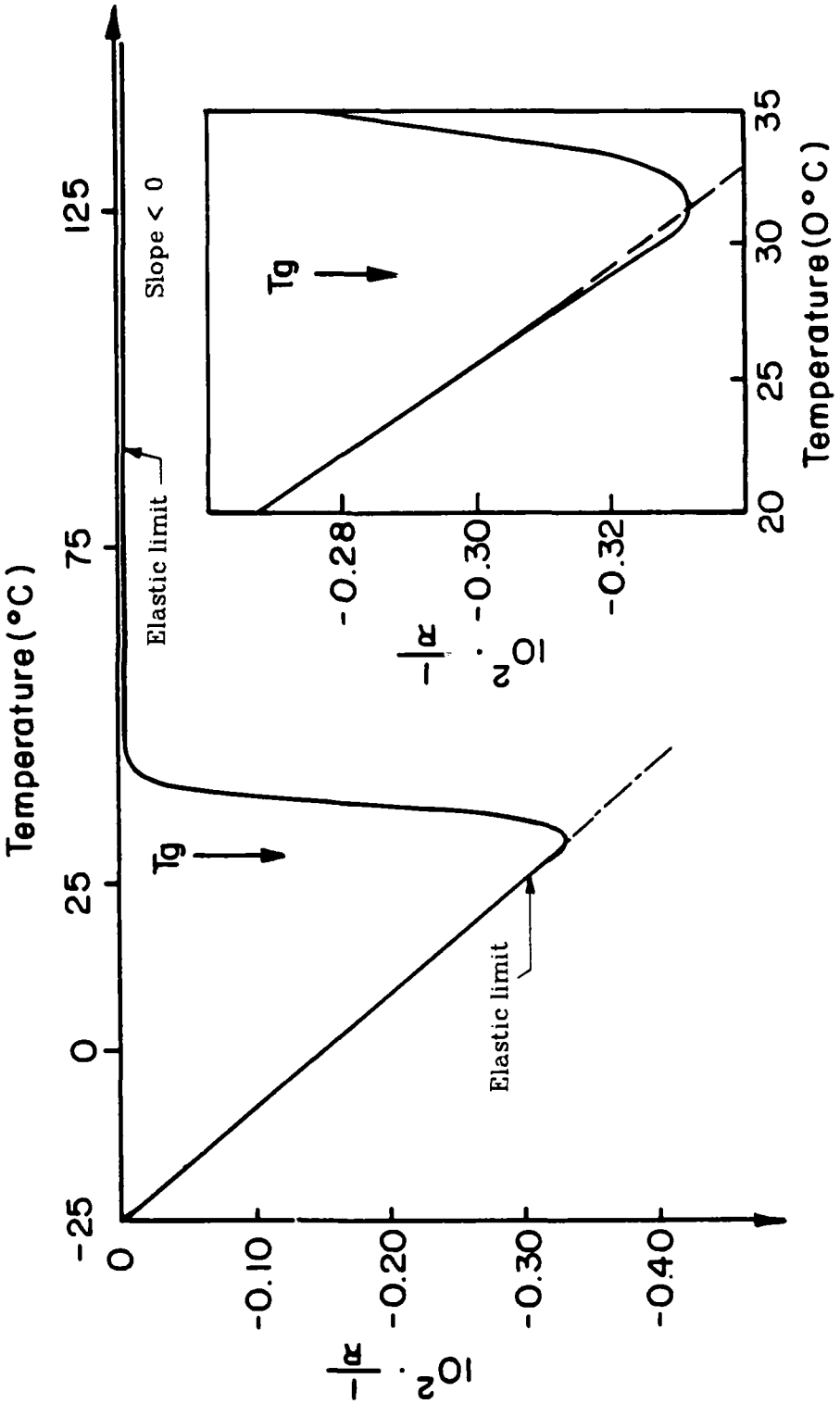

Figure 12. Curvature 1/R as a function of time (heating).

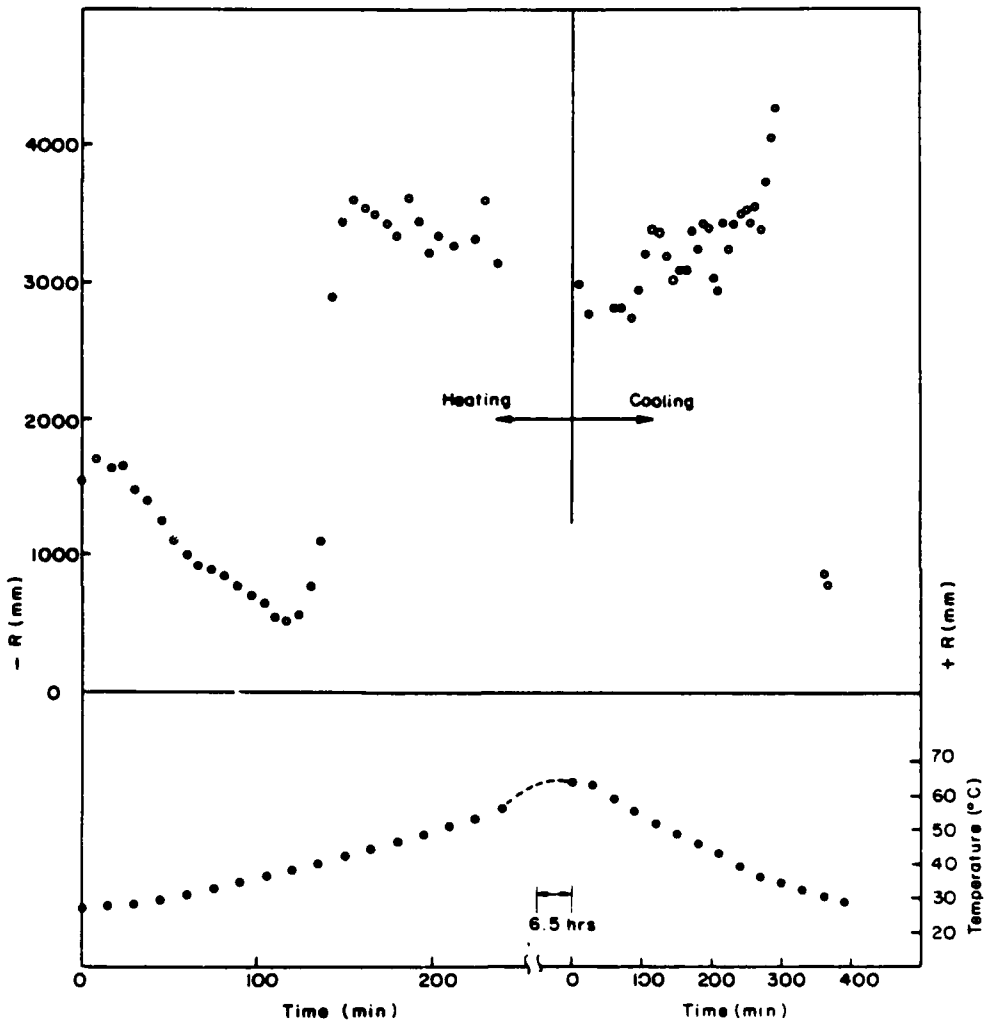

Figure 20. Radius of curvature of a bimaterial specimen as a function of time and temperature (thin glass slide).

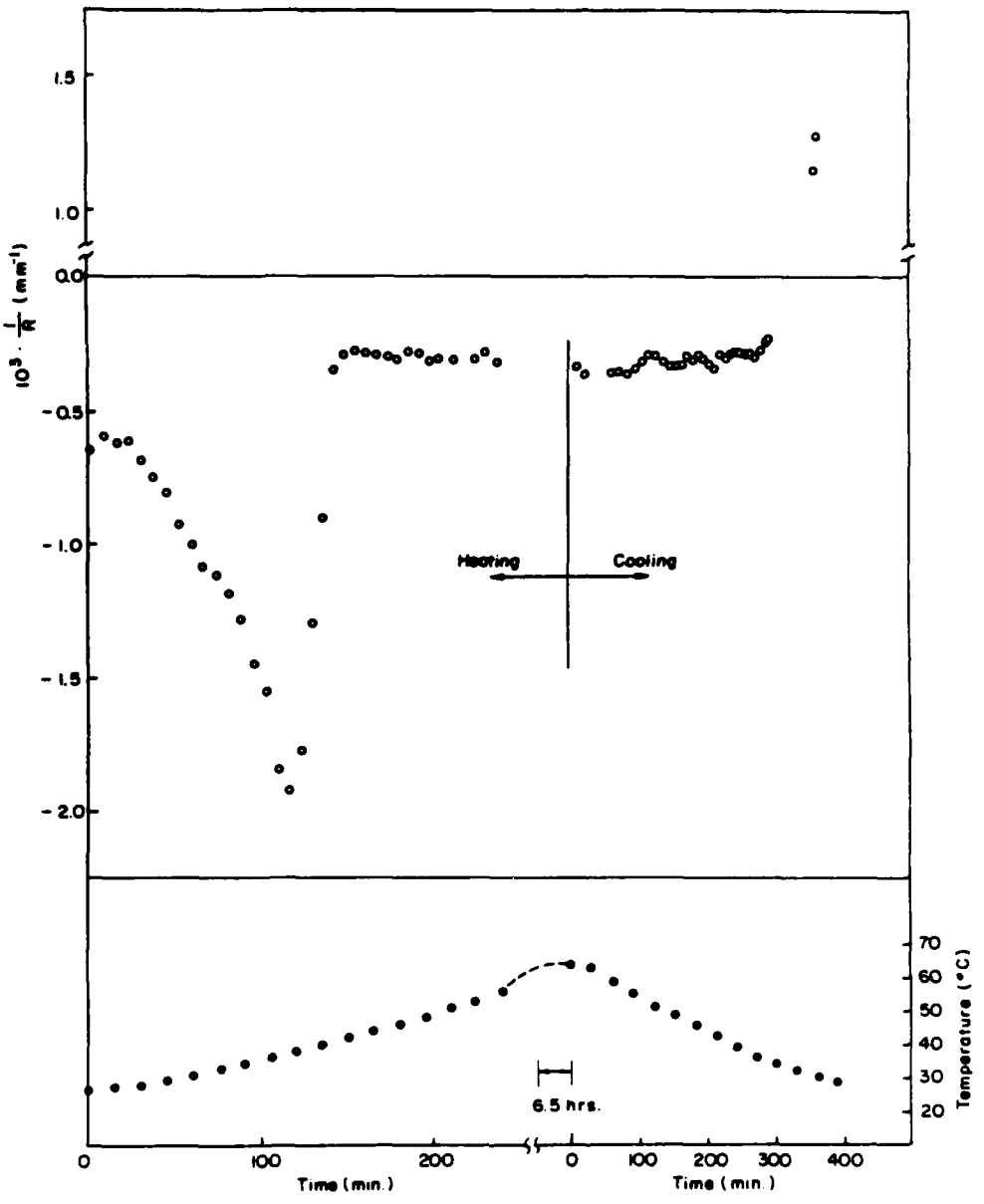

Figure 21. Curvature of a bimaterial specimen as a function of time and temperature (thin glass slide).

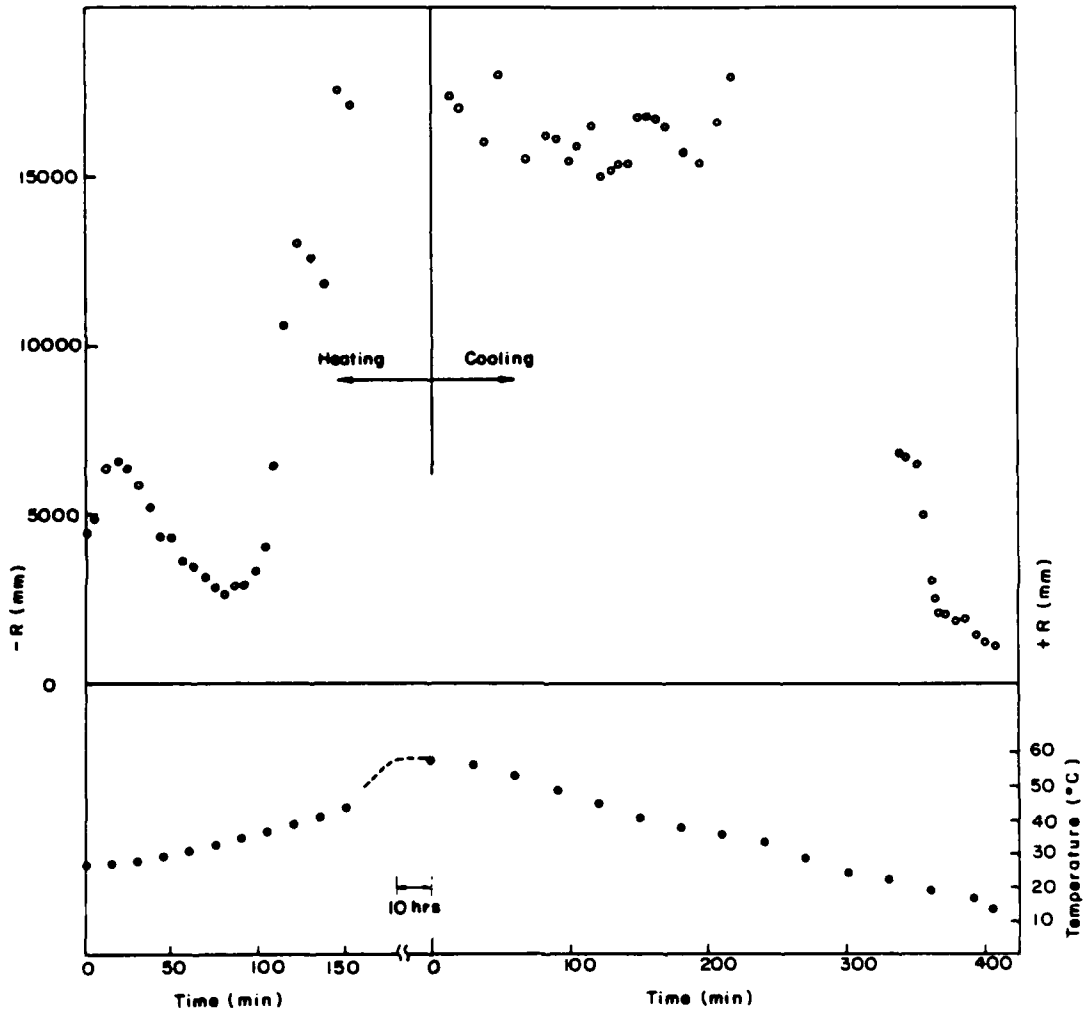

Figure 22. Radius of curvature of a bimaterial specimen as a function of time and temperature (thick glass slide).

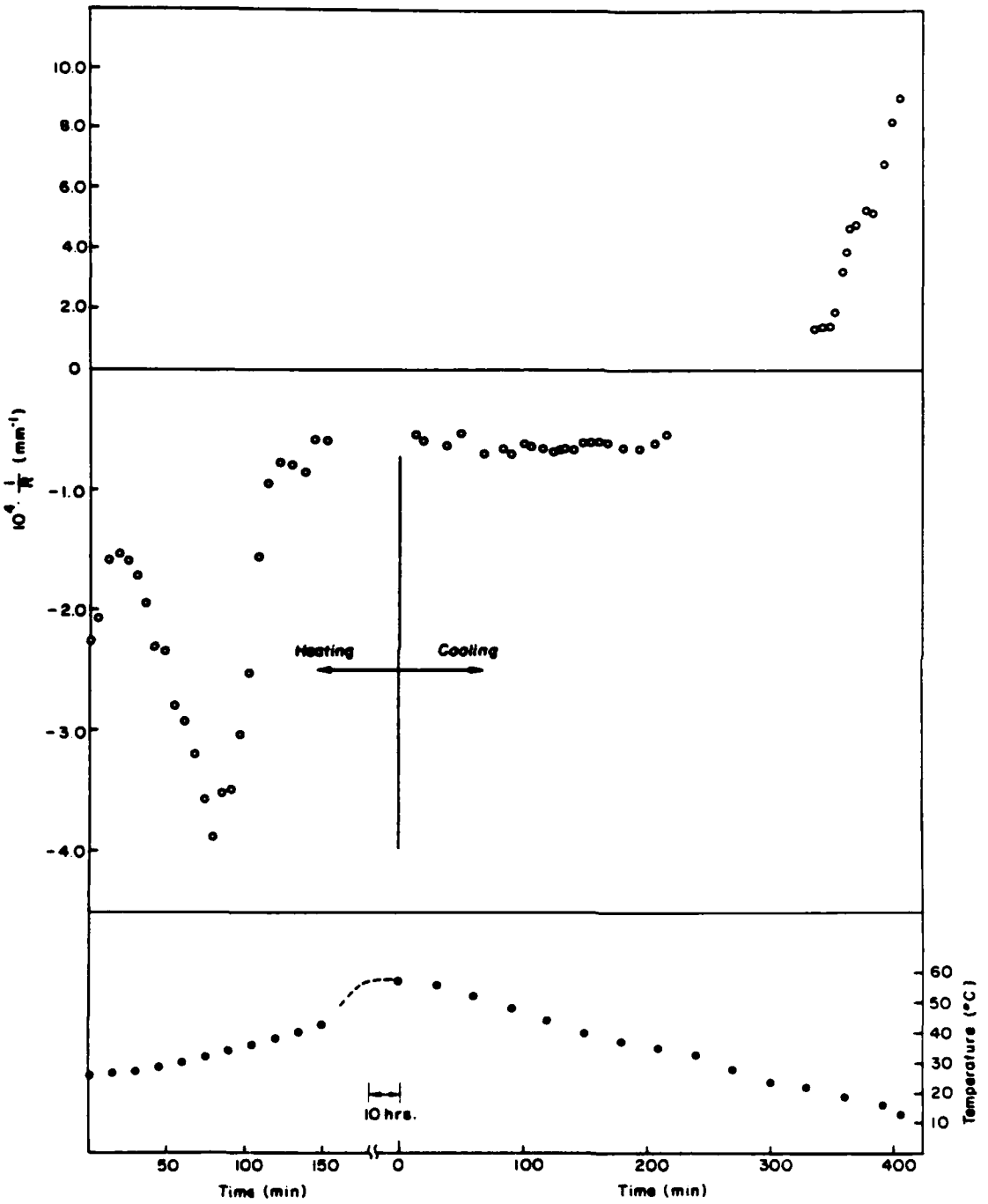

Figure 23. Curvature of a bimaterial specimen as a function of time and temperature (thick glass slide).

above a complicated fringe pattern appears which is definitely not axisymmetric.[8] The complicated, if not incoherent, fringe pattern which can be observed seems to transform into one commensurate with cylindrical bending. Several degrees below the glass transition temperature (T_g = 29 °C) the "regular" Newton's rings reappear.That fact is indicated by the data points on the far right of the time scale of Figures 20 through 23. In this temperature domain the "sign" of R and 1/R in Figures 20 through 23 is indicated as "positive". An explanation is presented in the analysis of the experimental results. It is worth stating that this "unstable" behavior of the sandwich around the glass transition domain during cooldown has been observed in every test run ; the "irregular fringe" pattern developed consistently and independently of the cooling rate imposed on the specimen.

4.4 Analysis of the Experimental Results

From the results of the first experiments involving the glass-PVA_c bimaterial specimens it became clear that it would be necessary to define a reference state to be used as a standard against which the induced strains could be compared through the measurement of the radius of curvature. The time dependent character of the material properties raises this question continuously ; this can be shown very easily by observing the change in curvature of a sample leaving the temperature unchanged. After four hours at room conditions (24 °C) the radius of curvature R was found to have nearly doubled its initial value, clearly demonstrating the relaxational behavior of the polymer. From these initial findings resulted the procedure followed during the measurements leading to the results shown in Figures 20 through 23. The plateau reached by R at about 30 °C above the glass transition temperature of PVA_c seems to meet the

8. The presence of this irregular fringe pattern is responsible for the lack of data points in the corresponding temperature domain of Figures 20 through 23.

requirements for the definition of a reference state. As mentioned previously any further increase in temperature does not appear to change R any more, thereby not varying the existing stress levels anymore. At these temperatures the material is approaching its viscous flow-region where additional stresses cannot build up any longer. Therefore it is postulated that this state represents a "stress free" reference state for the specimens, even though circular fringes can still be seen on the TV monitor. It was suspected that these remaining Newton's rings were caused mainly by the initial curvature of the glass slides. The validity of this assumption can be checked by measuring the curvature of the virgin glass slides ; for this purpose the polymer coating was removed from its substrate by submerging the samples in acetone in which polyvinyl acetate dissolves. The interference fringes generated in the air gap between the pristine glass slide and the optical flat accounted in part for the pattern observed at the higher temperatures, but also indicated that at the above mentioned reference state some residual curvature of the bimaterial specimen was still present. For the thin glass slides the residual curvature between our defined reference state and the curvature of the virgin glass slide equals 0.1×10^{-3}/mm. In the case of the thicker slides the amplitude of this residual curvature could not be determined because the experimental error is of the same order as this difference between the reference state and the curvature of a pristine glass slide.

We now proceed to make a comparison between the experimental results and the theoretical calculations outlined in Chapter 3 ; the heating and cooling thermal loading histories are analyzed separately. Because it is assumed that the theory only accounts for small deformations, linear superposition is applied in order to subtract the contribution of the reference state from the experimentally recorded fringe patterns. In accord with the nomenclature of Figure 17, the out-of-plane displacement d assuming spherical deflection is given

by :

$$d = R^2 - \sqrt{R^2 - r^2} \tag{39}$$

The thermally induced curvature to be compared with the theoretical results, is calculated from

$$\frac{1}{R_T} = \frac{2d_T}{r^2 + d_T^2} \tag{40}$$

where $d_T = d - d_o$,

in which d_T, d and d_o represent the thermally induced, experimentally recorded and reference out-of-plane displacement at a distance r from the point of contact between the sample and the reference plane respectively.

1. In Figures 24 through 27 experimentally obtained data for heating histories are plotted on a comparative basis with the theoretical curves, resulting from the viscoelastic stress analysis. The first two graphs refer to specimens with a thin glass slide. The main difference between theory and experiment lies in the maximum amplitude of the change in curvature ; in the four cases presented here the specimens undergo a maximum change in curvature with respect to their reference state ranging from 60% to 95% of the theoretically predicted value. In Figure 27 the influence of the value of the bulk modulus K_o is also included ; two theoretical curves corresponding to the indicated values of K_o are drawn. A 30% reduction in the amplitude of K_o does not constitute a sizeable difference and supports our assumption of a constant bulk modulus K_o.

Some characteristics common to the four cases are worth mentioning. In every case test data indicate that the specimen relaxes initially, indicated by a decline in the value of the curvature at an almost constant or very slowly increasing temperature. This phenomenon had been observed earlier when observing the relaxation of a specimen at constant temperature. Therefore the

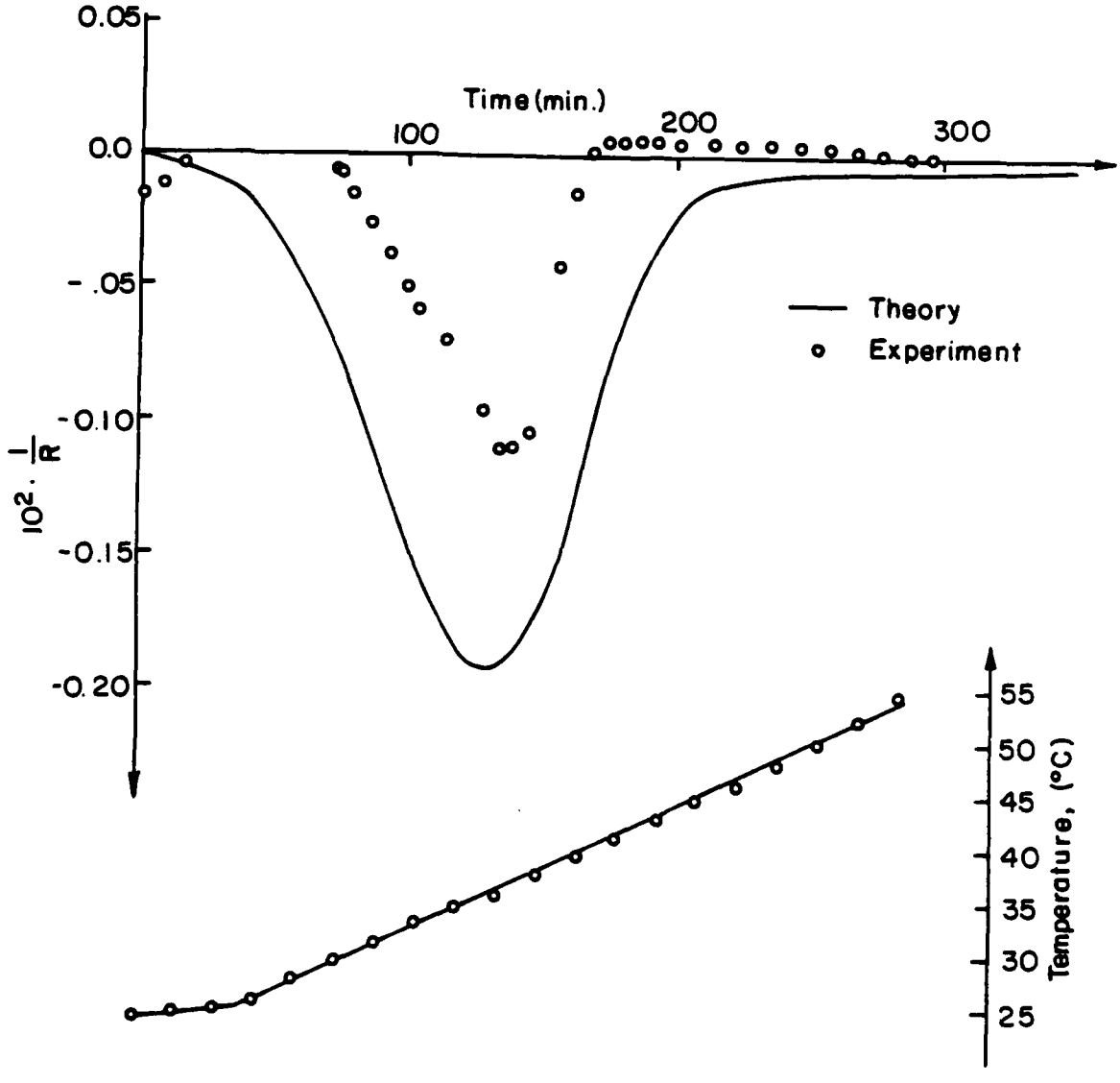

Figure 24. Change in curvature of a bimaterial specimen as a function of temperature (thin glass slide).

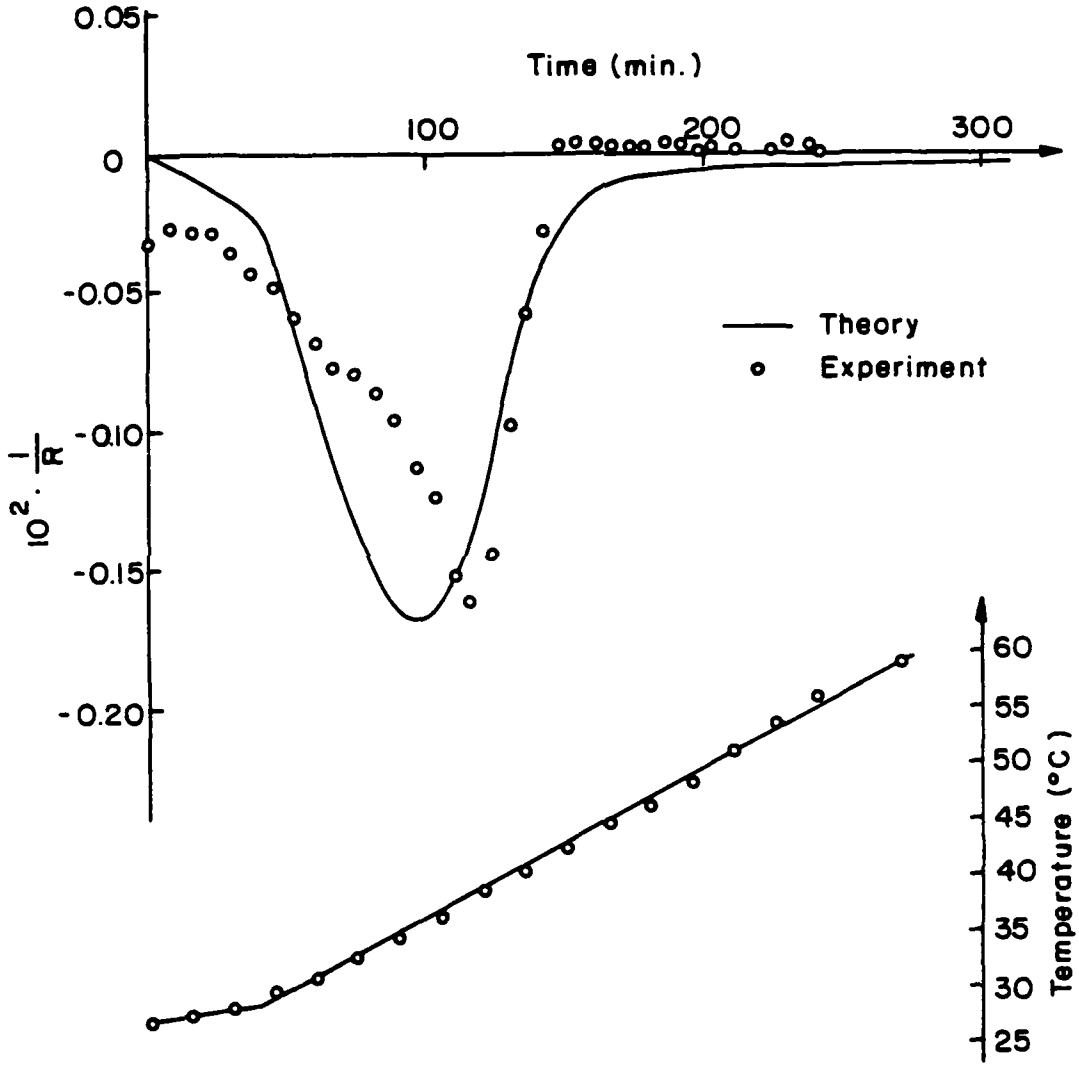

Figure 25. Change in curvature of a bimaterial specimen as a function of temperature (thin glass slide).

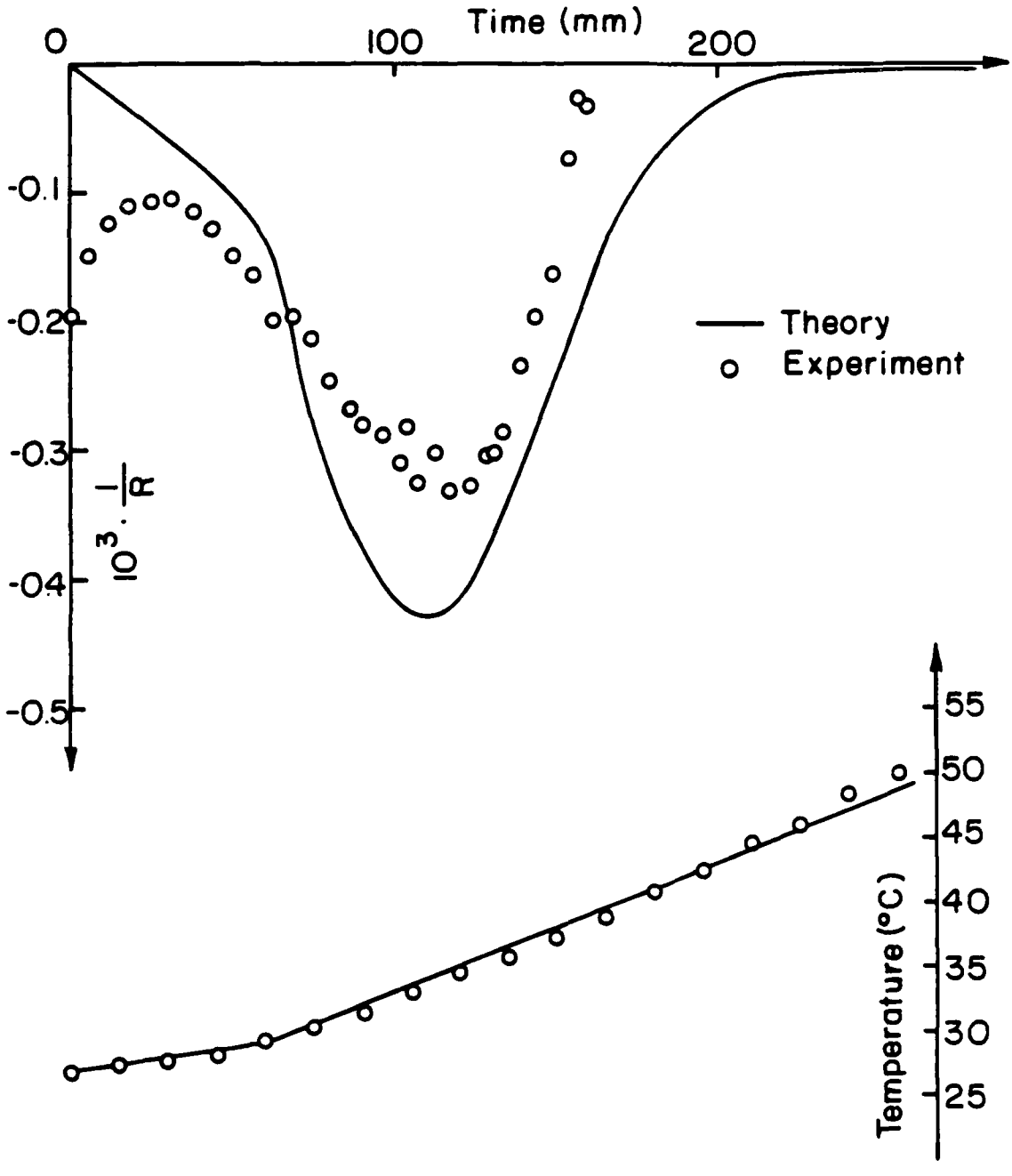

Figure 26. Change in curvature of a bimaterial specimen as a function of temperature (thick glass slide).

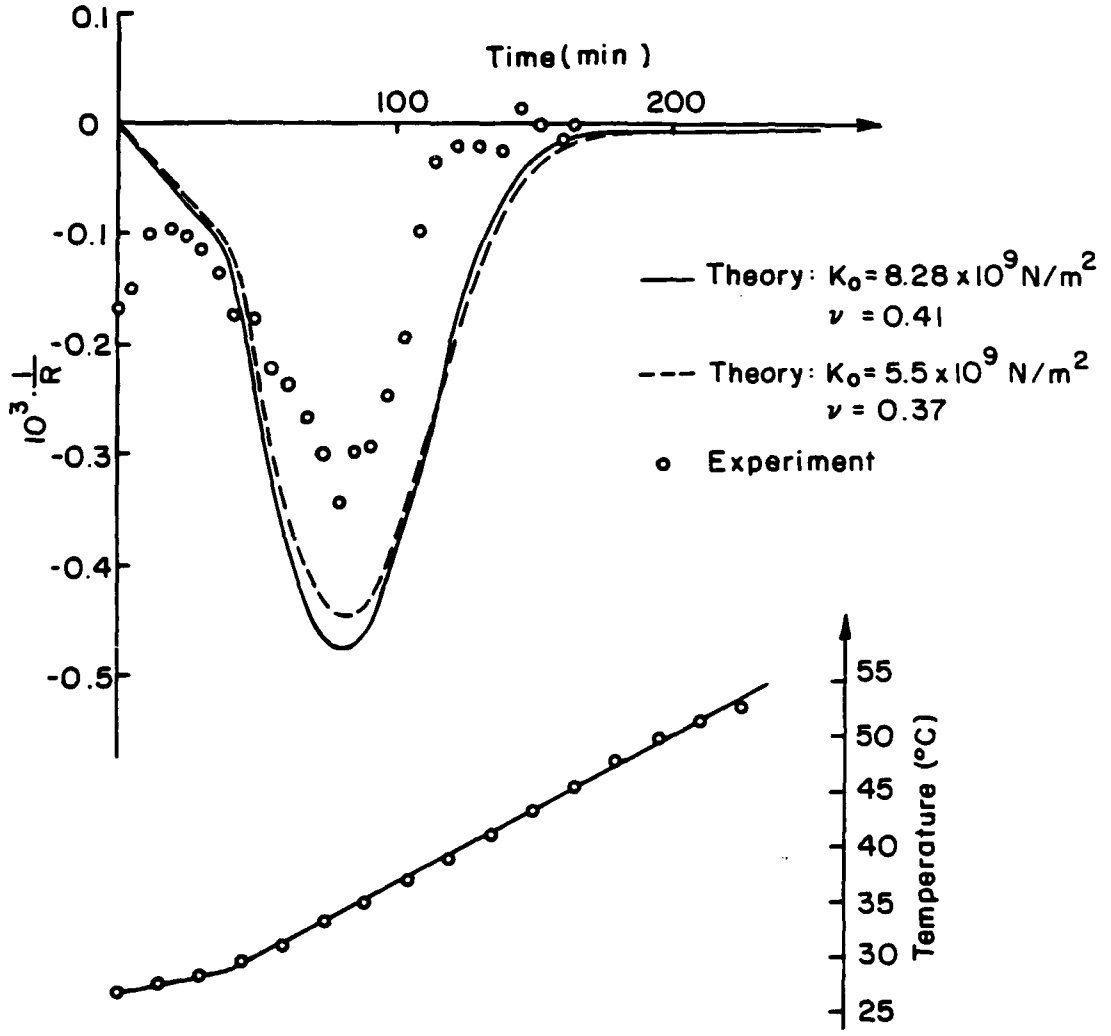

Figure 27. Change in curvature of a bimaterial specimen as a function of temperature (thick glass slide).

temperature profile used in the theoretical calculations has been approximated by a piece wise linear graph as indicated in Figures 24 through 27. In most of the cases the experimental data points lag behind the corresponding theoretical values, although the peak value is concurrently reached somewhere between 35 ° and 37 °C. The relaxation occurs somewhat faster than the theory predicts. This is a significant result of this investigation as it appears that full relaxation of the PVA_c does not start until about 7 °C after the glass transition has been passed.

It will be noted that some data points indicate apparent negative values of 1/R. This "behavior" results from taking a reference state equal to the one attained during the long time relaxation at the higher temperature. As can be seen in Figures 20 and 22, the radius of curvature corresponding to this reference state is smaller in absolute value than the ones reached immediately after pronounced relaxation occurs. This phenomenon is more pronounced in the specimens containing the thinner glass slide.

Two more assumptions made in the theoretical calculations need to be discussed. They involve the time dependence of the thermal coefficient of expansion as well as the uniformity of the temperature of the specimen. In our analysis no time dependence of the expansion coefficient is assumed. If one were to introduce some rate dependence of the thermal coefficient of expansion α in the analysis, the resulting effect would be a shift of the theoretical curves in Figures 24 through 27 parallel to the (horizontal) time or temperature axis. This time dependence of α could account for some of the discrepancies between theory and experiment, but its influence cannot be clearly identified from our measurements. We need to point out the measurements were performed at a heating rate similar to the one used in the determination of the thermal expansion characteristics of PVA_c reported on earlier in Chapter 2.

Concerning the uniformity of the temperature throughout a bimaterial specimen, we need to mention that the size of the specimen is chosen such that the bimaterial sample can respond "instantaneously" to temperature changes. It turns out however that the specimens are extremely sensitive to small temperature variations, which behavior results in the previously mentioned oscillatory behavior of the interference fringes in a certain temperature range. Nevertheless if the temperature is kept constant, the fringe motion ceases as was experimentally verified.

2. As indicated earlier in this chapter the cooling of the specimens from temperatures well above the glass transition temperature to ambient conditions resulted in unresolved experimental problems, namely the appearance of a complicated, non-circular fringe pattern. The repeatability of this phenomenon leads us to believe that some kind of instability develops when cooling through the glass transition range of polyvinyl acetate. It is believed that the bimaterial samples switch the "sign" of their curvature when cooled through the glass transition region. This phenomenon was also observed experimentally when heating bimaterial samples from temperatures well below ambient conditions (0 °C) to the glass transition temperature range.

'ENDIX 1

SION OF LINEARLY VISCOELASTIC MATERIAL SPECIMENS WITH CIRCULAR CROSS-

:TIONS

The relation between the creep compliance J(t) and the experimentally asured twist angle $\vartheta(t)$ as a function of time is derived for a linearly viscoe- tic material. The sample possesses a circular cross-section ; the geometry is)wn in Figure A1 :

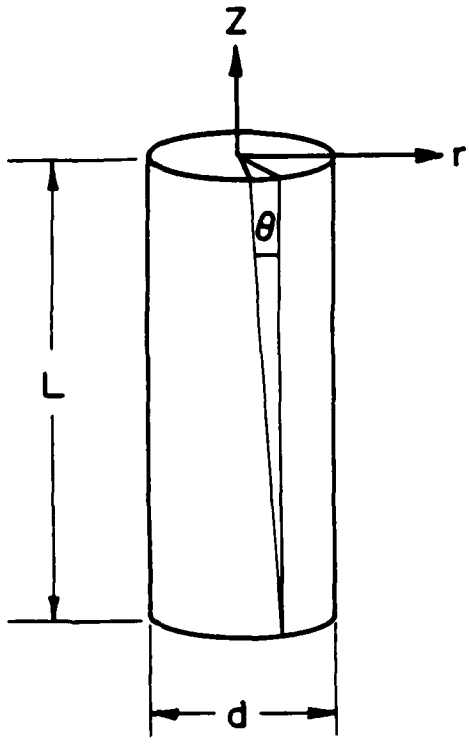

Figure A1. Torsion specimen

)m kinematic considerations the shear strain is given by,

$$2\,\varepsilon_{z\vartheta}(t) = \frac{r}{L}\vartheta(t) \qquad (A1.1)$$

l the corresponding shear stress is :

AD-A152 064 A STUDY OF THE TIME DEPENDENCE IN FRACTURE PROCESSES RELATING TO SERVICE..(U) CALIFORNIA INST OF TECH PASADENA GRADUATE AERONAUTICAL LABS W G KNAUSS

UNCLASSIFIED 30 JUN 84 GALCIT-SM-84-10 AFOSR-TR-85-0239 F/G 11/4 NL

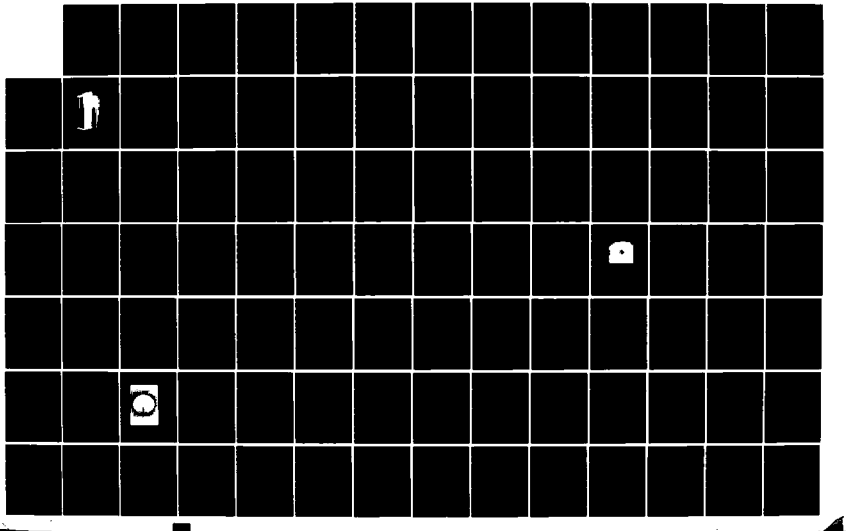

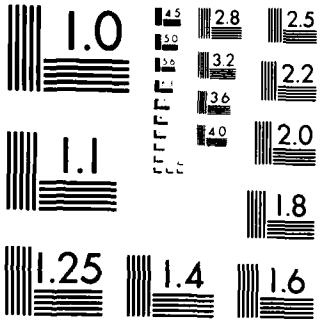

$$\tau_{z\vartheta}(t) = 2\mu * d\varepsilon_{z\vartheta} = \mu * d\left(\frac{r}{L}\vartheta\right) \dagger \tag{A1.2}$$

From statics the twisting moment M can be computed by :

$$M(t) = 2\pi \int_0^{d/2} \tau_{z\vartheta} r^2 \, dr = \frac{\pi}{32} d^4 \mu * d\left(\frac{\vartheta(t)}{L}\right) \tag{A1.3}$$

so that from equation (A1.3) the twist angle can be calculated as :

$$\vartheta(t) = \frac{32L}{\pi d^4} J(t) * dM(t). \tag{A1.4}$$

If the moment M(t) is applied in a step load fashion, such that

$$M(t) = M_o h(t) \tag{A1.5}$$

we can write:

$$\begin{aligned} J(t) * dM(t) &= \int_{-\infty}^{t} J(t-\xi)\, dM(\xi) \\ &= \int_{-\infty}^{t} J(t-\xi) d(M_o h(\xi)) \\ &= M_o J(t). \end{aligned} \tag{A1.6}$$

Combining equations (A1.4) and (A1.5) the creep compliance is then given by

$$J(t) = \frac{\pi d^4 \vartheta(t)}{32 L M_o} \tag{A1.7}$$

which yields equation (1). It is worth pointing out that this formula has exactly the same form as the one used for torsion of elastic specimens with circular cross-sections.

---

† The *star notation* (*) refers to Stieltjes convolution ; equation (A1.2) should read in full as follows

$$\tau(t) = \int_{-\infty}^{t} \mu(t-\xi)\, d\left(\frac{r}{L}\vartheta(\xi)\right).$$

APPENDIX 2

STRESS ANALYSIS CHECK FOR A BIMATERIAL INVOLVING ELASTIC MEDIA ONLY

If both materials forming the bimaterial specimen under consideration are elastic solids, the system consisting of equations (33), can be solved explicitly in terms of the material and geometric parameters.

The stress in either material is given by,

$$\sigma_{r_i}(z,t) = \frac{E_i}{1-\nu_i}\left[\varepsilon_o(t) - z\frac{\partial^2 w}{\partial r^2}(t) - \alpha_i(T(t))\,\vartheta(t)\right] \qquad \text{(A2.1)}$$

where i = 1,2 refers to the range either one of the materials. Substitution of (A2.1) into the equilibrium equations and integrating over the thickness of the specimen, yields a system of two equations and two unknowns, $\varepsilon_o(t)$ and $\frac{\partial^2 w}{\partial r^2}(t)$, which can be solved analytically. The solution of this system is :

$$\frac{\partial^2 w}{\partial r^2}(t) = -\frac{3\Phi_1\Phi_2 h_1 h_2}{\Delta}[T(t) - T_o]\,[\alpha_1(T(t)) - \alpha_2(T(t))]\,(h_1 + h_2) \qquad \text{(A2.2)}$$

$$\varepsilon_o(t) = \frac{[T(t) - T_o]}{\Delta}\left\{\left[\Phi_1^2\alpha_1(T(t))\,h_1^4 + \Phi_2^2\,\alpha_2(T(t))\,h_2^4\right]\right. \qquad \text{(A2.3)}$$

$$-\Phi_1\Phi_2\left[3h_2^2(h_1^2 + 2h_1h_2)(\alpha_1(T(t)) - \alpha_2(T(t)))\right.$$

$$\left.\left. - 4h_1h_2(\alpha_1(T(t))\,h_2^2 + \alpha_2(T(t))h_1^2)\right]\right\}$$

where

$$\Delta = \Phi_1^2h_1^4 + \Phi_2^2h_2^4 + 4\Phi_1\Phi_2h_1h_2(h_1^2 + h_2^2) + 6h_1^2h_2^2\Phi_1\Phi_2$$

$$\Phi_i = \frac{E_i}{1-\nu_i}.$$

REFERENCES

1. M.L. Williams, R.F. Landel and J.D. Ferry, The Temperature Dependence of Relaxation Mechanisms in Amorphous Polymers and Other Glass-forming Liquids, J. Am. Chem. Soc., 77 (1955) pp. 3701-3707.

2. W.G. Knauss and V.H. Kenner, On the Hygrothermomechanical Characterization of Polyvinyl Acetate, J. Appl. Phys., 51 (1980) pp. 5131-5136.

3. S. Timoshenko, Analysis of Bimetal Thermostats, J. Optical Soc. Am., 11 (1925) pp. 233-255.

4. M. Goland and E. Reissner, The Stresses in Cemented Joints, J. Appl. Mech., 11 (1944) pp. A17-A27.

5. A.J. Kinloch, The science of adhesion, Part 2 Mechanics and mechanisms of failure, J. Mater. Sci. 17 (1982) pp. 617-651.

6. A.J. Kinloch, The science of adhesion, Part 1 Surface and interfacial aspects, J. Mater. Sci., 15 (1980) pp. 2141-2166.

7. A.J. Durelli, V.J. Parks and C.J. del Rio, Stresses in Square Slabs, with Different Edge Geometries, when Bonded on one Face to a Rigid Plate and Shrunk, Experim. Mech., 7 (1967) pp. 481-484.

8. A.J. Durelli, V.J. Parks and C.J. del Rio, Stresses in a Square Slab Bonded on One Face to a Rigid Plate and Shrunk, Acta Mech. III (1967) pp. 352-359.

9. V.J. Parks, F.P. Chiang and A.J. Durelli, Maximum Stress at the Angular Corners of Long Strips Bonded on One Scale and Shrunk, Experim. Mech., 8 (1968) pp. 278-281.

10. D.R. Mulville and R.N. Vaishnav, Interfacial Crack Propagation, J. Adhesion, 7 (1975) pp. 215-233

11. Y. Weitsman, Residual Thermal Stresses Due to Cool-Down of Epoxy-Resin Composites, J. App. Mech., 46 (1979) pp. 563-567.

12. Y. Weitsman, Stresses in Adhesive Joints Due to Moisture and Temperature, J. Comp. Mat., 11 (1977) pp. 378-394.

13. Y. Weitsman, Interfacial Stresses in Viscoelastic Adhesive Layers due to Moisture Sorption, Int. J. Solids Structures, 15 (1979) pp. 701-703.

14. S.G. Abbott and N. Bumpton, The Effect of Moisture on Polyurethane Adhesives, J. Adhesion, 13 (1981) pp. 41-51.

15. J.P. Sargent and K.H. Ashbee, High Resolution Optical Interference Investigation of Swelling due to Water Uptake by Model Adhesive Joints, J. Adhesion, 11 (1980) pp. 175-189.

16. R. Muki and E. Sternberg, On Transient Thermal Stresses in Viscoelastic Materials With Temperature Dependent Properties, J. Appl. Mech., 28 (1061) pp. 193-207.

17. L.W. Morland and E.H. Lee, Stress Analysis for Linear Viscoelastic Materials with Temperature Variation, Trans. Soc. Rheol., IV (1960) pp. 233-263.

18. N. Bekkedahl, J. Res. Nat. Bur. Stand., 43 (1949) pp. 145-156.

19. ASTM, D864-52, Standard Method of Test for Coefficient of Cubical Thermal Expansion of Plastics.

20. A.J. Kovacs, Fortschritte der Hochpolymeren-Forschung, 3 (1963) pp. 394-507.

21. K.C. Rush, Time-Temperature Superposition and Relaxational Behavior in Polymeric Glasses, M. Macromol. Sci.-Phys. B2(2) (1068) pp. 179-204.

22. K.C. Rush, The Relaxational Behavior of Heterogeneous Polymers, J. Macro-

mol. Sci.-Phys., B2(2) (1968) pp. 421-447.

23. A.J. Kovacs, La Contraction Isotherme du Volume des Polymeres Amorphes, J. Pol. Sci., 30 (1958) pp. 131-147.

24. W.G. Knauss, V.H. Kenner and H. Chai, A Simple Creep Torsiometer and its Use in the Thermorheological Characterization of a Structural Adhesive, Experim. Mech., 22 (1982) pp. 75-80.

25. D.J. Plazek, The Temperature Dependence of the Viscoelastic Behavior of Polyvinyl Acetate, Polymer J., 12 (1980) pp. 43-53.

26. D.J. Plazek, The Temperature Dependences of the Viscoelastic Softening and Terminal Dispersions of Linear Amorphous Polymers, (unpublished).

27. J.D. Ferry, Viscoelastic Properties of Polymers, Wiley, New York (1970).

28. K. Ninomiya, An Extrapolation Method for Estimating Steady-Flow Viscosity and Steady State Compliance from Creep Data, J. Phys. Chem., 67 (1963) p. 1152.

29. I.L. Hopkins and R.W. Hamming, On Creep and Relaxation, J. Appl. Phys., 28 (1957) pp. 906-909.

30. A.C. Pipkin, Lectures on Viscoelasticity Theory, Appl. Math. Sci., 7 (1972).

31. V.H. Kenner, Personal Communication.

32. Optics Guide, Melles Griot,(1975), pp. 88.

33. F.A. Jenkins and H.E. White, Fundamentals of Optics, McGraw-Hill, New York (1957).

PART 2 - TIME DEPENDENT ADHESIVE FAILURE

1. INTRODUCTION

In this part of the thesis we are concerned with time dependent adhesive failure and long time integrity of adhesive systems ; emphasis is placed on the adhesion of rubbery materials to relatively rigid substrates. Besides the viscoelastic character of the polymeric coating, the amount of energy needed to generate new debond surfaces needs to be described quantitatively. When studying adhesive failure of rate sensitive materials one has to recognize the influence of the time dependent properties of the polymer on the fracture energy. Therefore, if one attempts to determine this surface energy experimentally, it is necessary to separate an intrinsic and a rate dependent interface energy from the measured fracture energy. The rate independent energy then corresponds to that obtained for infinitesimally slow interfacial crack propagation rates, and consequently should not vary if different test methods are used to measure it. The rate dependence needs to be clarified further. Let the fracture or adhesive energy measured at some rate of unbonding $\dot{c}$ be denoted by $\gamma(\dot{c})$. Then as originally formulated by Müller and Knauss [1] one may write

$$\gamma = \Gamma \, . \, g(\dot{c}) \tag{1}$$

where Γ is the intrinsic fracture energy and $g(\dot{c})$ is a nondimensional function of $\dot{c}$. In [1] the theory states specifically that the fracture energy can be represented by the product of an intrinsic adhesive failure energy Γ, which depends solely on the physical and chemical nature of the fracture interface, and a function $g(\dot{c})$ accounting for the rheological losses based on the description governed by the WLF equation. Efforts leading to establishing a characteristic measure of joint strength, independent of test geometry and loading conditions, were carried out by Gent and coworkers [2,3,4]. Their studies involved three types of testpieces, i.e. simple extension, pure shear and peeling samples.

The formulation exemplified by equation (1), was later confirmed by Andrews and Kinloch [5]. The details of their experimental work can be found in references [6,7].

In the determination of the intrinsic energy of adhesion Γ and the rate dependent adhesive energy γ many different test methods have been used over the years and newer ones are under study. The former ones include blister tests, cone tests, peel tests, lap shear and cantilever beam tests ; they have been extensively described in the literature [8]. A fairly complete overview of the various test methods for adhesive joints has been completed recently by Kinloch [9]. The choice of a specific method to measure the energy associated with interfacial fracture, whether it concerns Γ or γ , depends to a large extent on the function of the adhesive system.

Of particular interest in a fracture mechanics approach to adhesive failure is the interaction of the local crack tip deformation modes. In the theory of fracture mechanics this notion refers to the different types of deformations occurring in elastic media or adhesive systems with an initial flaw. In general, Mode I refers to a displacement during which the crack surfaces in the crack tip vicinity move directly apart, perpendicular to the plane of the crack. Mode II is associated with a displacement in which the crack surfaces slide over one another, i.e. perpendicular to the leading edge of the crack. In Mode III a similar motion occurs parallel to the leading edge of the crack. In monolithic materials displacements applied normal to and tangential to the crack plane result only in normal and tangential displacements of the crack tip respectively. In adhesive systems however combinations of various deformation modes appear in general under all loading conditions. Their existence has been demonstrated experimentally by Liechti [10], leading to the formulation of a vectorial crack opening displacement criterion in adhesive systems accounting for the presence of the

two fracture modes. This observation raises the question of the mode dependence of the adhesive energy. Several authors have reported a dependence of the adhesive fracture energy on the loading mode [11,12,13] resulting from a variety of test methods. Several reasons for this apparent variation can be mentioned however [12] ; among them we mention the different rates of viscous dissipation and the actual fracture surface area for each loading mode.

The viscoelastic character of the adhesive material is reflected in the rate dependence of the adhesive fracture energy. This characteristic also provides a way of checking whether a material is thermorheologically simple, if the amplitude of the residual thermal stresses is negligible. Under those circumstances, one can perform debonding experiments to measure the adhesive energy at different temperatures necessarily including the glass transition range of the polymer. If a master curve, displaying the adhesive energy versus the crack speed, can be constructed from the data by the time-temperature superposition principle, the material is said to be thermorheologically simple.

One needs to keep in mind, however, that the temperature itself remains a significant experimental parameter because it can be associated with one of several other potential sources of energy available to the debonding process, in addition to the mechanical load being applied during these tests. One energy source arises from the strain energy due to thermal stresses caused by the mismatch between the coefficient of expansion of adherend and substrate, if the tests are performed at temperatures far different from the one at which the polymer was deposited on its substrate. Furthermore the curing of the polymer and the attendant shrinkage causes straining and hence form an additional source of strain energy. The presence of these residual stresses has also to be accounted for in a quantitative manner.

Much attention has been directed towards the determination of the complex stress field around the interface crack tip. While investigating some problems of geophysical interest, Williams [14] established in the framework of the linearized theory of elasticity that the singular behavior of the stress is proportional to the inverse square root of the distance from the tip of the crack, but that the stresses possess a sharp oscillatory character confined to the immediate vicinity of the crack tip. Sih and Rice [15] confirmed Williams' finding of the oscillatory character of the stresses ; these authors also showed how the complex-variable method combined with eigenfunction expansion used in references [14,15] can be applied to formulate the problem of bonded dissimilar elastic planes containing cracks along the bond [16]. England [17] examined the problem of a crack opened under constant pressure between two dissimilar materials. Erdogan considered the case of two bonded semi-infinite planes containing cracks along the bond [18]. All these analyses possess the oscillatory singularities, which require the upper and lower surfaces of the crack to overlap near the ends of the cracks. In his work Erdogan concluded that in practical applications the phenomenon of stress oscillation may be ignored [18]. However more recently Knowles and Sternberg [19] showed that the oscillatory singularities arising in interface-crack problems stem from the linearization of such problems, as alluded to by England [17]. Knowles and Sternberg found the crack to open smoothly near its ends, regardless of the specific loading at infinity.

In their continuing effort to obtain a better understanding of time-dependent fracture in adhesive systems, researchers have tried to formulate equations governing fracture in viscoelastic solids. Williams [20] discussed the essential similarity between cohesive Griffith fracture and adhesive bond fracture, both of which in their elastic model possess singular stresses near the crack tip It then becomes natural to attempt to use similar fracture criteria for configurations

including adhesive bonds. In [21] Knauss formulates two fracture criteria applicable for cohesive crack propagation in viscoelastic materials. One is the crack-opening displacement criterion which states that continued fracture is possible when the displacement u at the trailing end of the cohesive zone attains some constant and critical value u_o. The other criterion equates the work done by the boundaries of the cohesive material on the disintegrating material which is equal to a fracture energy. In contrast to the description of fracture in rate-insensitive materials it appears that the size of the damage or process zone is a necessary parameter in the discussion on fracture in (linearly) viscoelastic solids. For many applications it is sufficient to assume that the growth law for steady crack propagation applies instantaneously. In [21] Knauss points out that if the stress intensity factor does not change much during the time interval in which the crack travels the length of the cohesive zone, the steady crack propagation equations still apply. In another paper Knauss [22] presented an expression for the rate of interfacial unbonding $\dot{c}$, if two poorly compressible viscoelastic solids are joined ; for plane strain conditions the crack speed is given by,

$$\frac{1}{2}\left[D_1\left(\frac{\alpha}{\dot{c}}\right) + D_2\left(\frac{\alpha}{\dot{c}}\right) \right] K^2[c,1,2] = \frac{\Gamma}{1-\nu^2} \qquad (2)$$

where

D_1 and D_2	=	the creep compliance of the two joined solids,
α	=	length of the process zone,
$c,\dot{c}$	=	crack size and crack tip velocity,
Γ	=	intrinsic surface energy required for unit crack extension,
$K[c, 1, 2]$	=	crack tip stress intensity factor.

The stress intensity factor K depends in general on the material properties of

the two solids which are indicated by the numerals 1 and 2. Numerical efforts to evaluate the stress intensity factors for bimaterial bodies have been carried out by Hong and Stern [23], and Smelser [24]. In the present study the strain energy release rate is chosen as the governing parameter for interfacial crack propagation.

Before we can attempt to carry out a failure analysis it follows from equation (2) that some other pertinent data need to be determined. Of special interest is the surface energy associated with the generation of new surfaces as indicated earlier. The measurement of the fracture energy forms the subject of the study in Chapter 2 where the influence of geometrical and environmental conditions is also investigated. Subsequently, in Chapter 3, two delamination models only involving elastic adherends and adhesives, are developed based on the strain energy release rate criterion ; this formulation leads to crack propagation criteria for elastic bimaterial specimens subject to thermal and moisture loading conditions. The next phase of this work also includes the influence of the viscoelastic character of the polymer layer in a bimaterial sandwich. Finally, results of debond tests are reported in order to verify the validity of the delamination criteria. In the experimental work a crosslinked polyurethane elastomer, Solithane 113, is used as the model adhesive. Its properties have already been extensively characterized in the past [1,25], and its weak bond to glass adherends, ensuring interfacial fracture, makes it a desirable material for these tests.

considerably smaller. These considerations are represented qualitatively in Figure 6. The combination of these two effects therefore shows a peak value for some intermediary value of the thickness of polymer films. Numerical values for the dissipation D calculated for the different film thicknesses in accord with equation (10) show a behavior similar to the one exhibited in the inset of Figure 4 in a qualitative manner.

An important remaining question, and unanswered in this study, is the deformation mode interaction in the peel test. One can expect the peel angle to play a role in determining the amount of Mode II loading at the crack tip. Anderson and coworkers contend [12] that in the 90° peel test, the major portion of the load should be in Mode I. However, it is reasonable to assume that some Mode II deformation is present, due to bending near the debond tip. In more recent work Crocombe and Adams [13] used the finite element method to show that the proportion of Mode II loading is essentially independent of the peel load and angle, and the adhesive or adherend modulus. The proportion appears significant, being about 30 % for compressible solids (ν = 0.3) and decreasing to about 12 % as the adhesive becomes incompressible. The results in the literature on this matter are still very limited. One can however conclude that an appreciable amount of Mode II deformation at the crack tip is present in the peel test.[4]

2.4.2 Temperature Effect in Fracture Energy Determination The temperature is expected to have two distinct effects on the debonding process.

1. First it influences the thermorheological behavior of the polymer

2. The temperature introduces thermal stresses and corresponding elastically

4. It was considered to investigate the interaction of the deformation modes in our test geometry through a finite element code, containing a bimaterial crack element. The TEXGAP computer code not being readily available we were unable to include these results in our study.

ment with other investigations [27,32] at least at first sight. In these referenced studies an increase of γ with thickness is reported, a conclusion that cannot be drawn from our data. Especially the results for the two thickest films need further explanation.

When plotting values of γ as a function of the thickness h for a particular crack speed $\dot{c}$, as indicated in the inset in Figure 4, one observes a peak for thickness value of h = 1.6 mm (1/16"). Let us attempt to explain this observation in terms of certain processes not explicitely accounted for in equation (3). The influence of the high stresses and strains as well as of the viscous dissipation around the moving crack tip is hard to determine directly. One can try, however, to estimate the bulk viscous dissipation D in the polymer sheet. Therefore we determine first the bending strain ε and the associated strain rate $\dot{\varepsilon}$ in the plate as :

$$\varepsilon = \frac{y}{R} \tag{8}$$

and

$$\dot{\varepsilon} = \frac{d\varepsilon}{dt} = \dot{c}\, y\, \frac{d\,(1/R)}{ds} \tag{9}$$

where y denotes a point location from the midplane of the polymer. The bulk viscous dissipation D is proportional to $\dot{\varepsilon}^2$ and the material volume V, according to :

$$D \sim \dot{\varepsilon}^2 V \sim \dot{c}^2 \int_0^{L_s} [\frac{d\,(1/R)}{ds}]^2\, ds \tag{10}$$

In this representation two counteracting effects are present. In the thinner films, which always form a full 90° bend, the strains and thus the strain rates are higher ; in the thicker films, which never display a complete 90° bend in these tests, the volume of the material remains higher, but the strain rates are

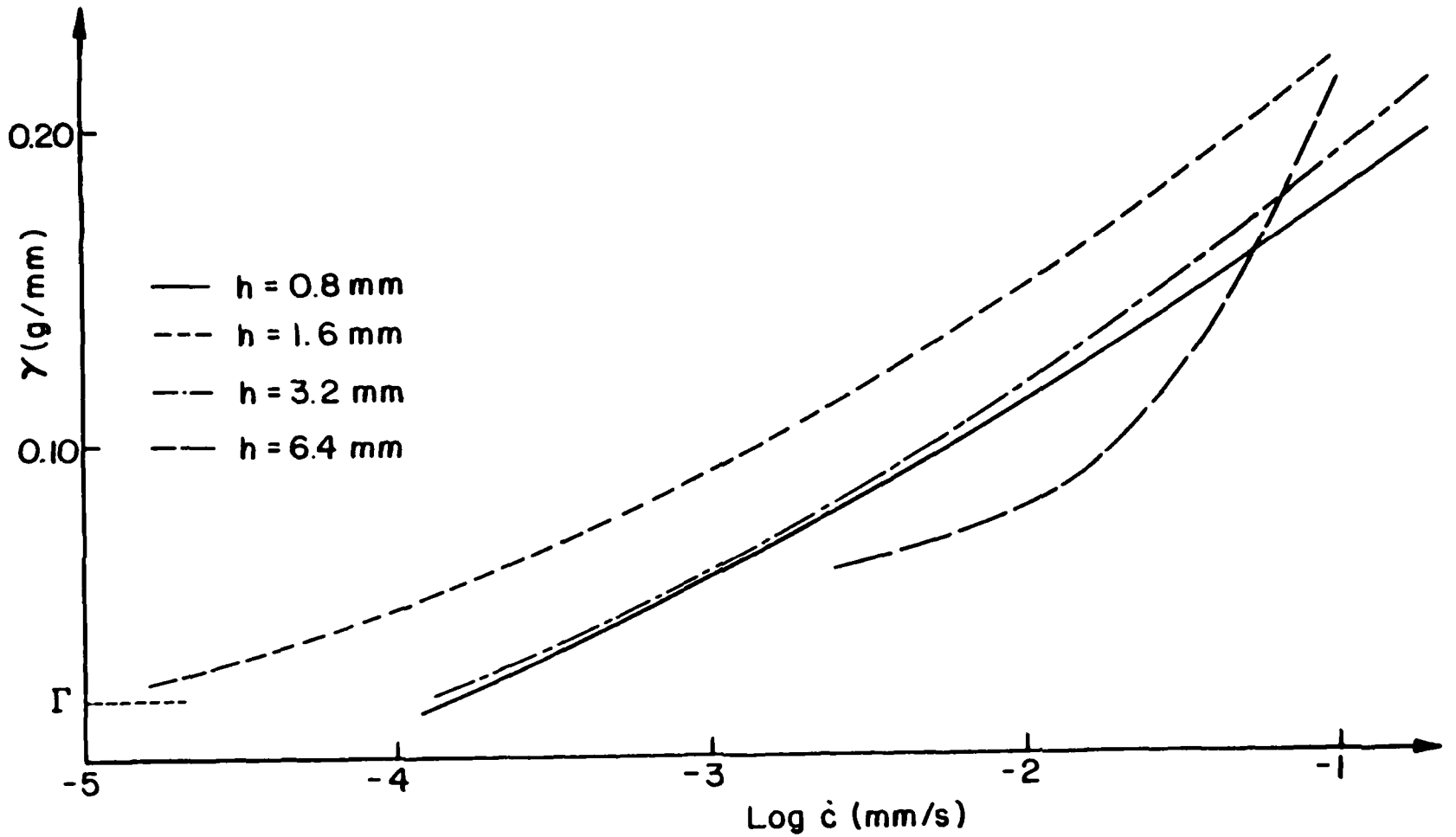

Figure 5. Polynomial (of degree 2) least squares fit through the experimental data of the peel tests.

restriction on the accuracy of these measurements derives from the limited resolution with which the debond position could be measured. This problem results from the need to monitor the tests from outside of the thermal chamber in which the experiments were performed. The resolution of the ruler indicating the crack propagation is around 0.5 mm. The accuracy of the various geometrical parameters is also subject to limitations, as they have to be obtained from photographic recordings. Figure 5 shows the results of a polynomial (of degree 2) least squares fit through the experimental data.

From Figures 4 and 5 it is apparent that the energy consumption in the separation process is a function of the adhesive thickness. As pointed out in the Introduction to Part II, one of the main points of interest remains the limiting value of the adhesive fracture energy for vanishing crack speeds. The data recorded for the four different thicknesses seem to converge to a common lower limit of about Γ = .02 g/mm ± 30%, which one identifies as the intrinsic energy of adhesion Γ ; for the limit value Γ of the adhesive energy the thickness effect seems to disappear.

We now discuss the reasons for the increase in the adhesive energy γ as the crack propagation increases. The deviation from the limiting value of the intrinsic energy of adhesion Γ is due to a number a processes which are not included in the energy balance equation (3). High stresses occur at the tip of the interface crack ; in addition to the strain energy associated with these stresses, viscous dissipation occurs in the viscoelastic material in the vicinity of the moving crack tip. This dissipation is clearly a function of the crack tip local strain rates which in turn are proportional to the crack speed $\dot{c}$. An additional energy absorbing process is the bulk viscous dissipation in the polymeric adhesive.

Even with these considerations in mind, these results are not in full agree-

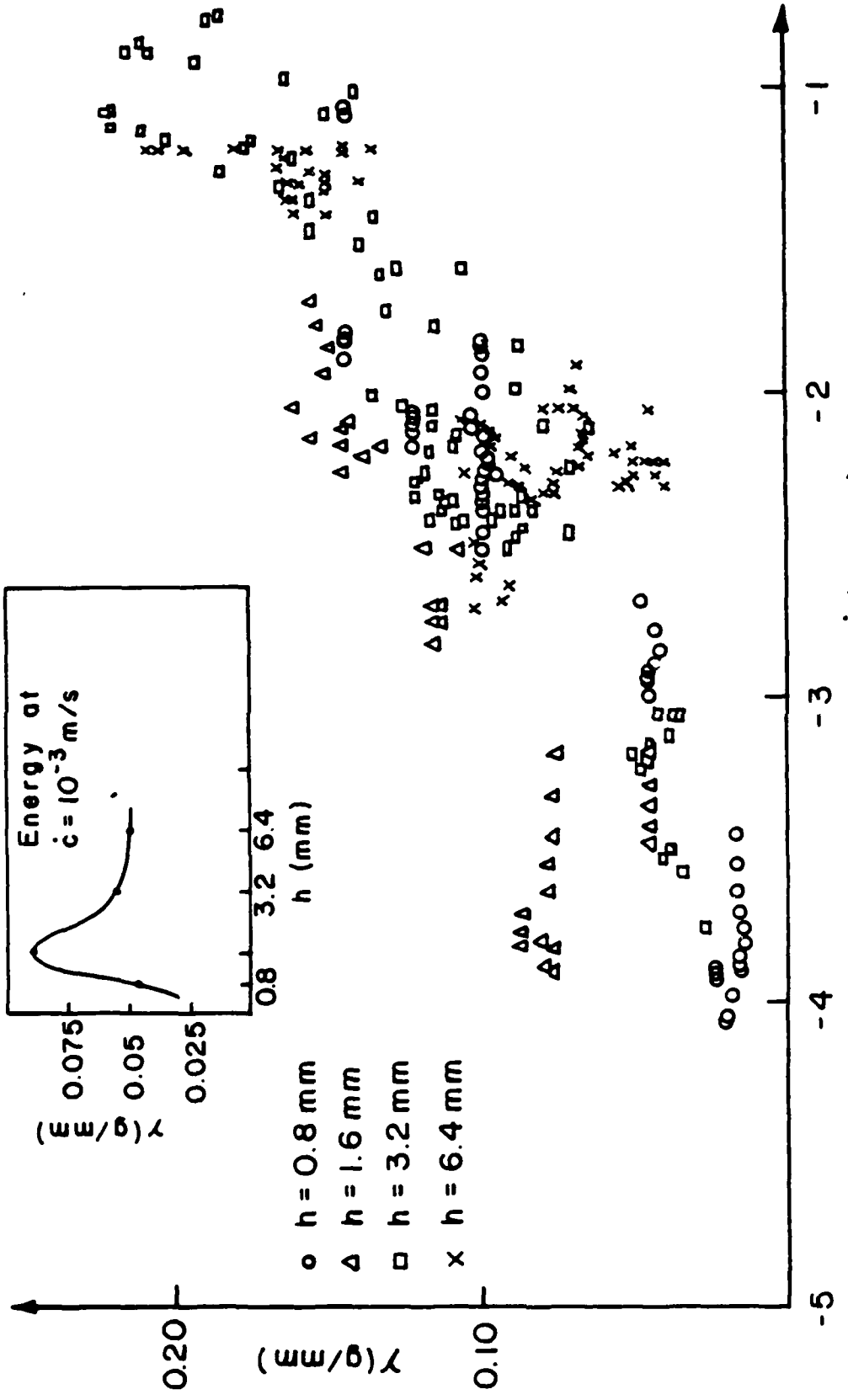

Figure 4. Adhesive energy γ versus crack propagation rate $\dot{c}$ for various film thicknesses at ambient temperature.

check whether the solution y(x) of equation (4) generates the experimentally recorded deflection.

In this comparison it is tried to match the experimental and calculated deflection and slope of the free end. Using the boundary conditions (5) does not yield the experimentally recorded deflection curve. Therefore the boundary condition describing the slope at the assumed "built-in" end (x = 0) needs some further clarification. The existing moment causes a rigid body like rotation of the debonded polymer film. Thus the second boundary condition in equation (5) is changed, allowing small initial angles varying (from 0° to 7°) at the clamped end ; this correction can be thought of as an elastic rotation correction at the built-in end. A similar consideration was formulated by Ripling and Mostovoy [31].

From equation (3) the adhesive peel energy γ can be calculated as a function of the crack propagation speed $\dot{c}$. During the tests with the thicker adherends when a constant 90° bend angle did not result, the effective loading varied and the debond speed seldom stayed constant, due to continuous variations in the geometry and thus the moment, hence the parameters L and l were also slowly varying functions of time.

2.4 Experimental Results and Discussion

2.4.1 Dependence of the Fracture Energy on Film Thickness Initial tests were performed at room temperature, using weights ranging from 1 g to 15 g, depending on the film thickness. The four different "film" thicknesses employed were : 0.8 mm (1/32"), 1.6 mm (1/16"), 3.2 mm (1/8") and 6.4 mm (1/4"). The results are shown in Figure 4 displaying the peel energy γ per unit crack extension versus the crack speed $\dot{c}$. The data exhibit distinct scatter, but that scatter is considerably smaller than that in many data reported in the literature [4]. One

soning the following relation results :

$$\begin{aligned} &F\,\dot{v} + \text{Body Force Work Rate} \\ &= \gamma\, b\, \dot{a} + \frac{1}{2}\frac{d}{dt}\left[\int_0^{L_s} (1-\nu^2)\,\frac{M^2}{EI}\,ds\right] \end{aligned} \tag{3}$$

where F and γ are the peel force and the adhesive energy respectively ; $\dot{v}$, $\dot{a}$, L_s, ν,E, I and b indicate the downward velocity of the free end of the cantilever plate, the crack speed, the length of the film (along its midplane), Poisson's ratio, Young's modulus, the section moment of inertia, and the width respectively ; M is the moment resulting from the applied peel force and the body forces. The energy associated with the longitudinal extension of the polymer was found to be negligible.

In order to calculate the work done by the body forces as well as its bending strain energy, the deflection shape of the cantilever plate needs to be known. In accordance with the theory of large deflections, the following differential equation governs the deflection y(x) (R = radius of curvature) :

$$\frac{1}{R} = \frac{M}{EI}(1-\nu^2) = \frac{y''}{[1+y'^2]^{3/2}} \tag{4}$$

subject to the boundary conditions :

$$\begin{aligned} y(o) &= 0 \\ y'(o) &= 0. \end{aligned} \tag{5}$$

Furthermore,

$$M = F\,(L-x) + \frac{q(l-x)^2}{2\cos\varphi} \quad \text{for} \quad 0 < x < l \tag{6}$$

$$M = F\,(L-x) \quad \text{for} \quad l < x < L \tag{7}$$

in agreement with the nomenclature of Figure 3 ; q denotes the weight of the polymer sheet per unit length. The results of the numerical calculations are compared with the data compiled from the photographic records, in order to

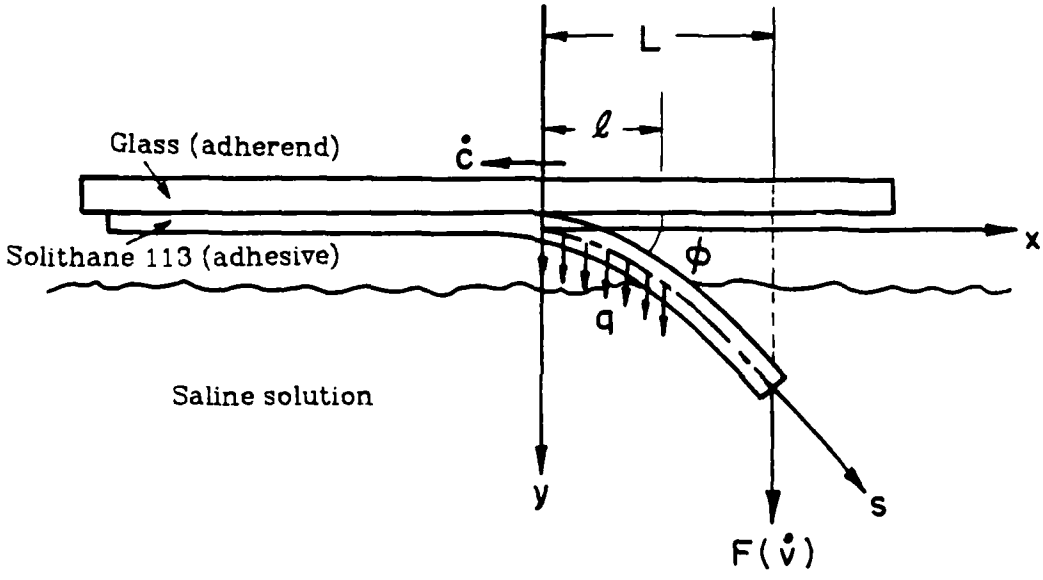

Figure 3. Geometry of the peel test.

At higher temperatures the dissolved gas in the saline solution formed bubbles on the specimen thus affecting the net weight on the specimen. In order to prevent the formation of air bubbles a 0.5% volume of Kodak Photo-Flo 200 solution is added to the fluid. In addition the latter was boiled before the actual testing to drive off the dissolved air.

2.3 Analytical Developments

As indicated in the Introduction to this chapter, one of the primary goals of this investigation remains the influence of the thickness of the adhesive on the adhesive energy γ. In addition we also want to include the viscoelastic character of the polymer film in our study.

When performing peel tests it is often desirable to obtain a 90° bend in the debonding adhesive film ; if the geometry remains constant during the time of the experiment, it makes the analysis necessary to evaluate the adhesive fracture energy relatively straightforward. For the range of thicknesses involved in our experiments it was found that the thicker films could not always form a full 90° bend ; this situation occurred for the range of peel weights used if the thickness exceeded 2 mm.

Next we proceed to formulate an energy balance to determine the fracture energy γ. The geometry of the peel test is shown in Figure 3. For analysis purposes we assume that the glass plate remains mechanically rigid. Work is being done by the descending peel force as well as by the body forces of the hanging portion of debonded polymer. The latter part includes work as a result of the translation of the "film" as well as of the rotation of the free hanging polymer in the case of thicker films when the peel angle does not remain constant. The energy thus generated serves to create new surfaces and is also stored as bending strain energy in the debonded film. Hence, using "strength of materials" rea-

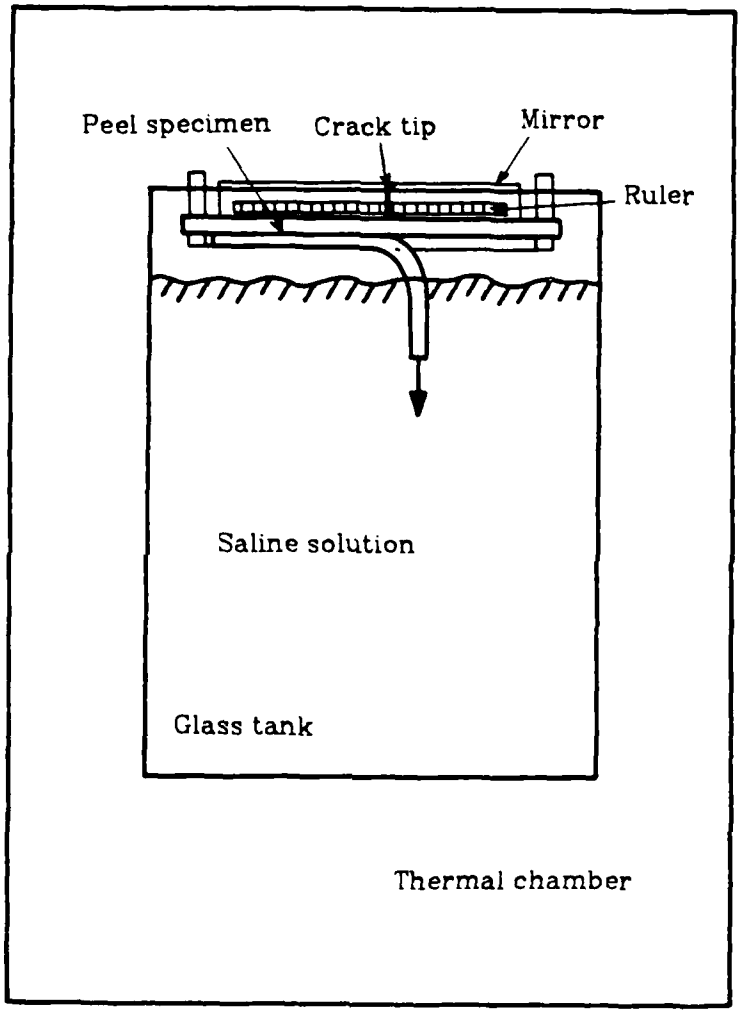

Figure 2. Schematic of the peel test setup.

a prescribed load orientation to the adhesive and aimed at gradually removing it from its adherend with a more or less constant rate. This can be achieved by either prescribing a constant displacement rate or by applying a constant load to the adhesive joint. In the former configuration the peel testing apparatus needs to include a system that allows continuous adjustment of the peel angle in order to be performed in a tensile testing apparatus [13,26]. In the present work preference is given to the second way of loading, i.e. a constant weight is applied. The experimental set-up in the latter case also is simpler to assemble. In addition the need to enclose the testing apparatus in an environmental chamber allowing control of the test temperature pointed towards the use of a simple method.

In addition to the dead weight, we have to account for the increasing weight of the debonded polymer film as peeling progresses. The large thickness of the Solithane 113 films in these measurements (from 0.8 mm to 6.4 mm) gives rise to body forces on the order of the applied peel force. Therefore it was decided to submerge the debonded portion of the adhesive in a fluid with a density that matches that of Solithane 113. A 5% by weight saline solution [30] satisfies this requirement.[3] The peel testing apparatus is shown schematically in Figure 2. It consists of a stainless steel frame which supports the specimen and rests on the edges of a water tank. The latter is made out of glass so that the test geometry can be monitored during peeling.

The motion of the crack tip is monitored via a mirror and using a transparent ruler mounted on the glass adherend. At regular time intervals pictures of the peel test geometry are taken in order to keep track of the debonding process. Kodak technical pan film 2415 provided high contrast records.

3. The potential effect of salt deposition at the interface on the values of the adhesive energy remains an unknown and is unaccounted for in this work.

weight is thoroughly degassed and mixed. The liquid polymer is then pressure injected into the gap between the center plate of the mold and the glass adherends, through feeding channels drilled in the center plate. The mold gap is then sealed and the polymer cured at room temperature for one week ; the peel specimens are used within a month after the cure has been completed. The symmetric design of the fixture permits the simultaneous casting of two specimens of equal thickness. This procedure reduces somewhat the possibility of differences in material adhesive properties between specimens. In order to prevent sticking of the Solithane 113 to the metal parts of the mold, these were sprayed with a thin layer of KRAXO 1711 Release Agent (Contour Chemical Company). The Solithane 113 specimens are approximately 290 mm long, 50.8 mm wide, the thickness varying according to the spacer used, bonded to the glass ; the dimensions of the latter exceed those of the Solithane 113 by about 1 cm all around.

The cure at room temperature eliminates the residual stresses, resulting from the different thermal expansion properties of adherend and adhesive. However, the cure shrinkage of the latter introduces residual stresses. Their magnitude has been estimated by Liechti [10] ; the cure shrinkage was determined to be $\Delta V / V = 1.34 \times 10^{-2}$ which corresponds to a thermal cool down of 25 °C.[2]

2.2 Experimental Method for Peel Testing

The adhesive peel test can be performed in different ways, including stripping, floating roller and climbing drum tests. All these methods are designed to apply

1. The terms "Resin" and "Catalyst" are commercial designations. Chemically the "Resin" is a trifunctional isocyanate which is the product of a reaction between Castor Oil and Tolylenediisocyanate. The "Catalyst" is a triol and consists essentially of Castor Oil.
2. The thermal expansion characteristics of Solithane 113 were determined previously in the dilatometer described in Chapter 2 of Part I. Above the glass transition the linear coefficient of thermal expansion equals 1.79×10^{-4}/°C.

Figure 1. Peel test specimen and casting fixture.

2. MEASUREMENT OF THE ADHESIVE FRACTURE ENERGY

In this chapter the determination of the adhesive energy is presented. The peel method has been widely used, because it is an easily applied technique [4,7,13,26,28,29]. However, as will be seen below, the peel test is not free of interpretational difficulties. It is in part for this reason that we investigate the interfacial failure process in terms of the peel test. The specific goals of the peel tests are :

1. To determine a value for the intrinsic energy of adhesion Γ, as well as to study the rate dependence of the fracture energy γ at ambient temperature.
2. To examine the effect of the thickness of the polymer as well as of its viscoelastic nature on the value of the fracture energy γ. The latter influence manifests itself through relaxational behavior and viscous dissipation *phenomena*.
3. To investigate the influence of residual (cure) and thermal stresses on the basis of the thermorheological behavior of the polymer.

The next two sections describe the materials used and the experimental method. Section 2.3 presents the energy balance considerations leading to the value of γ. The experimental results and the discussion form the object of Section 2.4.

2.1 Test Materials and Specimen Preparation

In order to allow visual monitoring of the peel test, glass was chosen as the transparent adherend. In the Introduction the reasons for choosing Solithane 113 as the model adhesive have already been given.

A specimen and the casting mold are shown in Figure 1. By means of set-screws the glass plate is forced against a spacer which determines the thickness of the polymer film. A mixture of 50% Solithane "Resin" and 50% "Catalyst" [1] by

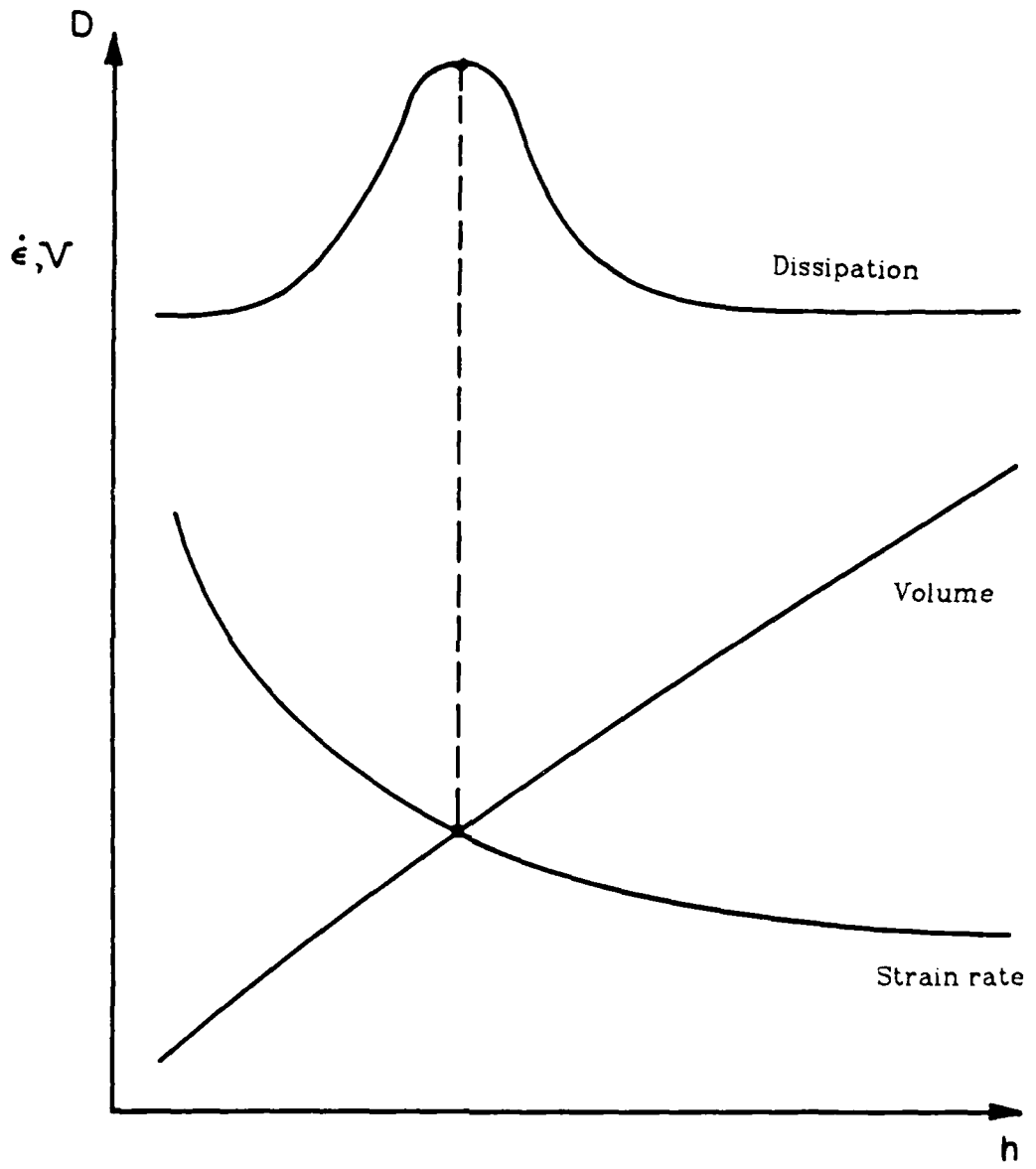

Figure 6. Qualitative representation of the volume V of the polymer film, the strain rate $\dot{\epsilon}$, and the dissipation D as a function of the film thickness h.

stored energy.

In all testing data available in the literature at this time only the first of these effects is considered, and the effect of the second, the temperature influence is not considered. Therefore, it is appropriate to examine whether this second effect can be neglected, and if so, under what conditions.

The enclosure of the set-up in the thermal chamber allowed measurements in the temperature interval ranging from 0 °C to 70 °C. The lower limit was imposed by the freezing point of the saline solution (around −3 °C) [30] ; at temperatures above 70 °C excessive evaporation of the solution made it more difficult to keep the fluid level constant over protracted periods of time. In order to keep the crack propagation speeds at the low end of the velocity domain, test periods of 12 hours were common.

The test results for the 0.8 mm (1/32") and 1.6 mm (1/16") thick films, are displayed in Figure 7. These data show the interfacial crack propagation rate c as a function of the test temperature, the arrows pointing downward in Figure 7 represent zero crack speed data at the corresponding temperatures. The peel tests were performed using the same constant weight at all temperatures. The measurements were limited to the thinner films, which keep their geometry essentially constant during the peeling process. In both cases the crack speed seems to reach a maximum value around 10 ° to 20 °C above room temperature At higher temperatures the crack speed becomes vanishingly small. This latter observation is in direct contradiction to the thermorheological effect

For the purpose of an explanation we note that equation (2) can be written as :

$$\frac{1}{2} D \left(\frac{\alpha}{\dot{c}\, a_T} \right) = \frac{\Gamma}{E_\infty G} \qquad (11)$$

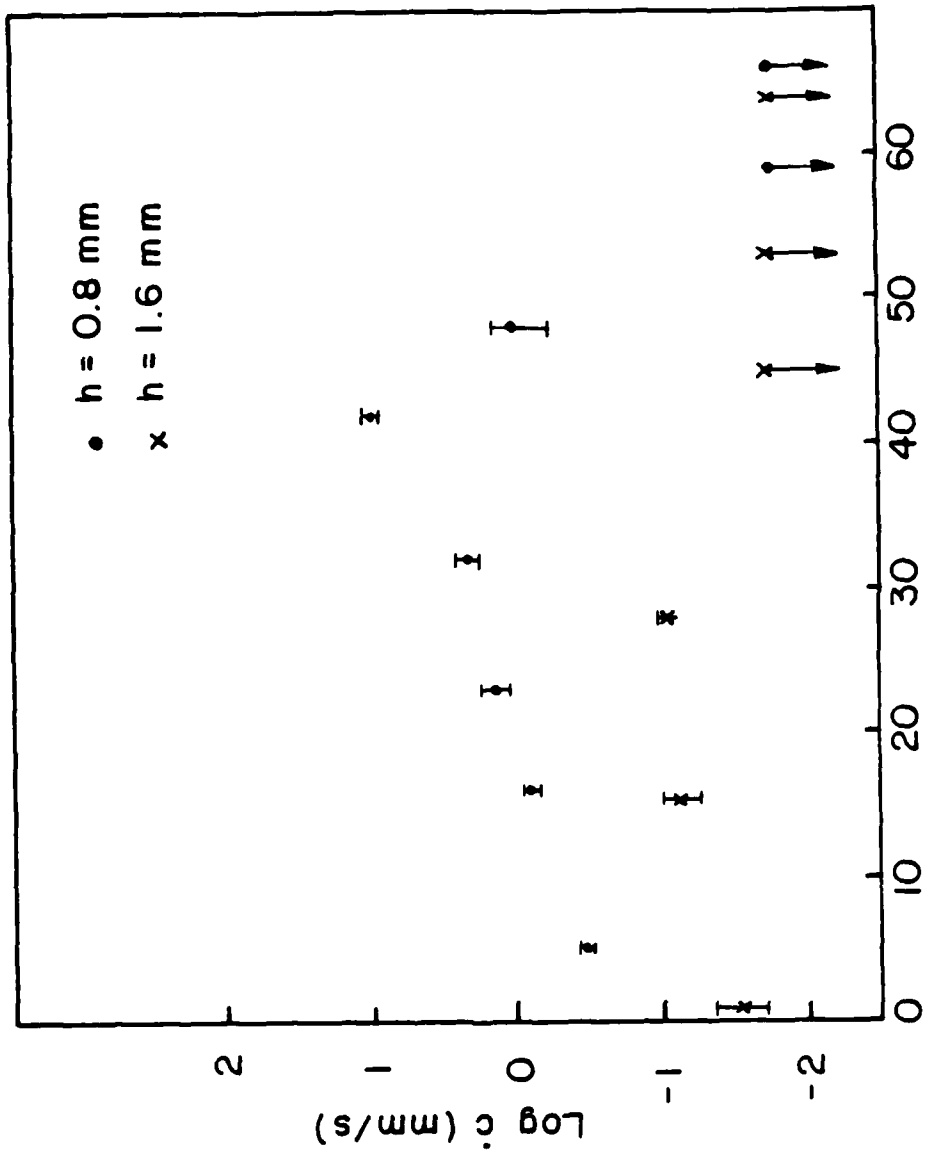

Figure 7. Crack propagation rate ċ as a function of the test temperature.

where E_∞ is Young modules for Solithane 113 in its rubbery domain and G is the energy strain release rate. The contribution of the glass adherend on the left hand side of equation (2) has been neglected. In this analysis the sources of energy driving the crack propagation are twofold. One arises from the strain energy stored in the polymer as a result of the cure shrinkage. The strain energy release rate due to curing amounts to :

$$G_c = \frac{Eh}{1-\nu}\left(\frac{\Delta V}{3V}\right)^2 \left[\frac{T_o - T}{T_c}\right]^2 \qquad (12)$$

where

$\frac{\Delta v}{v}$ = cure shrinkage (numerical values from ref. [10])

T_c = cure temperature (room temperature) taken equal to 25 °C

T_o = T_c + 25 °C. T_o represent the temperature at which the curing induced strains would vanish as determined by Liechti [10].

For reasons of simplicity the strain energy release rate due to the peel load, is taken to be :

$$G_P = \frac{F}{b} \qquad (13)$$

Introducing equations (12) and (13) into equation (11) yields :

$$D\left(\frac{\alpha}{\dot{c}\, a_T}\right) = \frac{2}{E\left[\frac{Eh}{\Gamma}\cdot\frac{1}{1-\nu}\left(\frac{\Delta V_c}{3V}\right)^2 + \frac{F}{\Gamma l}\right]} \qquad (14)$$

From equation (14) the crack velocity $\dot{c}$ can be calculated as a function of the temperature T with the intrinsic energy of adhesion Γ as a parameter ; the results of such a computation are presented in Figure 8. For lower values of Γ, i.e. up to $\Gamma \simeq 0.020$ g/mm, a continuous relation is obtained over the complete temperature interval. For higher values of Γ, equation (14) is no longer satisfied

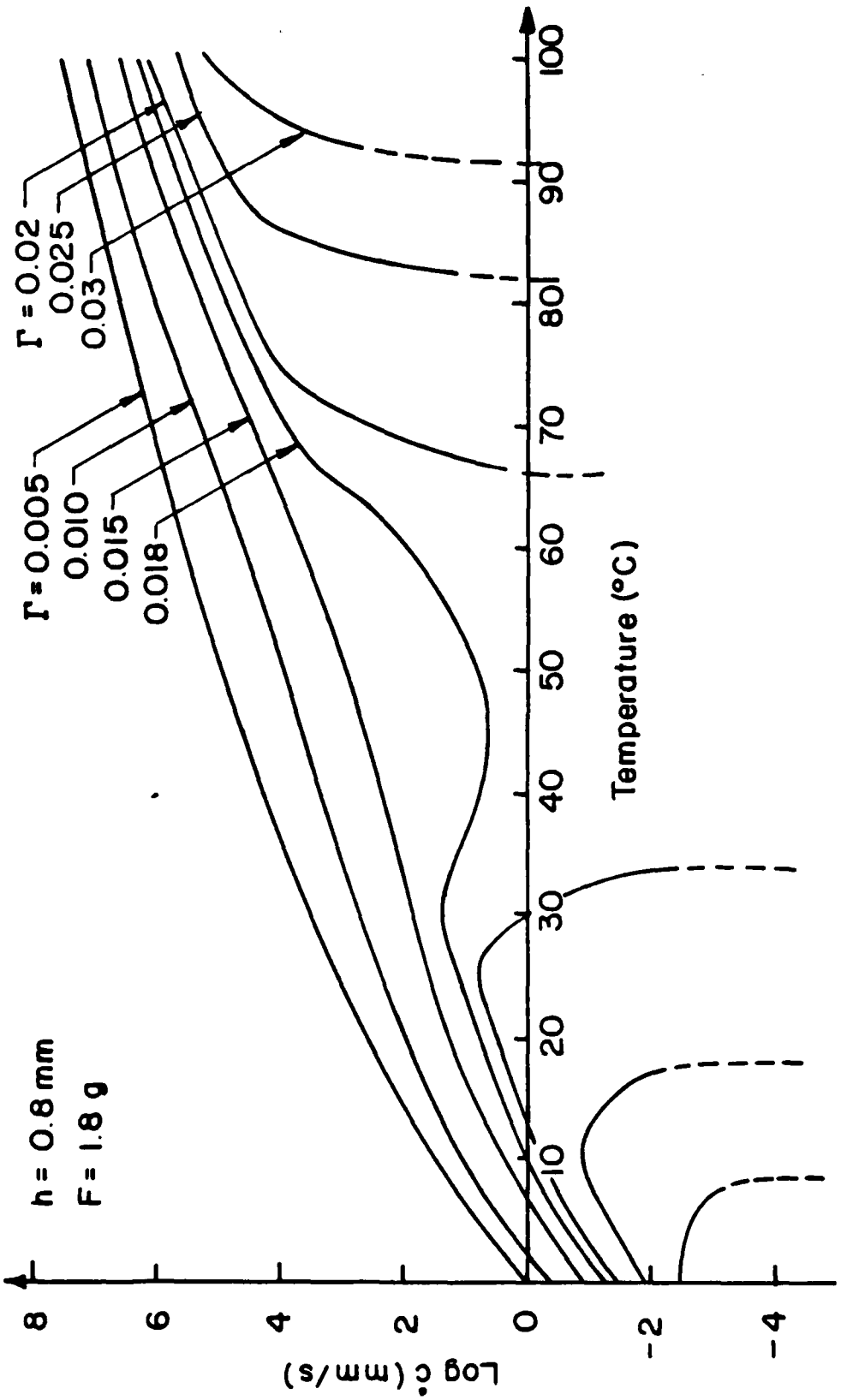

Figure 8. Calculated crack propagation rate ċ versus temperature.

over the whole temperature domain and hence the criterion for crack propagation is no longer met for all values of T. In order to compare experimental and theoretical results, one tries to match the results of Figure 7 with one of the theoretical curves of Figure 8 for a constant value of Γ. The theoretical curve corresponding to Γ = 0.02 g/mm displays a behavior very similar to the one exhibited by our experimental data as exemplified in Figure 9 for a film thickness h = 0.8 mm. It should be borne in mind that the cure shrinkage strain energy vanishes around 50 °C, thus reflecting the correspondence of the cure shrinkage to a thermal cooldown of 25 °C [10]. At temperatures removed from 50 °C, the strain energy stored in the material volume as a result of curing becomes much more important. From our experimental results it appears that this source of strain energy plays a significant role in the lower end of the test temperature range. We can also conclude that the value of the intrinsic fracture energy is somewhat less than 0.02 g/mm.

Two more considerations concerning equation (14) deserve attention. The first one concerns the value of F to be substituted in equation (14). Besides the peel weight, the body forces connected with the unbonded polymer not yet submerged in the saline solution, also pull on the still adhering portion of the Solithane 113 sheet. Therefore estimates were made to account for the body forces in some sample calculations ; no significant change from the previous calculations was obtained however.

Another point of interest is the length of the damage zone α. In order to effect a fit of the analysis represented in Figure 8 with the experimental data of Figure 7 a value of α = 2Å was necessary. In connection with Figure 8 it should be pointed out however, that small variations in Γ result in rather significant changes in the value of $\dot{c}$. Hence variations in Γ, corresponding to vertical shifting in Figure 8, can easily raise the value of α up to 100Å. For comparison the

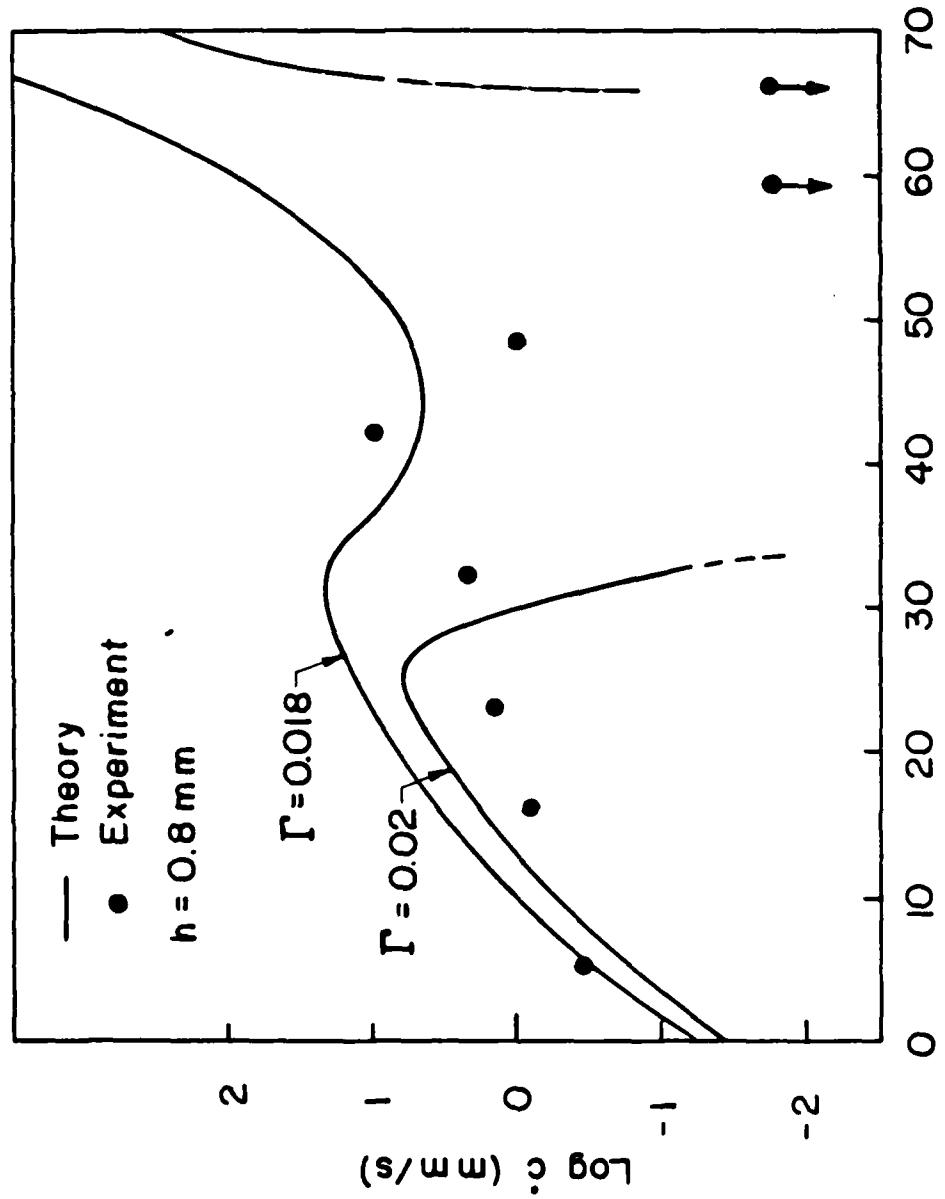

Figure 9. Comparison between calculated and experimentally obtained crack propagation rate as a function of temperature.

value of α in cohesive fracture in Solithane 113 obtained by Knauss and Müller can be referred to, i.e. $\alpha = 150\text{Å}$ [1]. Hence our theoretical results seem to constitute a reasonable source for comparison with the experimental data, and underline the importance of the residual (cure) stresses.

3. DELAMINATION MODELS

In this section two examples of failure progression are considered ; they exemplify the fracture mechanics approach to two typical adhesive failure processes germane to protective film debonding. An energy criterion is applied in order to predict crack propagation, for the case that initial imperfections (debond) are present at the polymer-substrate interfaces.

In one example case shown in Figure 10a, one is concerned with the growth of a debond at the edge of a interface between a polymer and a rigid substrate. Straining, induced by, say, a decreasing temperature or by outgassing of the polymer, initiates and drives the crack propagation. The second example outlined in Section 3.2, involves the buckling of the adhesive layer, after a portion of the coating has separated from the substrate. Subsequent heating or solvent water infusion into the polymer coating of the bimaterial structure may cause the debond to grow.

In both cases the circular geometry of the specimen favors axisymmetry of the problem. It is also appropriate to summarize the assumptions made in the sample calculations, namely :

1. The coating material behaves like a linearly elastic material except possibly in the highly stressed region at the crack tip. This assumption describes well the general behavior of a polymer far away from its glass transition. Viscoelastic effects will be discussed later on.
2. The adhering layer possesses a uniform temperature throughout its volume.

In each example the elastic strain energy release rate G is calculated which equals to the derivative of the elastic energy with respect to the crack surface increase. The crack propagation criterion used in order to predict the onset of

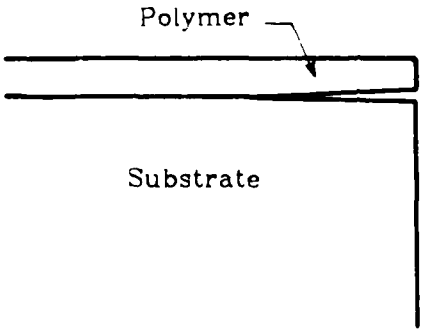

(a) Edge Delamination

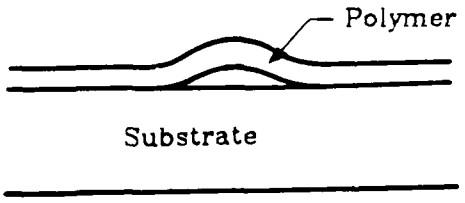

(b) Central Delamination

Figure 10. Delamination configurations.

additional debonding, was originally formulated by Griffith ; it states that crack propagation will occur if the energy released upon crack growth is sufficient to provide all the energy required for crack growth. For an axisymmetric geometry the criterion can be written as,

$$G = \frac{\partial U}{\partial A} = \frac{1}{2\pi R} \frac{\partial U}{\partial R} \geq \Gamma \qquad (15)$$

where ∂A is the area to be debonded, while R and Γ is the radial coordinate and the energy required to create a new surface, respectively. The study of the edge delamination is complemented with experimental results of debond tests, delineated in Section 3.4.

3.1 Edge Delamination

The geometry of the edge delamination case is shown in Figure 11. A circular polymer film of thickness h and radius R_o is bonded to a rigid substrate over a circle of radius R so that an annulus $R_o - R$ is unbonded, where $R >> R_o - R$ and $R_o - R >> h$. The latter assumption allows neglecting the more complex stress analysis necessary if the size of the debond were comparable to the film thickness. Upon changing the temperature, the film tends to contract or expand, but because of the partial bond, an equibiaxial homogeneous stress field is established inside a circle of radius r_c , where $r_c >> h$. We aim at calculating the temperature T at which unbonding will occur if T_o is the temperature at which bonding was effected.

In the circular region, where $r < r_c$, one finds the stress field :

$$\begin{aligned} \sigma_r &= \sigma_\vartheta = \sigma \\ \sigma_z &= 0 \end{aligned} \qquad (16)$$

Due to adhesion to the rigid substrate, the in-plane mechanical strains vanish, namely,

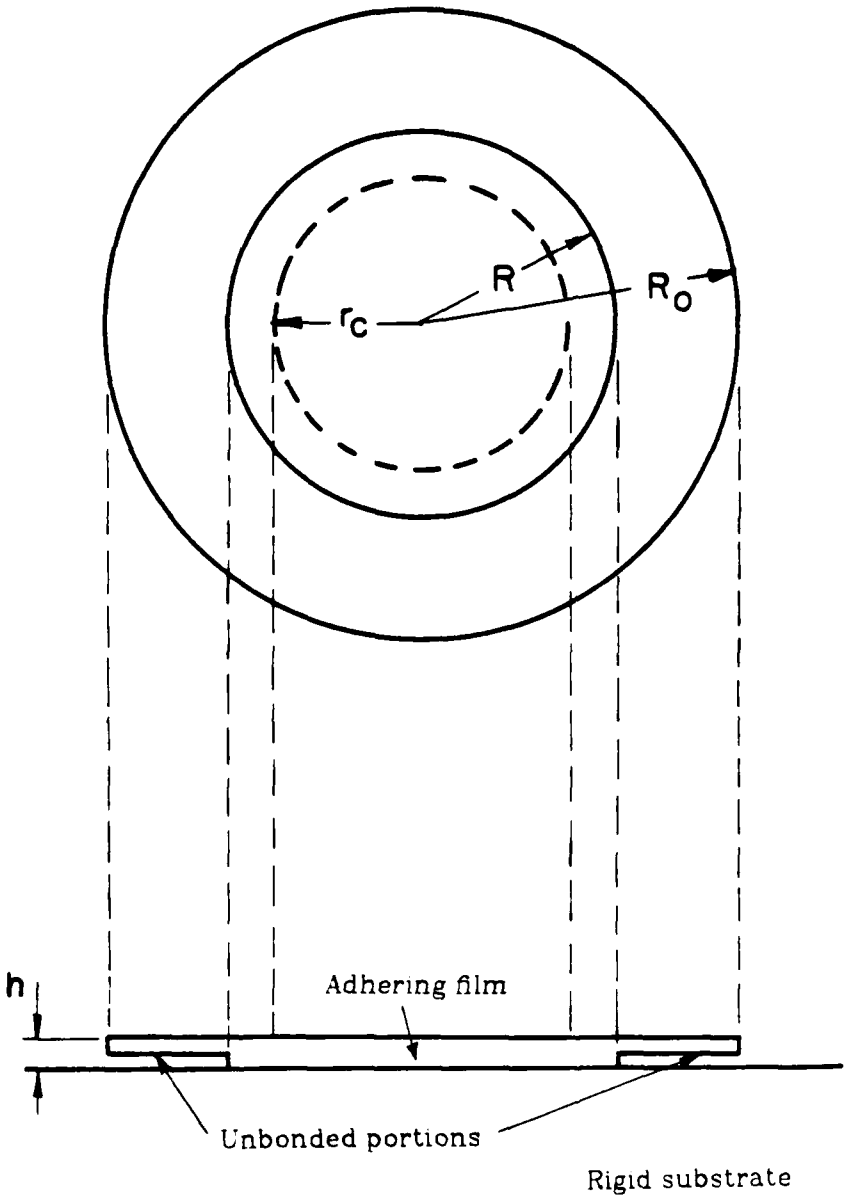

Figure 11. Geometry of the edge delamination.

$$\varepsilon_r = \varepsilon_\theta = 0 \tag{17}$$

and hence,

$$\sigma = \frac{-E\,\varepsilon_T}{1-\nu} \tag{18}$$

where $\varepsilon_T = \alpha\,(T - T_o)$; E and ν are Young's modulus and Poisson's ratio respectively ; $\Delta\alpha$ is the difference between the coefficients of thermal expansion of the polymer and the substrate ; the value of the latter can be neglected with respect to the one for the polymer, and hence $\Delta\alpha \cong \alpha$. The equibiaxial character of the stress field yields the strain energy per unit volume

$$u = \frac{1}{E}\sigma^2\,(1-\nu) \tag{19}$$

so that the total stored energy U is given by

$$\frac{\sigma^2}{E}\pi r_c^2 h(1-\nu) \cong \frac{\sigma^2}{E}\pi R^2 h(1-\nu) . \tag{20}$$

In order to create a new annular surface Δa (of radius R with width ΔR) as the debonding continues, the energy ΔS required is

$$\Delta S = 2\pi R\ \Delta R\ \Gamma . \tag{21}$$

During the unbonding process, energy stored elastically in the sheet is released. The rate at which this occurs per unit bond radius equals

$$\frac{\Delta U}{\Delta R} \rightarrow \frac{\partial U}{\partial R} = \frac{2\sigma^2}{E}\pi R h(1-\nu) \tag{22}$$

Upon substituting equation (18), one obtains :

$$G = \frac{1}{2\pi R}\frac{\partial U}{\partial R} = Eh\,\frac{\alpha^2 (T - T_o)^2}{1-\nu} . \tag{23}$$

According to equation (15) unbonding can occur when

$$T - T_o > \frac{1}{\alpha} \left| \frac{\Gamma(1-\nu)}{Eh} \right|^{1/2} \tag{24}$$

Note that the strain energy release rate G is independent of the bond size R, namely

$$G = \frac{\sigma^2 h}{E}(1-\nu) . \tag{25}$$

As already suggested earlier, a more detailed analysis is needed for small values of $(R_o - R)/h$ as indicated in Figure 12. Numerical methods seem more appropriate to solve problems relating to the early stages of this particular kind of crack growth, namely crack initiation and/or small initial flaws. In the region where $R/h > R^*/h$, debonding will proceed continuously, and presumably, at a constant rate if enough energy is being provided to create new crack surfaces, i.e. if $G \geq \Gamma$. If $G < \Gamma$, no separation will take place.

Finally one notes that strain energy release rate G may result from causes other than temperature induced straining, namely solvent (water) swelling and mass loss (outgassing migration of low molecular weight components). Then the non-dimensionalized strain energy release rate is given by

$$\frac{G}{Eh} = \frac{1}{1-\nu} \varepsilon_o^2 \tag{26}$$

as long as ε_o is the strain due to thermal and/or moisture loading and/or due to outgassing of the polymer, i.e.

$$\varepsilon_o = \Delta\alpha\,(T - T_o) + \alpha_{H_2O}\, C - \beta \tag{27}$$

where α_{H_2O}, C, β are the coefficient of expansion due to water (or other solvent) absorption, the water (or solvent) concentration and the shrinkage due to outgassing respectively

we account for the cure shrinkage stresses, the strain energy release rate G can be written as :

$$G = \frac{Eh}{1-\nu}\left[\alpha\,(T_o - T + \Delta T_c)\right]^2 \qquad (37)$$

where ΔT_c = 25 °C represents a thermal cooldown equivalent to the cure shrinkage [10].

According to equation (37) debonding could start for a ΔT = 35 °C and ΔT = 24 °C for the two thicknesses involved in the debond tests. From equation (37) one concludes that

$$G \sim h\,(T_o - T + \Delta T_c)^2 \qquad (38a)$$

$$\sim h\,(\Delta T)^2 \qquad (38b)$$

When evaluating equation (38b) the ratio of the average strain energy release rate G associated with each polymer film thickness, is equal to :

$$\frac{G_1}{G_2} = \frac{h_1(\Delta T_1)^2}{h_2(\Delta T_2)^2} = \frac{0.8(100)^2}{1.6(90)^2} = 0.62 \qquad (39)$$

One has to consider once more the contribution of the viscoelastic character of the coating in order to explain this result. As was also experimentally observed in the peel tests involving several different thicknesses, it appears that the thicker films require a higher adhesive fracture energy γ and consequently a higher strain energy release rate G in order for interfacial crack propagation to occur. It remains difficult to estimate the absolute value of the temperature at which debonding will proceed on the basis of the elastic (rubbery) properties of Solithane 113. One should note that no debond could be observed experimentally unless at temperatures well below the glass transition range of the polymer, which induces a pronounced change in material properties. In addition the observed debond does not occur in the crack speed range of the intrinsic frac-

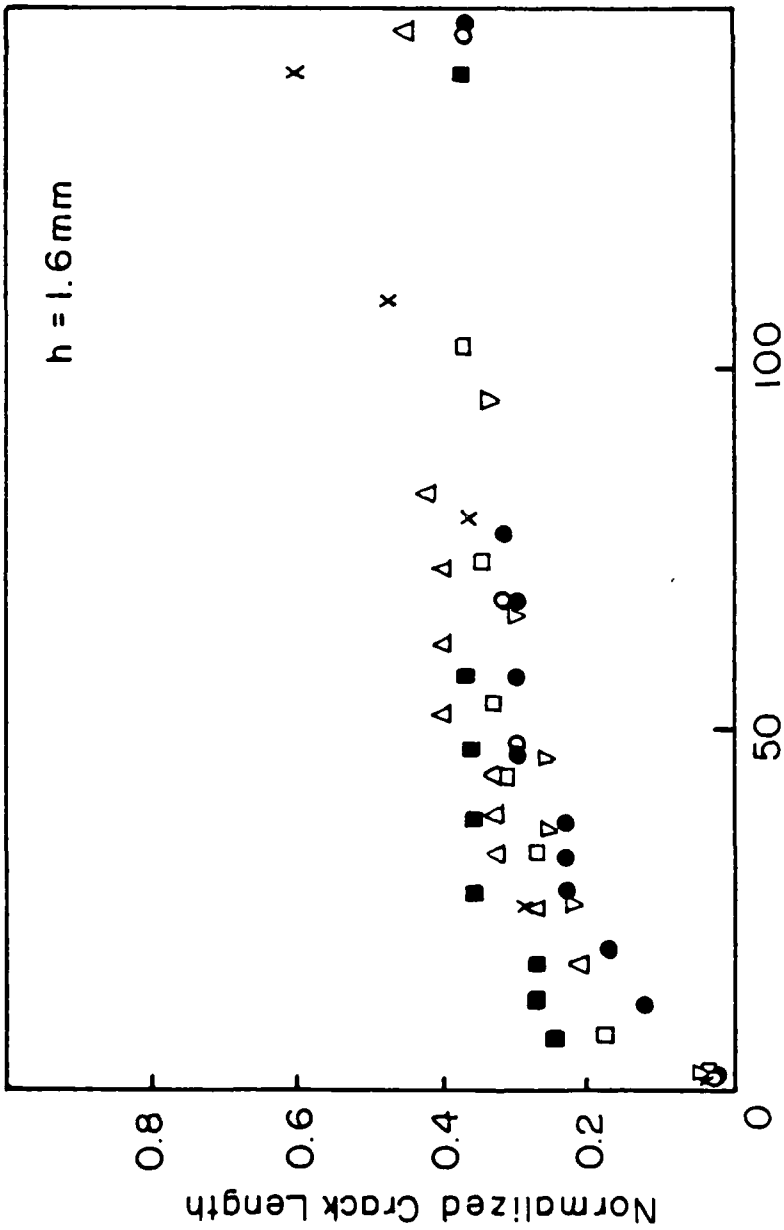

Figure 17. Debond progression as a function of time.

eight times the thickness of the adhesive. Some specimens were allowed to cool down as the chamber lowers its temperature ; others were quench cooled once the test environment has reached its desired temperature. This different cooling history is reflected in the initial debond rates, as shown in Figure 17. The latter represents the crack progression as a function of time. The specimens cooled at a lower rate start debonding at a slower pace than the quenched specimens. Eventually the crack propagation arrests, as the built-in stresses are continuously relieved due to relaxation in the viscoelastic material for both the slow and fast cooling histories. In addition the viscosity of Solithane 113 increases significantly below its glass transition temperature, previously determined to be ± 25 °C [5] ; this certainly influences the value of the fracture energy γ, a phenomenon illustrated by the experimental data of the previous chapter where the influence of the temperature on γ was investigated. It must be pointed out that the debond does not progress in a perfect axisymmetric fashion.

Some of the immediate, practical results of the tests are the temperatures at which debonding could first be noticed after a waiting period of about 12 hrs for the slowly cooled specimens and about half an hour for the quench cooled samples. For the larger thickness this occurred around −42 °C , for the thinner film T=−51 °C to see continuing crack propagation, which seems consistent with the smaller amount of strain energy stored in the thinner coating. For the quench cooled specimens debond started to be noticeable a few degrees below the corresponding temperature for the slowly cooled samples. We now proceed to calculate a lower bound estimate for the temperature at which debonding should start, using the (elastic) material properties of Solithane 113 in its rubbery domain. It should be recalled that the strain energy release rate G associated with the propagation of an edge delamination is given by equation (26) ; if

5. The thermal expansion characteristics of Solithane 113 were determined in the dilatometer, used in the material characterization of PVA_c in Chapter 2 of Part I.

Figure 16. Specimen for debond testing.

3.4 Debond Testing

In the final section of this chapter the experimental results of debond tests are presented. The tests are performed in order to make a comparison with the failure analysis outlined previously in Section 3.1 of this Chapter.

3.4.1 Experimental Method In order to relate the fracture energy from the peel tests to these measurements Solithane 113 is used as the model adhesive. To monitor the debond progression glass is also again selected as the adherend. Because of the wide test temperature range involved it appears necessary to use Pyrex glass which can sustain large temperature differentials. Before the polymer is cast on to the circular glass substrate, the latter is coated with a thin (0.075 mm or 0.003") self-adhesive Teflon film, except for a centered circular portion with a diameter of 25.4 mm (1.0"). The Solithane 113 polymer is then cast on the glass slab following a procedure similar to one used to make the peel test specimens. The cure at room temperature eliminates the residual thermal stresses, but cannot avoid the cure shrinkage stresses whose magnitude has been determined previously [10].

The specimens, an example of which is shown in Figure 16, were tested in a Missimers temperature test chamber whose temperature can be controlled to within ± 1 °C. The temperature is recorded with the help of a Chromel-Alumel thermocouple.

3.4.2 Experimental Results

1. The first series of tests concentrated on cooling specimens from room temperature to temperatures well below ambient conditions. The thermal loading history is motivated by the analysis outlined before. Two different thicknesses are involved in the measurements, namely : 0.8 mm (1/32") and 1.6 mm (1/16"). The thickness is chosen such that the initial debond is equal to at least

the adhesive energy γ from its lower limit Γ reflects the rheological or dissipative properties of the polymer. This observation underlines the distinction between a rate independent, intrinsic energy of adhesion Γ and its rate dependent counterpart γ as stated by Müller and Knauss [1].

For very slow crack propagation one deals essentially with the intrinsic energy of adhesion Γ ; in this case the bulk of the polymeric coating does not experience pronounced viscoelastic effects. It seems prudent however to allow for viscous dissipation which occurs in any case near the crack tip, by increasing somewhat the value of the required adhesive energy γ. At higher crack speeds the rate-sensitivity of the viscoelastic material becomes much more significant and consequently one needs to use values of γ higher than Γ in an analysis in order to account for some viscous dissipation at non-zero crack growth rates.

If the layered structure is subject to temperature or moisture variations which induce viscoelastic behavior in the bulk of the polymer one needs to consider severe changes in material properties as well as the influence of the environment on the adhesive fracture energy. The former can be avoided by working in the temperature range far above the glass transition region of the polymer coating. The sensitivity of the fracture energy to temperature and moisture makes it necessary to determine the adhesive fracture energy γ under a wide range of environmental conditions. The influence of the temperature can be significant as experimentally verified in Chapter 2. By allowing variations on the value on γ, accounting for viscous effects as well as environmental conditions, the results of the elastic analyses enable us to make engineering estimates of the environmental conditions under which time-dependent adhesive failure of rubbery materials can occur.

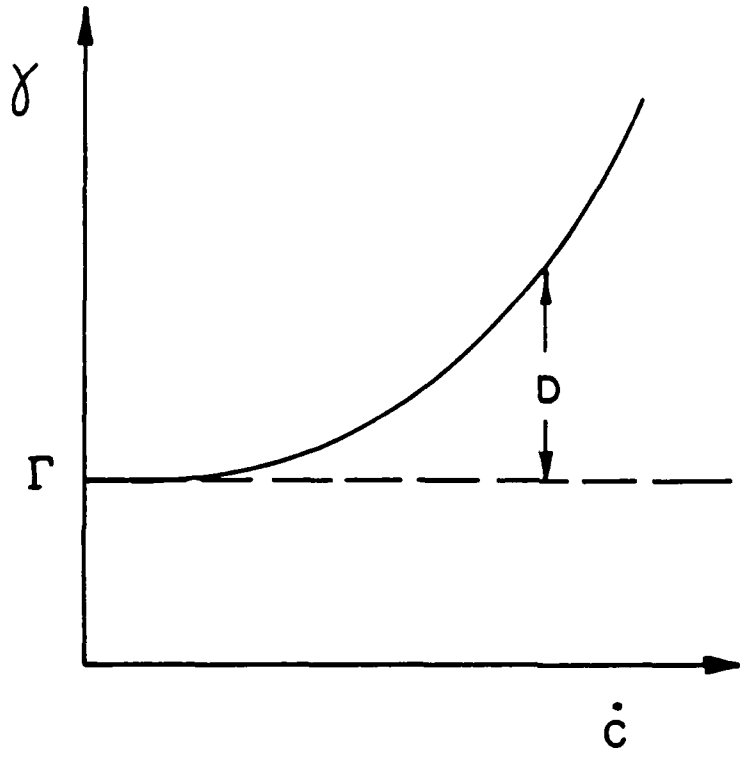

Figure 15. Schematic representation of the relation between the adhesive energy γ and the crack speed $\dot{c}$.

face energy Γ ; once this situation develops, the interface crack keeps running, i.e. no arrest phenomenon occurs as indicated in Figure 14.

3.3 Viscoelastic Effects

The two delamination configurations were analyzed for linearly elastic and isotropic materials. Most encapsulating and adhesive materials however display viscoelastic behavior when a wide range of temperatures is involved.

One might then question the wisdom of using the results of theses sample calculations presented in the previous sections, when time-dependent failure of rubbery materials is the subject of this study. First, it is worth noting that we restricted ourselves to the fracture behavior of a crosslinked polymer above its glass transition temperature range. Thereby pronounced viscous flow in the bulk of the polymer does not arise as well as significant nonlinear viscoelastic response to deformation which is more likely to occur below the glass transition and at the very tip of the interface crack. Some bulk relaxation could still occur, but its magnitude is very limited compared to the relaxation which a viscoelastic material experiences when going through the glass transition zone. Hence a corresponding variation of the elastic properties in the delamination sample calculations can account for any potential relaxation.

We still have to deal with the viscous dissipation occurring in the vicinity of the crack tip. Although the bulk dissipation can be calculated more easily, the precise contribution of the viscous processes in the immediate vicinity of the crack tip remains somewhat of an unknown. In order to be able to incorporate the importance of the dissipation on the unbonding process, one needs to take a closer look at the relation between the adhesive energy γ and the interfacial crack speed $\dot{c}$; such a graph is shown schematically in Figure 15, its shape being in agreement with the results of Chapter 2 (Figures 4 and 5). The deviation of

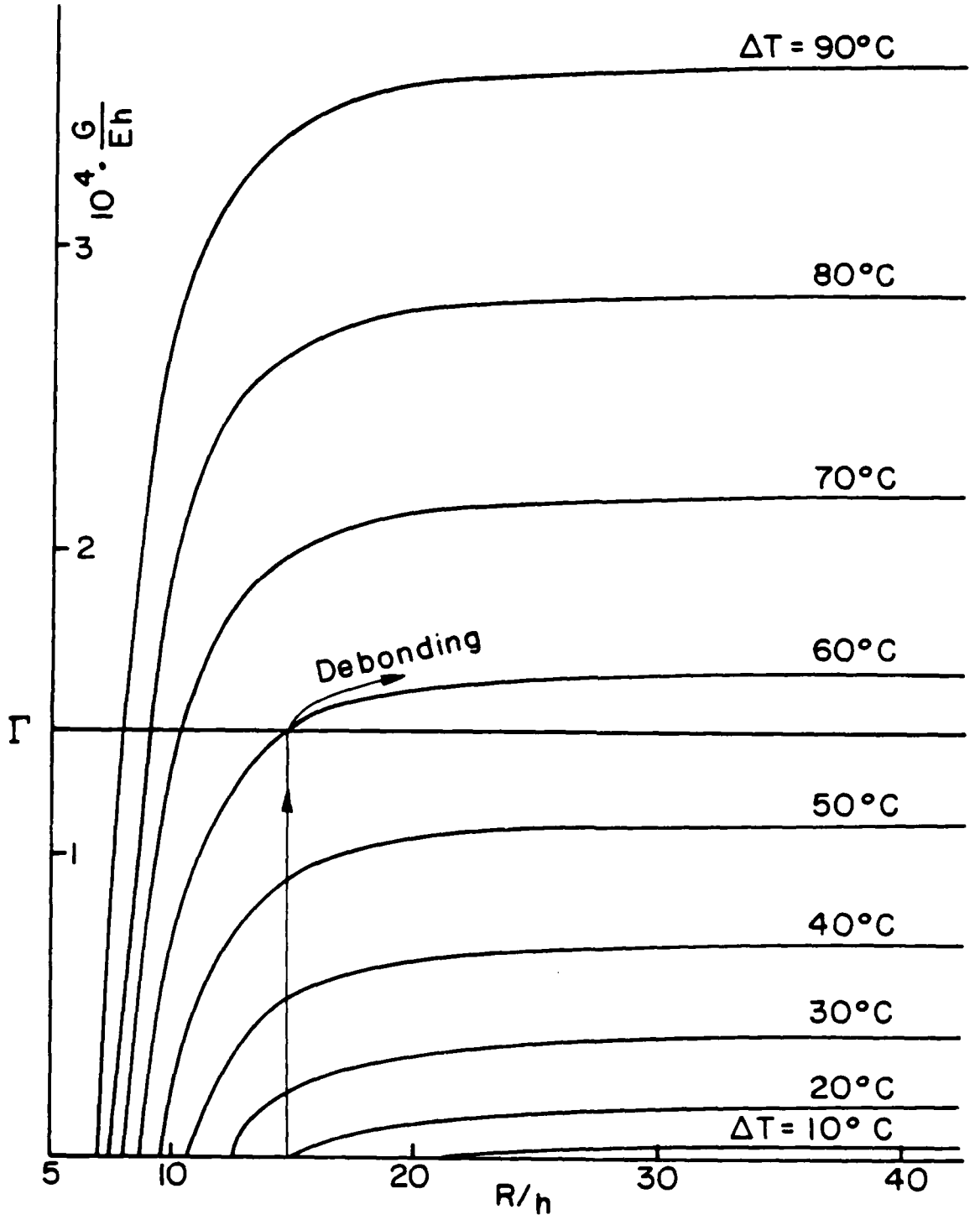

Figure 14. Strain energy release rate as a function of R/h for the central delamination.

$$\frac{R}{t} < \sqrt{\frac{1.223}{\alpha(1+\nu)} \cdot \frac{1}{T-T_o}} \qquad (35)$$

The elastic strain energy comprises the strain energy of bending and the strain energy of compression in the plate ; the total elastic energy using large deflection theory is given by :

$$U = \pi D \int_o^R \left[\ddot{w}^2 + 2\nu \ddot{w} \frac{\dot{w}}{r} + \left(\frac{\dot{w}}{r}\right)^2 \right] r\,dr$$

$$+ \frac{\pi Eh}{1-\nu} \int_o^R \left[\left(\dot{u} + \frac{1}{2}\dot{w}^2 \right)^2 + 2\nu \left(\dot{u} + \frac{1}{2}\dot{w}^2 \right) \frac{u}{r} + \left(\frac{u}{r}\right)^2 \right] r\,dr \qquad (36)$$

where a dot denotes differentiation with respect to r. The closed form evaluation of equation (36) using the expressions for for u and w (equations (30) and (31)) is intractable. We therefore prefer to evaluate the strain energy, given by equation (36) numerically, where ε_o involves a thermal strain only. Before applying the crack propagation criterion the energy, stored in an annulus of radius R and width Δ R, which is about to debond, has also to be accounted for. This material volume contains an amount of thermally induced energy equal to :

$$\Delta E_{th} = 2\pi R \Delta R \frac{Et}{1-\nu} \alpha^2 (T-T_o)^2 . \qquad (37)$$

For the delamination geometry the energy criterion formulated by equation (15) can then be written as :

$$G = -\frac{1}{2\pi R} \cdot \frac{\partial U}{\partial R} + \frac{1}{2\pi R} \cdot \frac{\partial E_{th}}{\partial R} \geq \Gamma \qquad (36)$$

which is evaluated numerically for thickness of h = 2.5 mm (0.1") and the mechanical properties of Solithane 113 [25]. The results are presented in Figure 14 where the strain energy release rate is non-dimensionalized by (Eh). If the temperature remains constant the crack starts growing if the debond is sizeable enough for the strain energy release rate G to exceed the necessary sur-

$$w(r) = b \cdot \frac{J_o(\gamma R) - J_o(\gamma r)}{J_o(\gamma R) - 1} \tag{30}$$

where b is the deflection at the center of the plate (r = 0) ; its amplitude still needs to be determined ; J_o denotes the Bessel function of zero order. A further result of the perturbation analysis is the in plane displacement,

$$u(r) = -\frac{P(1-\nu)}{Eh} r + \frac{b^2 \gamma}{4[J_o(\gamma R) - 1]^2} \Big\{ (1+\nu) J_o(\gamma r) J_1(\gamma r)$$

$$+ \nu \gamma r [J_o^2(\gamma R) - J_o^2(\gamma r) - J_1^2(\gamma r)] - \gamma r J_o^2(\gamma R) \Big\} \tag{31}$$

where the load P per unit length of circumference is :

$$P = P_c + 3.009 \frac{b^2 D}{R^2 h^2} \tag{32a}$$

and the buckling load P_c is

$$P_c = 14.68 \frac{D}{R^2} . \tag{32b}$$

The amplitude b of the deflection w(r) is now determined from the prescribed displacement at the clamped edges of the circular plate. At r = R one has :

$$u(R) = \varepsilon_o R = -\frac{1-\nu}{Et} R \left[P_c + 3.009 \frac{b^2 D}{R^2 t^2} \right] - \frac{\gamma^2 b^2}{4[J_o(\gamma R) - 1]^2} R J_o^2(\gamma R) \tag{33}$$

from which b^2 can be extracted as :

$$b^2 = -\frac{\left[\varepsilon_o + \frac{1.223}{(1+\nu)} \left(\frac{h}{R}\right)^2 \right]}{\left[\frac{0.51}{(1+\nu)} \frac{1}{R^2} + \frac{J_o^2(\gamma R)}{[J_o(\gamma R) - 1]^2} \frac{3.67}{R^2} \right]} \tag{34}$$

In equations (33) and (34) ε_o carries the same meaning as previously defined through equation (27). From equation (34) there follows a limiting value for R below which no buckling can occur for a prescribed specified strain $\varepsilon_o = -\alpha(T - T_o)$, a solution for b > 0 exists only if

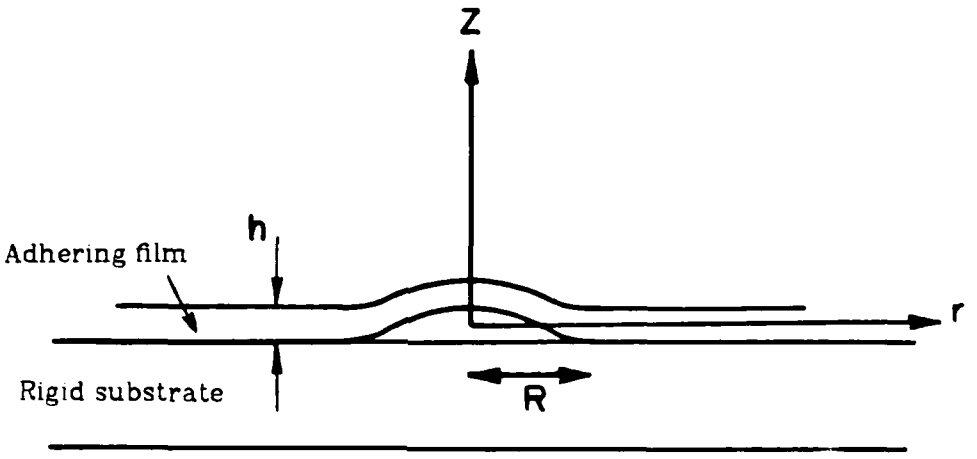

Figure 13. Geometry of the central delamination.

3.2 Central Delamination

The second example involves a blister type configuration which may be the result of prior loading or of defective manufacturing procedures where portion of the coating material has separated from its substrate as indicated in Figure 13. Subsequent heating expands and buckles the film, leading to possibly further crack propagation. Let a circular section of radius R be detached from the underlying adherend. As in the case of the edge delamination T_o is the temperature at which the bond was effected. In order to calculate the strain energy release rate G, we first proceed to find the deflection curve, which identifies the shape of the partially debonded coating.

Within the framework of plate analysis the problem reduces to thermally induced buckling of a circular plate with clamped edges. Assuming that the deflection surface is a surface of revolution, and denoting by φ the slope of the deformed plate, one finds [33]:

$$\varphi(r) = A_1 J_1(u) + A_2 Y_1(u) \tag{28}$$

where $J_1(u)$ and $Y_1(u)$ are Bessel functions of first order of the first and second kinds respectively, and

$$u = \lambda r$$

$$\frac{P_c}{D} = \lambda^2 \tag{29}$$

where r, P_c and D are, respectively, the distance of any point from the center of the plate, the critical (buckling) load per unit of circumference and the flexural rigidity of the plate. Thompson and Hunt [34] present the results of a continuum perturbation analysis of initial postbuckling behavior. The deflection of the circular plate is given by

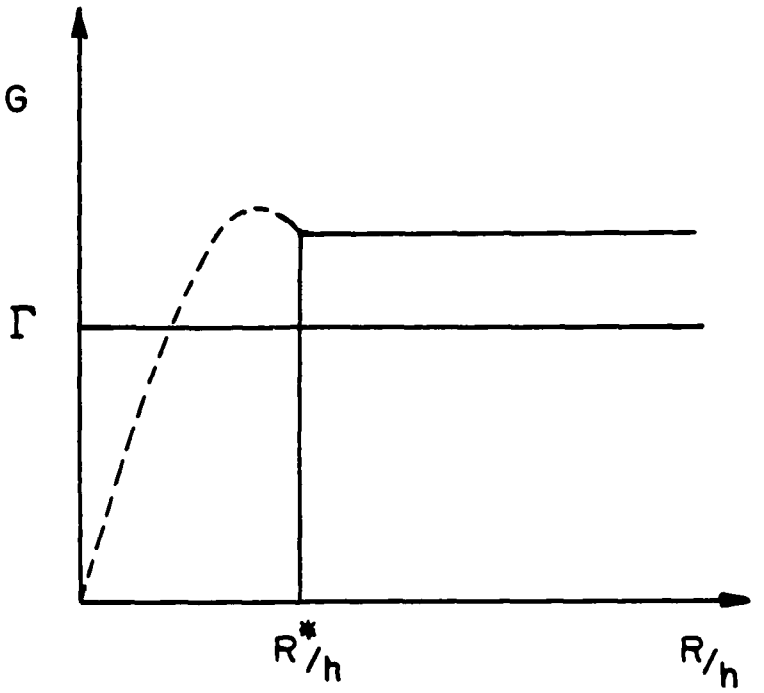

Figure 12. Strain energy release rate as a function of R/h for the edge delamination.

ture energy Γ. However, if one uses equation (2) to predict the temperature at which interfacial crack propagation can occur, there results that one needs to cool the bimaterial assembly (at least) below -10 °C in order for debonding to proceed. This calculation includes the zero time glassy response of the Solithane 113 adhesive layer ; the result also corresponds more closely with the experimentally observed temperature domains where adhesive failure occurs.

2. It was also attempted to cause debonding by heating the specimen well above ambient conditions. This effort proved futile as apparently no high enough stresses to cause crack propagation could build up. When heating the bimaterial specimens the Solithane 113 expands more than its substrate ; this expansion thus puts the crack tip under compression, thereby preventing further delamination.

REFERENCES

1. H.K. Müller and W.G. Knauss, The Fracture Energy and Some Mechanical Properties of a Polyurethane Elastomer, Trans. Soc. Rheol., 15 (1971) pp. 217-233.

2. A.N. Gent and R.P. Petrich, Adhesion of Viscoelastic Materials to Rigid Substrates, Proc. Roy. Soc. London, A 310 (1969) pp. 443-448.

3. A.N. Gent, Adhesion of Viscoelastic Materials to Rigid Substrates II. Tensile Strength of Adhesive Joints, J. Poly. Sci., Part A-2, 9 (1971) pp. 283-293.

4. A.N. Gent and A.J. Kinloch, Adhesion of Viscoelastic Materials to Rigid Substrates III. Energy Criterion for Failure, J. Poly. Sci. , Part A-2, 9 (1971) pp. 659-668.

5. E.H. Andrews and A.J. Kinloch, Mechanics of Elastomeric Adhesion, J. Polymer Sci. Symposium No. 46, (1974) pp. 1-14.

6. E.H. Andrews and A.J. Kinloch, Mechanics of Adhesive Failure I, Proc. Roy. Soc. London, 332 (1973) pp. 385-399.

7. E.H. Andrews and J. Kinloch, Mechanics of Adhesive Failure II, Proc. Roy. Soc. London, 332 (1973) pp. 401-414.

8. G.P. Anderson, S.J. Bennett and K.L. Devries, Analysis and Testing of Adhesive Bonds, Academic Press, New York (1977).

9. A.J. Kinloch, The Science of Adhesion, Part 2 Mechanics and Mechanisms of Failure, J. Mat. Sci., 17 (1982) pp. 617-651.

10. K.M. Liechti, Ph.D. Dissertation, California Institute of Technology (1980).

11. G.G. Trantina, Combined Mode Crack Extension in Adhesive Joints, J. Comp. Mat., 6 (1972) pp. 371-385.

12. G.P. Anderson, K.L. Devries and M.L. Williams, The Influence of Loading Direction upon the Character of Adhesive Debonding, J. Colloid & Interface Sci. 47 (1974) pp. 600-609.

13. A.D. Crocombe and R.D. Adams, Peel Analysis Using the Finite Element Method, J. Adhesion, 12 (1981) pp. 127-139.

14. M.L. Williams, The Stresses Around a Fault or Crack in Dissimilar Media, Bull. Seism. Soc. of America, 49 (1959) pp. 199-204.

15. G.C. Sih and J.R. Rice, The Bending of Plates of Dissimilar Materials with Cracks, J. Appl. Mech., 31 (1964) pp. 477-482.

16. J.R. Rice and G.C. Sih, Plane Problems of Cracks in Dissimilar Media, J. Appl. Mech., 32 (1965) pp. 418-423.

17. A.H. England, A Crack Between Dissimilar Media, J. Appl. Mech., 32 (1965) pp. 400-402.

18. F. Erdogan, Stress Distribution in Bonded Dissimilar Materials with Cracks, J. Appl. Mech. 32 (1965) pp. 403-410.

19. J.K. Knowles and E. Sternberg, Large Deformations Near a Tip of an Interface Crack Between Two Neo-Hookean Sheets, Technical Report No. 48, Contract N00014-75-C-0196, California Institute of Technology, September 1981.

20. M.L. Williams, Stress Singularities, Adhesion and Fracture, Proceedings 5th U.S. National Congress of Applied Mechanics, Minneapolis (1966).

21. W.G. Knauss, On the Steady Propagation of a Crack in a Viscoelastic Sheet : Experiments and Analysis, Deformation and Fracture of High Polymers, Ed. H.H. Kausch, J.A. Massell and R.I. Jaffee, Plenum Press, (1973) pp. 501.

22. W.G. Knauss, Fracture Mechanics and the Time Dependent Strength of Adhesive Joints, J. Comp. Mat., 5 (1971) pp. 176-192.

23. C.C. Hong and M. Stern, The Computation of Stress Intensity Factors in Dissimilar Materials, J. Elasticity, 8 (1978) pp. 21-34.

24. R.E. Smelser, Evaluation of Stress Intensity Factors for Bimaterial Bodies Using Numerical Crack Flank Displacement Data, Int. J. Fracture, 15 (1979) pp. 135-143.

25. W.G. Knauss and H.K. Mueller, The Mechanical Characterization of Solithane 113 in the Swollen and Unswollen State, GALCIT SM 67-8, California Institute of Technology, Pasadena, California, (1968).

26. G.P. Anderson, K.L. Devries and M.L. Williams, The Peel Test in Experimental Adhesive Fracture Mechanics, Experim. Mech., 14 (1974) pp. 89-97.

27. K. Kendall, Peel Adhesion of Solid Films, J. Adhesion, 5 (1973) pp. 179-202.

28. D.W. Aubrey and S. Ginosatis, Peel Adhesion Behaviour of Carboxylic Elastomers, J. Adhesion, 12 (1981) pp. 189-198.

29. A.D. Crocombe and R.D. Adams, An Elasto-Plastic Investigation of the Peel Test, J. Adhesion, 13 (1982) pp. 241-267.

30. N.A. Lange, Handbook of Chemistry, Mc Graw-Hill, New York (1961) p. 1194.

31. E.J. Ripling and S. Mostovoy, Fracture Mechanics: A Tool for Evaluating Structural Adhesives, J. Adhesion, 3 (1971) pp. 107-123.

32. J.L. Gardon, Some Destructive Cohesion and Adhesion Tests, Treatise on Adhesion and Adhesives, Ed. R.L. Patrick (1967), pp. 269-324.

33. S.P. Timoshenko and J.M. Gere, Theory of Elastic Stability, Mc Graw-Hill (1961).

34. J.M.T. Thompson and G.W. Hunt, A General Theory of Elastic Stability, Wiley, New York (1973).

CRACK PROPAGATION IN VISCOELASTIC MATERIALS UNDER TRANSIENT LOADING WITH APPLICATION TO ADHESIVELY BONDED STRUCTURES

Thesis by

Samuel K.Y. Chang

In Partial Fulfillment of the Requirements

for the Degree of

Aeronautical Engineer

Graduate Aeronautical Laboratories

California Institute of Technology

Pasadena, CA 91125

December 1983

ACKNOWLEDGEMENTS

I would like to express my appreciation and grattitude to Professor W.G. Knauss for his guidance, inspiration and encouragement.

I would like to thank Clarence Hemphill and Francis Waiyaki for their help in the laboratory, and I would also like to thank Marta Nyiri for the excellent work in typing this thesis.

This work was performed under the sponsorship of the Airforce Office of Scientific Research, Grant No. AFOSR-81-0127, with Major David Glasgow as the technical monitor. This support, as well as Major Glasgow's understanding assistance, is gratefully acknowledged.

I dedicate this thesis to my parents, my wife, Rita, and my sister, Dora, for their prayers and supports.

TABLE OF CONTENTS

ABSTRACT

Linear viscoelasticity theory is applied to the fatigue problem of solids sensitive to the deformation rate. A series of experiments have been performed to investigate the range of applicability in which the theory is valid and to examine the accuracy of the theory. The experimental results are compared with an existing theory.

1. INTRODUCTION

Compared to 10 or 20 years ago there are many situations in engineering today where polymers are used for structural purposes. This use occurs in the civil engineering sector; in water- and gas piping constructed from Polyvinylchloride; in agriculture for irrigation and desalination purposes; in many household goods and in particular in the automotive industry. In the transportation industry polymers are widely used in automobile tires as well as in automotive body components. In the aerospace industry polymers are used to a large extent as sealants, as structural bonding agents, as well as bonding together fibers to make composite materials. The composite materials may be either of continuous, or chopped fiber type. Inasmuch as a very large percentage of engineering application of any materials encounters transient or periodic loading, it is appropriate that one give attention to the fracture behavior of these types of materials in a fatigue-type of environment.

We associate with the terminology "fatigue" the phenomenon that failure or fracture of a component occurs under a cyclic load environment at stress or load levels that are significantly lower than those that might have been sustained by the part if only a steady continuous load had been imposed. In the context of time-dependent failure of polymeric material this definition may or may not be appropriate. We know, for example, that even when steady loads are imposed on a viscoelastic material, fracture will occur in a time-delayed manner due to the slow and time-dependent growth of cracks in such a material. This phenomenon has often been associated with the term of "static fatigue". Under such circumstances it would be appropriate by the classical definition of fatigue to add into that definition some measure of a comparative time length or life so as to assess whether a cyclic or repetitive loading leads to an acceleration over the appropriate steady-state environment to which a part might be subjected.

By and large the study of fatigue in polymeric materials has been, to date, confined essentially to rigid polymers. In this connection fatigue in polymers has been treated by virtually the same methods that are normally applied to the fatigue of structural metals. Because a detailed understanding of the fatigue process in metals and also in the rigid polymers does not exist from a basic point of view, one has generally resorted to analyzing crack propagation rates under fatigue type loading as a function of the difference between maximum and minimum stress intensity factor. The resulting test curves have often come to represent essentially the fatigue material behavior instead of the S-N curves that were part of standard fatigue analysis only three decades ago.

From an engineering point of view, this may be quite an acceptable approach for dealing with the fatigue problem when the polymer is definitely in the rigid state. However, there are many situations, in particular in aerospace applications, where the material is exposed to elevated temperatures to such a degree that while substantial softening is not achieved the load duration and the fatigue environment may last long enough so that a substantial amount of damage is incurred in this elevated temperature stage. Inasmuch as at elevated temperatures polymers tend to become significantly viscoelastic, the question arises as to how the fatigue process is governed in this kind of environment when strong viscoelastic effects are present.

It appears reasonable to view the fracture behavior or failure behavior of polymeric materials from the point of view of fracture mechanics, that is, the failure behavior of these materials in the presence of preexisting cracks. In this context, it becomes reasonable therefore to inquire as to how cracks propagate in a material when strong viscoelastic material behavior is present and when the load history of the component is cyclic in nature. Inasmuch as there is at this time only an approximate theory [1] that deals with crack propagation in

polymers under cyclic conditions of loading it is appropriate to examine this problem in some detail and to do so from an experimental point of view.

At this time our foundation for understanding the propagation of cracks in viscoelastic material is based on linear viscoelastic material response. For the case of linearly viscoelastic behavior this foundation is outlined essentially in [2], while similar developments based on special material representation are covered in [3] and [4]. These developments are documented specifically for propagation theory at constant velocities, where the underlying assumption is that the crack propagation is applicable instantaneously in situations where the stresses at the tip of the crack change continuously with time. It turns out that for many situations this underlying assumption is not a serious restriction at all. However, it appears questionable to what extent these relations are applicable when the stresses change rather rapidly at the tip of the moving crack. As has been pointed out in [5], if the crack-tip stresses change rapidly compared to a length parameter characterizing a thin zone of fracturing material along the crack path, then these approximations involving constant rates of crack propagation may no longer be applicable. The fully analytical exploration of this question seems too cumbersome at this time. Rather, one would feel that it is more appropriate to examine this problem initially experimentally. Subsequent to such an experimental investigation one would then find more justification or motivation to explore particular ranges of material behavior where perhaps more suitable approximation are appropriate.

2. REVIEW OF EXISTING LINEAR FRACTURE THEORY

We shall summarize here briefly the developments in [2]. Consider the tip of a crack moving through a (linearly) viscoelastic material. This tip is characterized by a damage or process zone in which the material behaves non-linearly. If this zone is sufficiently small, one may make use of the linearized theory of viscoelasticity along with a line model for the process zone according to Prandtl, Barenblatt or Dugdale. The process zone needs to be incorporated to provide a length scale parameter that couples the material viscosity to a crack propagation speed. In *Ref. 2* two criteria of fracture were explored: a crack-opening displacement and an energy criterion. Both gave essentially identical results. It suffices, therefore, to consider only one, the energy criterion.

The energy criterion states that the rate of work done by the unloading tractions on the displacements in the (line) plastic zone equals the rate of fracture energy absorption, which, in the simplest form, may be considered to be a constant Γ times the crack speed $\dot{c}$. Under the assumption of *constant* crack propagation speed that criterion leads to the relation (for Poisson's ratio $\nu = 1/2$)

$$K^2\Theta\left[\frac{\alpha}{\dot{c}}\right] = \frac{4}{3}E_\infty\Gamma \tag{1}$$

where

K = stress intensity factor

α = length of (line) cohesive or process zone

Γ = rate independent fracture energy

$\dot{c}$ = rate of crack growth

$$\frac{\Theta(t)}{E_\infty} = \int_0^t\int_\rho^\infty \{D\left[\frac{\alpha}{t}(r-\rho_o)\right] - D(o)\}\frac{dF^+(r)}{dr}\,dr\,d\rho = D \tag{2}$$

$$F^+(r) = \sqrt{1-r} + \frac{1}{2}\left[\frac{1-r}{2}\ln\frac{\sqrt{1-r}+1}{\sqrt{1-r}-1} - \sqrt{1-r}\,r\right]$$

$D(t)$ = uniaxial creep compliance

$$E_{\infty} = \frac{1}{D(\infty)}$$

In this context we note that eqn. (1) holds rigorously for $\dot{c}$ = const. and approximately for $\dot{c}$ const. ***provided*** (see Ref. 2)

$$\frac{|\dot{K}(t)|}{K(t)} << \frac{\dot{c}(t)}{2a(t)} \tag{3}$$

This question of describing crack growth analytically by an equation like (1) was addressed in a previous analysis which was based on crack growth by small but finite increments [1] but which did not limit itself to the cases allowed by [2]. The net result of that analysis was that if viscoelastic transients become important (i.e. if the equation (3) above is violated) then crack propagation per cycle should occur more rapidly than if only the quasi-steady relations (1) is involved ($\dot{c}$ = const.). Inasmuch as equation (1) is much easier to apply than the work in Ref. 1 one may raise the question whether the deficiency associated with violation of (3) is really important: After all, a problem may exist only near $\dot{c}$=0, so that the total amount of crack growth accumulated near the "crack growth boundary"[1] is very small to begin with and thus possibly an important contribution to the total crack length. The constraint (3) is always violated when a crack tip experiences loading that passes through the limit for possible crack propagation: Below and at this limit $\dot{c}$ = 0 but $\dot{K}(t) \neq 0$; the same is true for conditions above this limit where both $\dot{K}$ and $\dot{c}$ exceed zero, but still close enough to the propagation limit so that the order relation is violated. The question arises thus to what extent equation (1) can represent crack growth under conditions when the propagation boundary is passed, particularly passed repeatedly as in a cyclic history. It is possible that equation (1) would be more powerful than the analytical estimates would indicate. It appears, however, reasonable to expect

1. Crack growth is not possible if the stress intensity is below a certain value say K^*; above K^* crack growth occurs. We call K^* the crack growth boundary.

that the range of validity of (1) is somehow limited by the inequality (2) and that the argument of "small crack growth contribution" means that the propagation boundary may only extend the range of validity for (1) somewhat.

In view of this situation it is appropriate to examine the crack growth behavior under transient rather than steady loading conditions experimentally. The results of such an investigation would then provide further input to analytical formulations that elucidate the behavior of crack growth under rather arbitrary transient loading histories. Because of its technical importance as well as the ease with which small crack growth can be accumulated over many cycles into a readily measurable quantity, cyclic deformation histories seem to be well suited to this study.

For later reference it should be pointed out that evaluation of crack growth under transient load histories, if governed by equation (1), was carried out in considerable detail in [6]; this study will serve as a guide and reference against which the experimental results can be compared.

We proceed next to a description of the experimental set-up and analysis of the experimental technique (caustics). Following these developments we turn to the recording and then analysis of the experimental results.

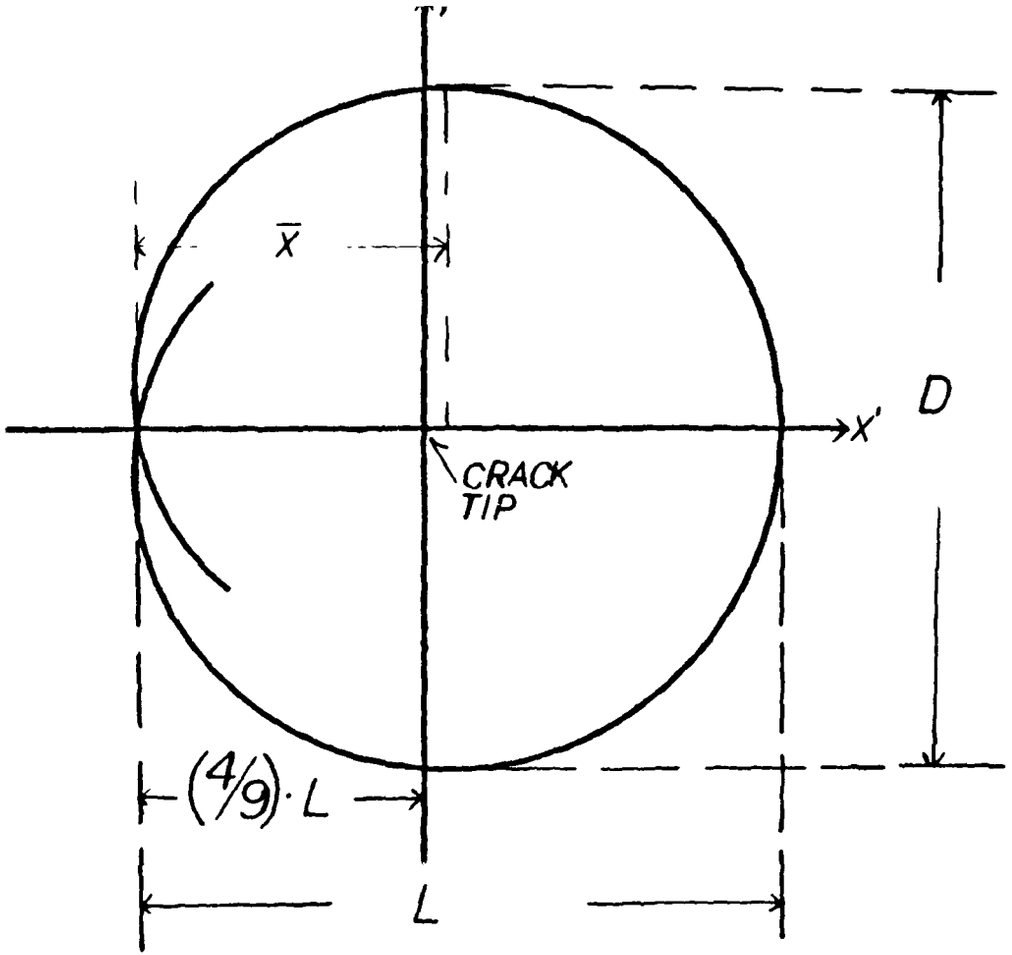

Figure 3.8 Location of crack tip relative to caustic.

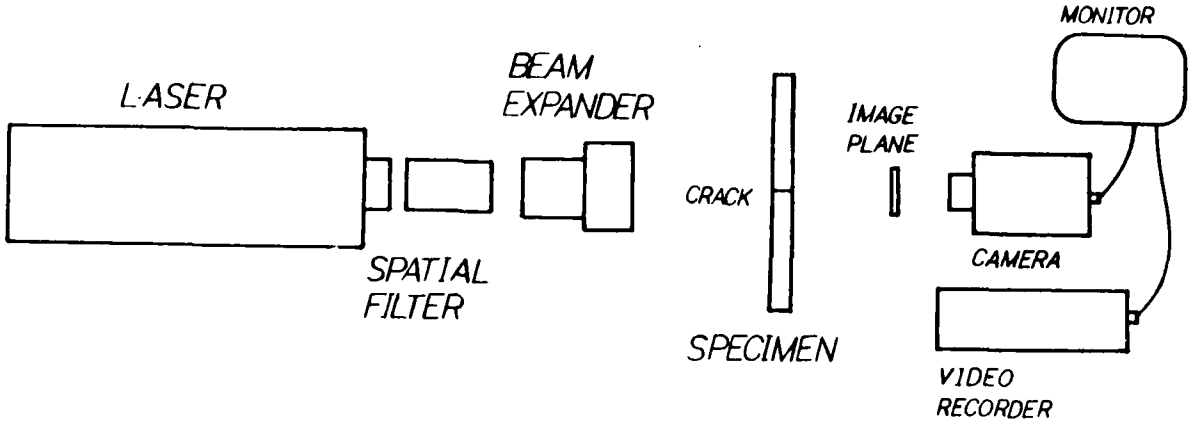

Figure 3.7 Experimental set-up for cyclic crack growth experiment.

It should be mentioned that we shall be interested in a moving crack, while the caustic relation (15) corresponds to a stationary crack. However, the crack will be moving so slowly that dynamic effects are irrelevant so that the present analysis is totally adequate to deal with the later test situations.

3.3 Experimental Procedure

We shall attempt to study crack growth as a function of the *maximum* stress intensity during any cycle. Thus it will be necessary to record the maximal caustic diameter D during any cycle. This is accomplished in the set-up shown in Figure 3.7.

A Spectra Physics Model 120 Laser shines light through a spatial filter and beam expander onto the crack tip of a specimen supported in a (servo-hydraulic) test machine. The image plane is formed by a translucent piece of paper with mm rulings . This arrangement allows virtually continual monitoring of the caustic size by means of a video camera and recorder. Data is reduced later from the video tapes.

3.4 Caustic Data Analysis

In order to avoid buckling of the specimen, only tension-tension cycling was performed such that there was always tension on the specimen. The lowest value of the caustic was used to locate the tip of the crack relative to the boundary. It turns out that the location of the crack tip is determined relative to the caustic by the discussions shown in Figure 3.8. The computation of these dimensions are shown in Appendix B. The diameter of the caustic under maximum load is measured (off the video-play back) as a function of crack length in the same cycle. It will be noted from equation (15) that the stress intensity factor can be determined if all the parameters characterizing the material as well as the experimental set-up are known. It turned out that some of this informations was

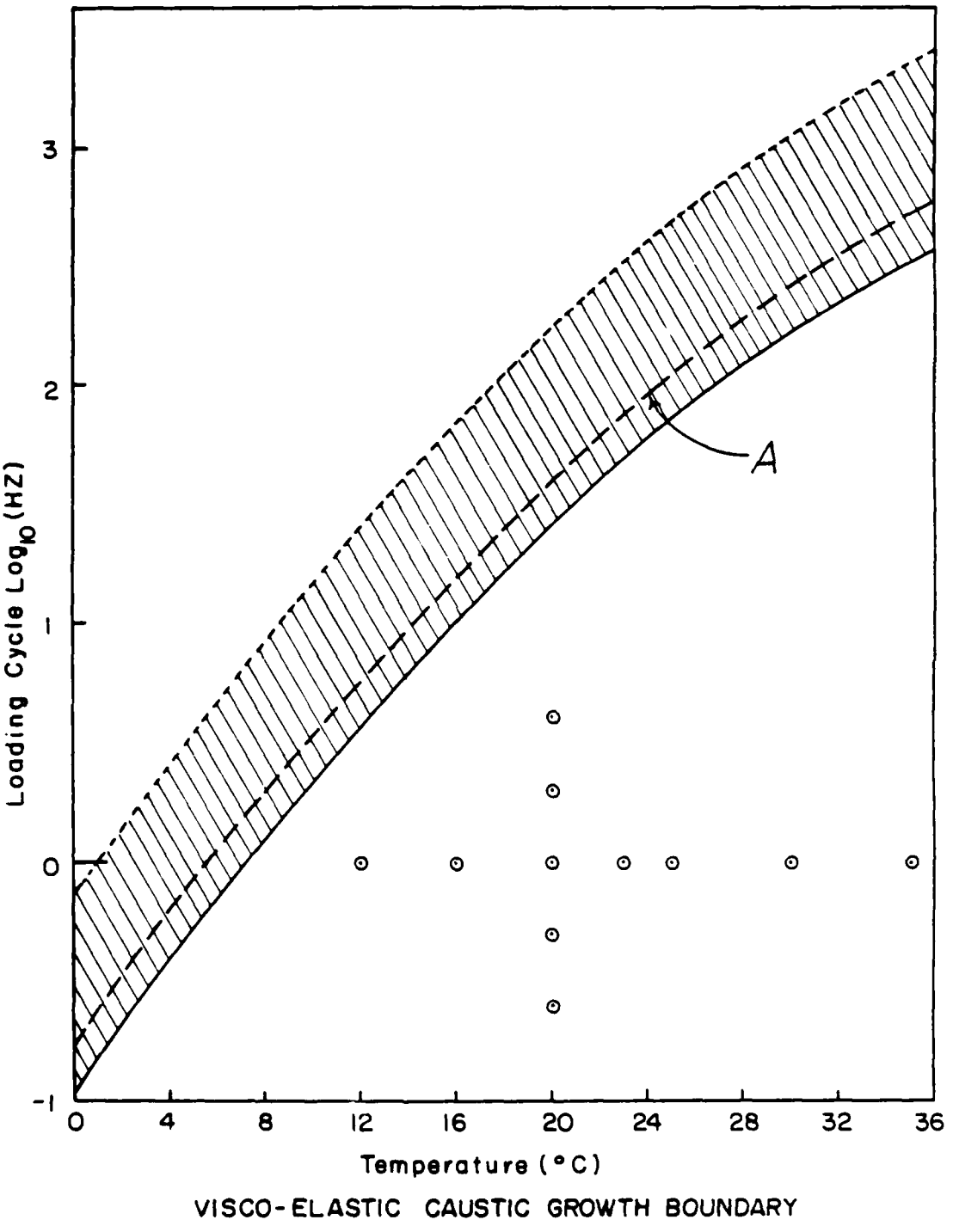

Figure 3.6 Curve A corresponds to 10^{-1} minutes in Figure 3.5

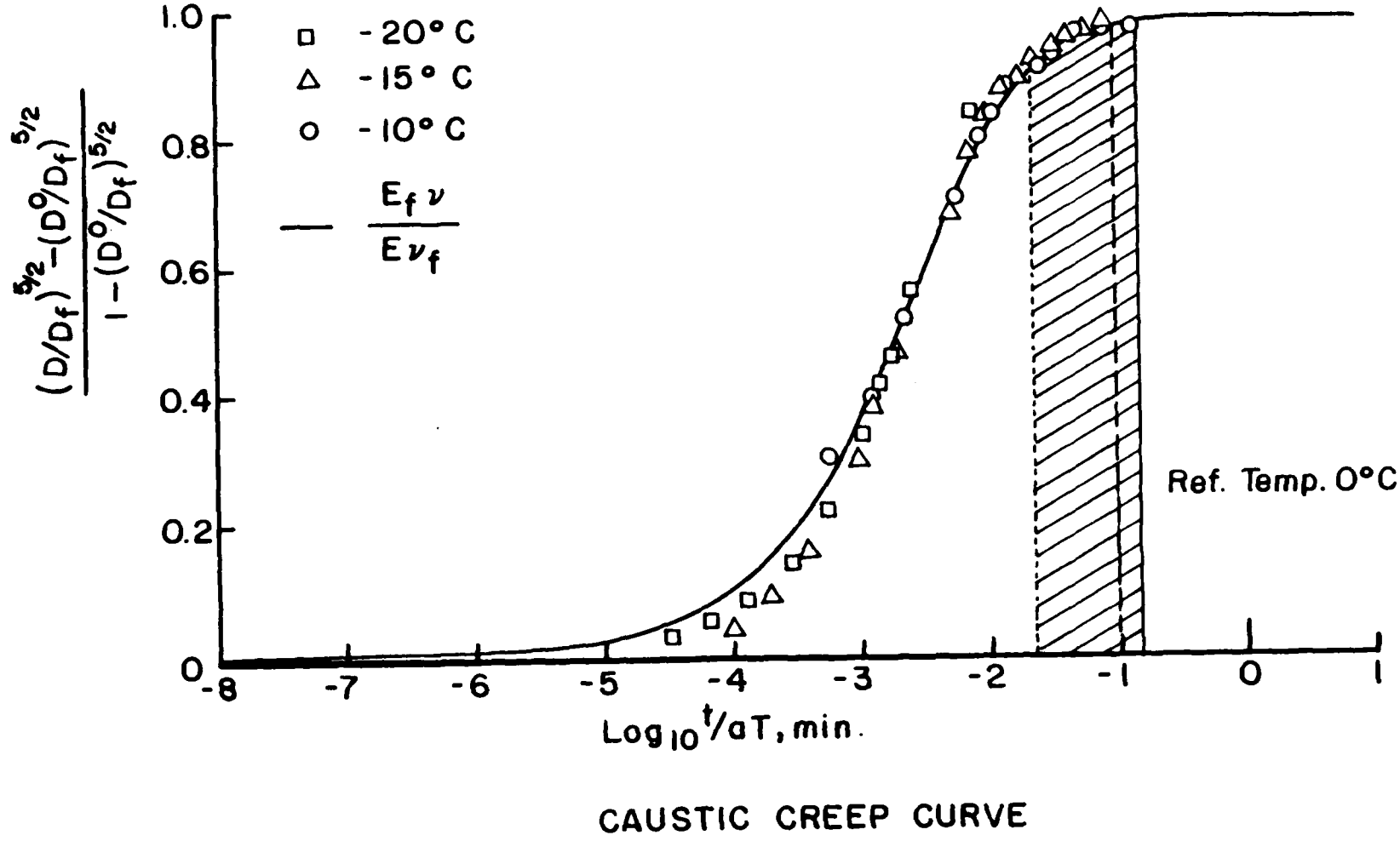

Figure 3.5 Experimental and analytical dependence of the caustic diameter on time for step loading (from Ref. 7).

$$K_I(t) \bullet \lambda(t) = \frac{2\sqrt{2\pi}}{3f^{\frac{5}{2}} \cdot h \cdot z_o} D^{\frac{5}{2}} \tag{14}$$

Thus by measuring the "caustic diameters" D(t) as a function of time, the corresponding stress intensity factor K can be calculated from (14).

The determination of K requires the solution of an (convolution) integral equation; this is not a trivial matter, in general. For further work here we therefore make use of results in [7] which establishes an excellent approximation for the test material and load histories used in this investigation. In [7] it was established that essentially elastic conditions prevail for times longer than 10^{-1} min (cf. Figure 3.5) at a temperature of 0°C. It was also shown that the time-temperature equivalence principle holds. With this information it is possible to determine those conditions on temperature and test frequency for which elastic rather than fully viscoelastic conditions prevail. With this information one is able to construct a curve of frequency vs. temperature that "separates" the elastic from the viscoelastic behavior[1]

This relation is shown in Figure 3.6 along with the test conditions (as points) used in the later experiments. It is clear from these considerations that the caustic data gathered in the subsequent tests can be used to compute the stress intensity factor from the elastic solution represented by equation (15) where the constant λ (definition following equation (3)) incorporates the long time or rubbery Young's modulus of the test material.

$$K_I(t) = \frac{2\sqrt{2\pi}\, D(t)^{\frac{5}{2}}}{3f^{\frac{5}{2}} h z_o \lambda} \tag{15}$$

1. This curve shown is, of course, a sharp demarcation instead of the "region" in which viscoelastic behavior is weak. For this reason the curve is adjoined by a shaded region, in which viscoelasticity behavior is minimal.

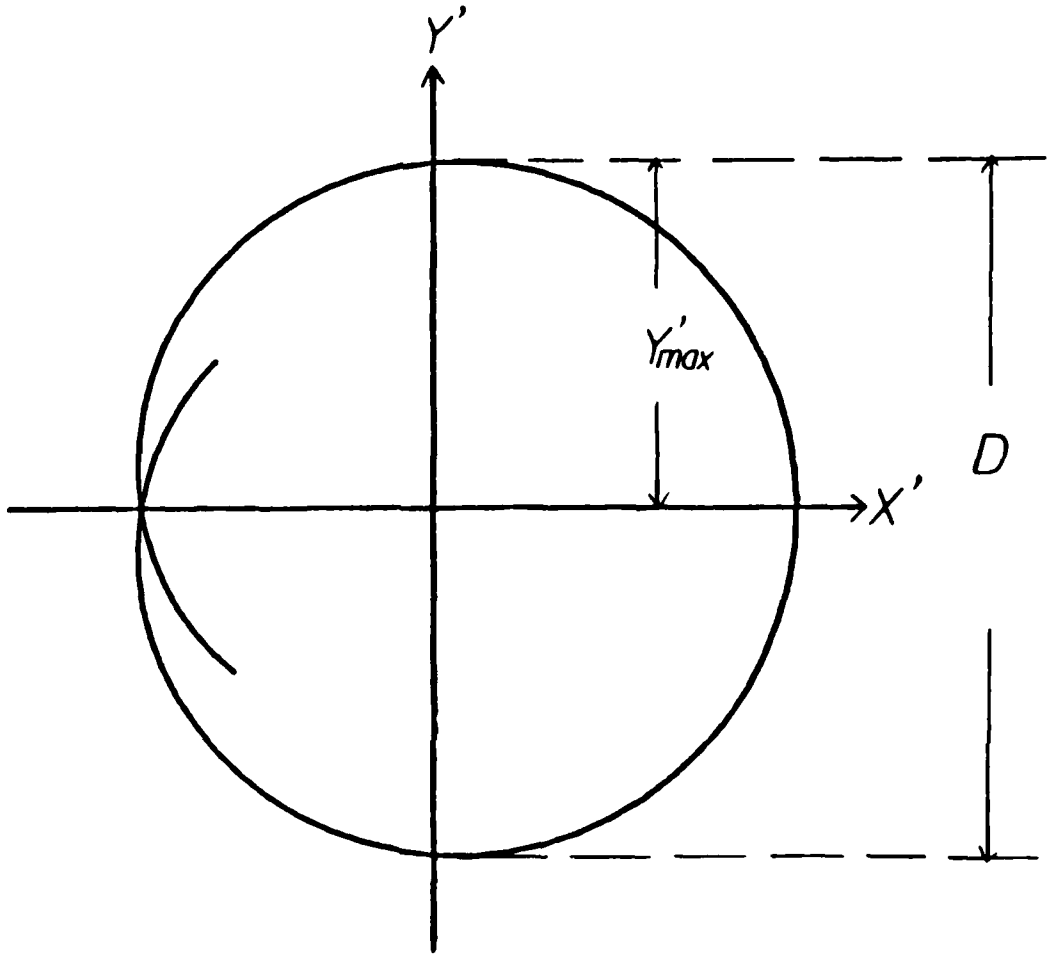

Figure 3.4 Computed caustic.

singularity condition (J = Jacobian of x', y'with regard to r, φ)

$$J = \frac{\partial x'}{\partial r}\frac{\partial y'}{\partial \varphi} - \frac{\partial x'}{\partial \varphi}\frac{\partial y'}{\partial r} = 0 \tag{10}$$

If we define the curve $r(\varphi)$ in the object plane from which the rays fall on the caustic curve in the image plane as $r = r_s(\rho)$, then this relation yields that

a. The radius r_s is independent of ρ; i.e., the curve is a circle with center at the crack tip; this curve is called the "initial curve."

b. the radius r_s of the initial curve is given by

$$r_s = \left\{ \frac{3}{2} \frac{hz_o}{\sqrt{2\pi}} [\, \lambda(t) \cdot K_I(t) \,] \right\}^{\frac{2}{5}} \tag{11}$$

The image of that initial curve (circle), i.e., the caustic is given by equation (9) together with (11) as

$$X' = r_s(\cos\varphi + \frac{2}{3}\cos\frac{3}{2}\varphi) \tag{12a}$$

$$Y' = r_s(\sin\varphi + \frac{2}{3}\sin\frac{3}{2}\varphi) \tag{12b}$$

A plot of equations (12) is given in Figure 3.4 for a particular time when r_s is some constant. Now define $D=2Y'_{max}$ (cf. Fig. 3.4). Then

$$\begin{aligned} D &= 2 \cdot \max [\, r_s (\sin\varphi + \frac{2}{3}\sin\frac{3}{2}\varphi) \,] \\ &= 2r_s \max (\sin\varphi + \frac{2}{3}\sin\frac{3}{2}\varphi) \\ &= r_s f \end{aligned} \tag{13}$$

where

$$f = 2 \cdot \mathrm{Max}(\sin\varphi + \frac{2}{3}\sin\frac{3}{2}\varphi)$$

Use of (13) together with (11) renders the convolution relation

$$\Delta s = h \cdot \lambda(\sigma_1 + \sigma_2) . \tag{4}$$

For viscoelastic and optically isotropic materials the corresponding relation is in the form of a convolution, namely

$$\Delta s = h \cdot \lambda \ * \ \sigma \tag{5}$$

where the star (*) notation signifies the Stieltje's Integral. Thus, the optical path change within the material is a function of the stress and deformation history. Recall that in linear elasticity the stresses near the crack tip (in the object plane) are

$$\sigma_x = \frac{K_I(t)}{\sqrt{2\pi r}} \cos\frac{\varphi}{2}\left(1 - \sin\frac{\varphi}{2}\sin\frac{3\varphi}{2}\right) + \cdots \tag{6a}$$

$$\sigma_2 = \frac{K_I(t)}{\sqrt{2\pi r}} \cos\frac{\varphi}{2}\left(1 + \sin\frac{\varphi}{2}\sin\frac{3\varphi}{2}\right) + \cdots \tag{6b}$$

$$\tau_{xy} = \frac{K_I(t)}{\sqrt{2\pi r}} \cos\frac{\varphi}{2}\sin\frac{\varphi}{2}\cos\frac{3\varphi}{2} \quad + \cdots \tag{6c}$$

It follows that the stress invariant $\sigma_1 + \sigma_2 = \sigma_x + \sigma_y \equiv \sigma$ is

$$\sigma = \frac{K_I(t)}{\sqrt{2\pi r}} 2\cos\frac{\varphi}{2} . \tag{7}$$

Therefore equation (1) becomes, with the help of Equations (5) and (6)

$$\vec{r}' = \vec{r} + dz_o(\lambda(t) \ * \ K_I(t)) \nabla \left(\sqrt{\frac{2}{\pi r}} \cos\frac{\varphi}{2}\right) \tag{8}$$

which, in Cartesian components is equivalent to

$$x' = r\cos\varphi - dz_o[\ \lambda(t) \ * \ K_I(t)\ ] \frac{1}{\sqrt{2\pi}} r^{-\frac{3}{2}} \cos\frac{3}{2}\varphi \tag{9a}$$

$$y' = r\sin\varphi - dz_o[\ \lambda(t) \ * \ K_I(t)\ ] \frac{1}{\sqrt{2\pi}} r^{-\frac{3}{2}} \sin\frac{3}{2}\varphi \tag{9b}$$

We next observe that in the image plane, the caustic is the envelope of all singular points for equations (9a) and (9b). Thus the caustic can be expressed by the

be deflected to intersect the image plane at the point P''. By the geometry in Figure 3.3, we have then

$$\vec{r}' = \vec{r} + \vec{w}(r,\varphi) \tag{1}$$

where $\vec{w}(r,\varphi)$ is a deviation vector. Applying the theory of the eikonal one has

$$\vec{w}(r,\varphi) = z_o \nabla \left(\Delta s(r,\varphi) \right) \tag{2}$$

where $\Delta s(r,\varphi)$ is the total change in light path orientation as the ray passes through the material. By the Maxwell-Neumann stress optic law and Hooke's law one has for Δs

$$\Delta s = h \cdot \lambda \left[(\sigma_1 + \sigma_2) \pm (\sigma_1 - \sigma_2) \cdot p \right] \tag{3}$$

where the following definitions hold

$$\lambda = \frac{\lambda_1 + \lambda_2}{2} - (n-1)\frac{\nu}{E}$$

$$p = \frac{\lambda_1 - \lambda_2}{\lambda_1 + \lambda_2 - 2(n-1)\frac{\nu}{E}}$$

h = thickness of the plate

λ_1, λ_2 = stress optical constants

σ_1, σ_2 = principal stresses

E = modulus of elasticity

ν = Poisson's ratio

n = index of refraction

If $\lambda_1 \neq \lambda_2$ the material is called optically anisotropic, or birefringent. The consequence is that $p \neq 0$ and therefore Δs has two values. Therefore there will be two vectors $\vec{w}$, i.e. there will be two caustics. It turns out, *practically* speaking, that Solithane 113 (50/50) is optically isotropic, i.e. $\lambda_1 = \lambda_2$, and $p = 0$, so that only one caustic is observed. For optically isotropc materials

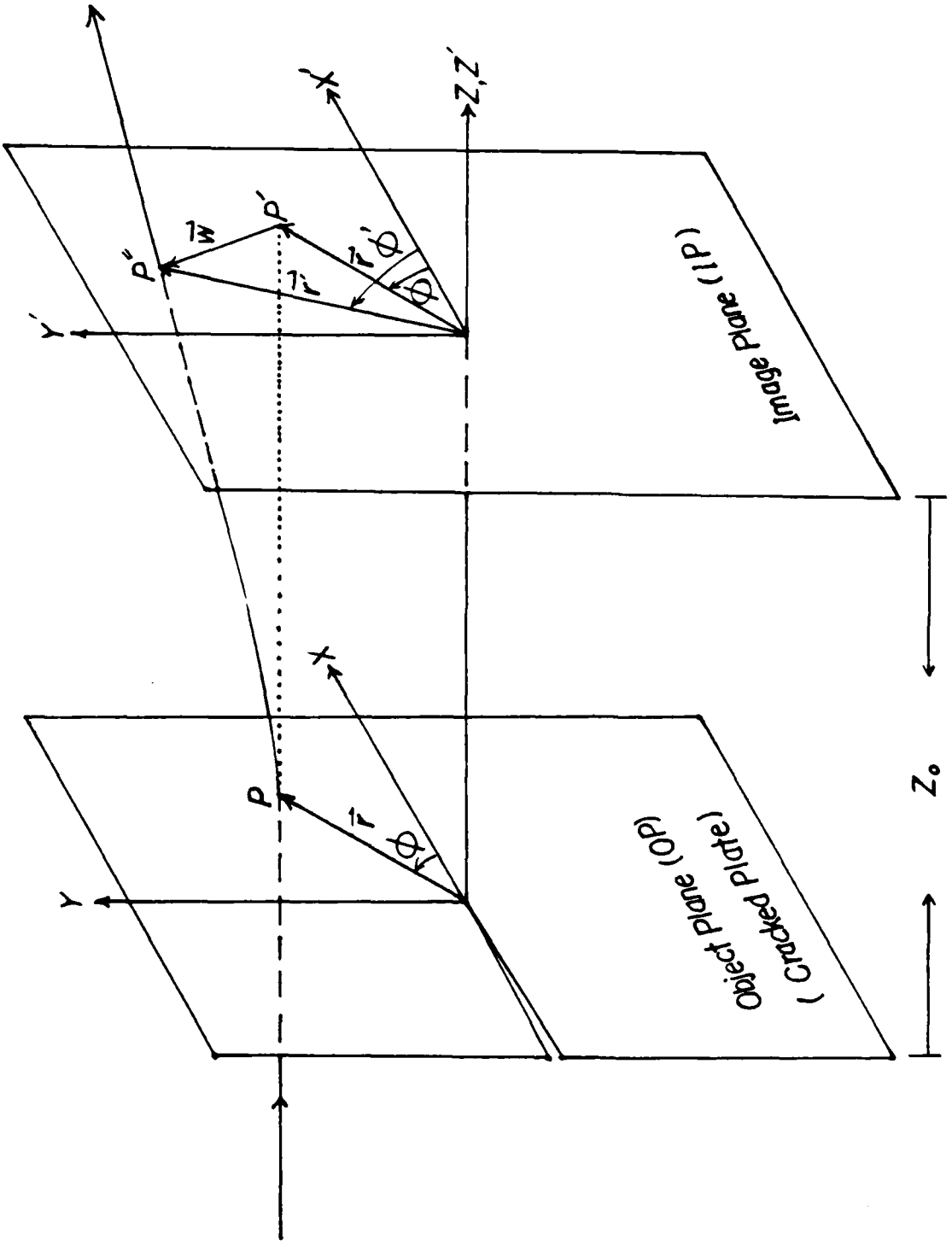

Figure 3.3 Optical paths for development of caustic.

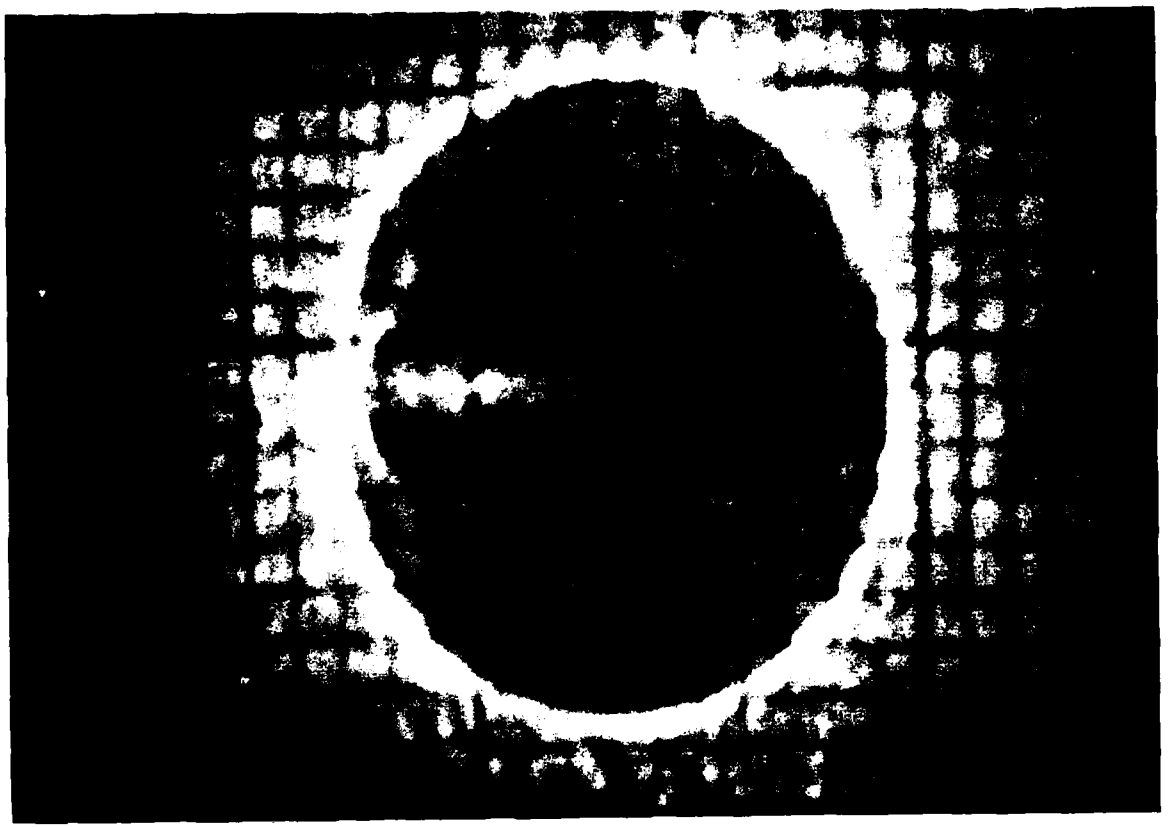

Figure 3.2 Photo of a caustic spot (Solithane 113 (50/50)).

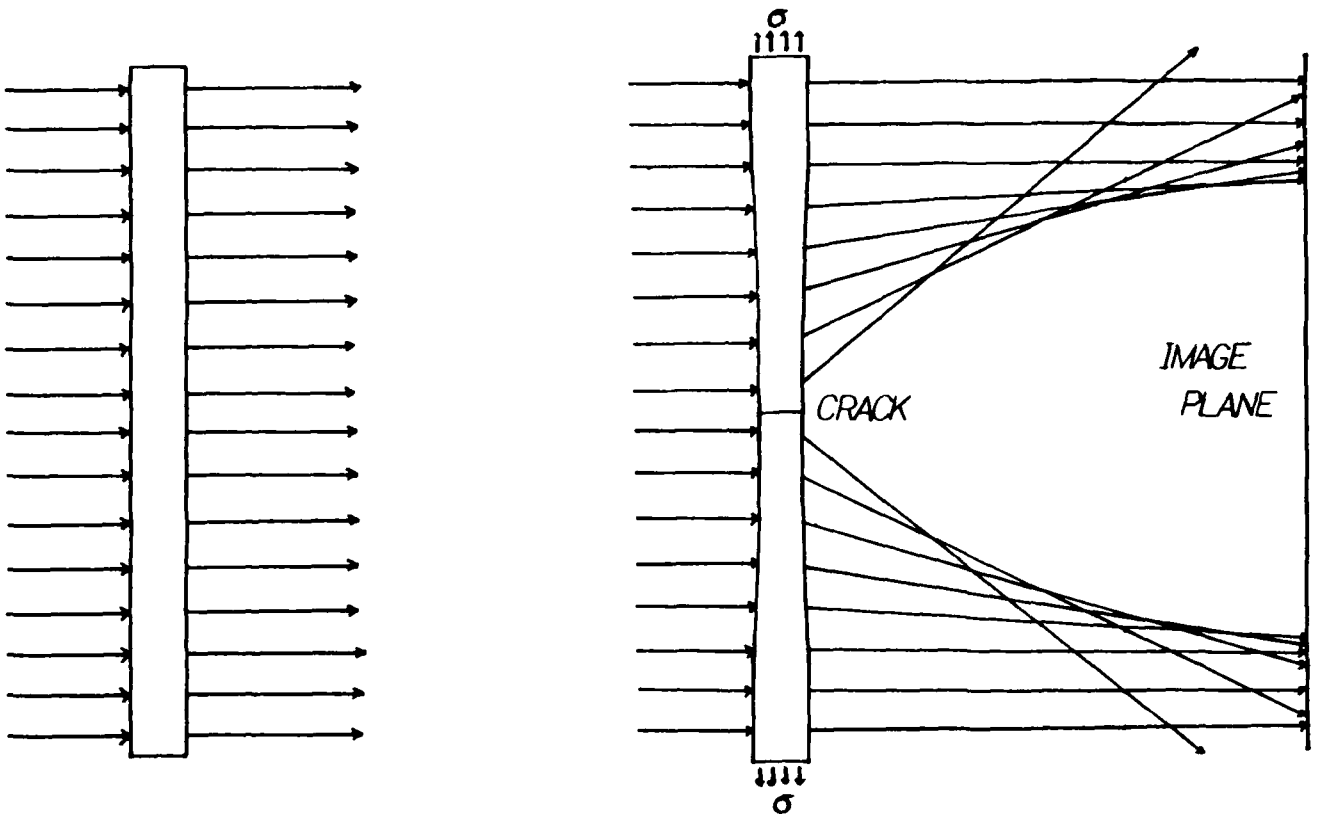

Figure 3.1 Effect of crack tip stresses on light paths.

3. EXPERIMENTAL PROCEDURES

For measuring the stress intensity factor K(t) and the crack length c(t) in the same time frame, the method of caustics is adopted. This method, also called "shadow spot method", or "the method of shadow pattern", was recognized by Schardin and analyzed by Mannog in 1959. Through the works of Theocaris, Kalthoff and others (Knauss, Rosakis, Kim, Ravi-Chandar) this method is not only useful for elastic materials, but also for viscoelastic ones [7].

3.1 Physical Description of the Method of Caustics

When a beam of parallel light is incident normally on a stress free plate of transparent material, the beam of light just passes through. However, if there is a crack in the plate, say under Mode-1 loading, the light rays will be deflected, particularly in the crack tip region. Due to the stress field in the material the index of refraction of the material will change. Also, around the crack tip the shape of the plate surface is altered. Both effects will cause the transmitted light to deviate from the original straight path. By the Maxwell-Neumann elasto-optical law the refraction index is decreased; this fact plus that of the non-homogeneous surface deformation makes the crack tip act like a divergent lense (cf. Figure 3.1). The light around the crack tip is deflected outward so that on an image plane the area around the crack tip is devoid of light and a dark spot is formed. A photograph of a test situation is shown in Figure 3.2.

3.2 Mathematical Description

Consider the optical arrangement in Figure 3.3 of a cracked plate represented by the object plane and a viewing plane or image plane IP is located at a distance z_0 from and parallel to the object plane. Let a light ray be incident at point P on the object plane with coordinates $P = P(r, \varphi)$. If the light were not deflected, it would intersect the image plane at the point P'. Actually the ray will

not available, in particular the stress-optic coefficient for Solithane 113. In terms of equation (15) this means that the parameter λ is not known. The determination of the stress-optic coefficient is not a trivial matter. Therefore it was deemed more time-efficient to ascertain this parameter λ in a separate calibration process, rather than the stress optic coefficient.

3.5 Caustic Calibration

To this end a typical specimen (cf. Figure 3.9) is mounted in an Instron test machine (screw-type loading device) with a C-type load-cell in the 0-20 lb range. Under a given load the caustic is recorded and the corresponding crack length noted. Using the analytical results for this geometry (infinitesimal elasticity solution [8]), one notes, as for example from equation (15), that the 5/2 power of the caustic diameter D is linearly proportional to the stress intensity factor. Thus, if one plots $D^{\frac{5}{2}}$ against the theoretically determined stress intensity factor one should obtain a straight line. This stress intensity factor would be based on the conditions prevailing in the experiment (load and crack length as well as the rest of the geometry). As can be seen from Figure 3.10, the resulting experimentally determined points fall very neatly along a straight line. A best straight line fit to this data, is then accomplished as shown; this line determines the value of $\lambda f^{5/2}$ in equation (15) and, by deduction, the long-time value of the stress-optic coefficient. It should be remarked that the experimental points in Figure 3.10 are obtained by varying the applied stress as well as by varying the crack length for computing the "theoretical" value of the stress intensity factor.

For purposes of completeness let us record here the pertinent equation for this computation. From [8] we have for the stress intensity factor (Mode-I)

$$K_I = 1.1215\sigma \sqrt{\pi a} \cdot F\left(\frac{H}{b}\right)$$

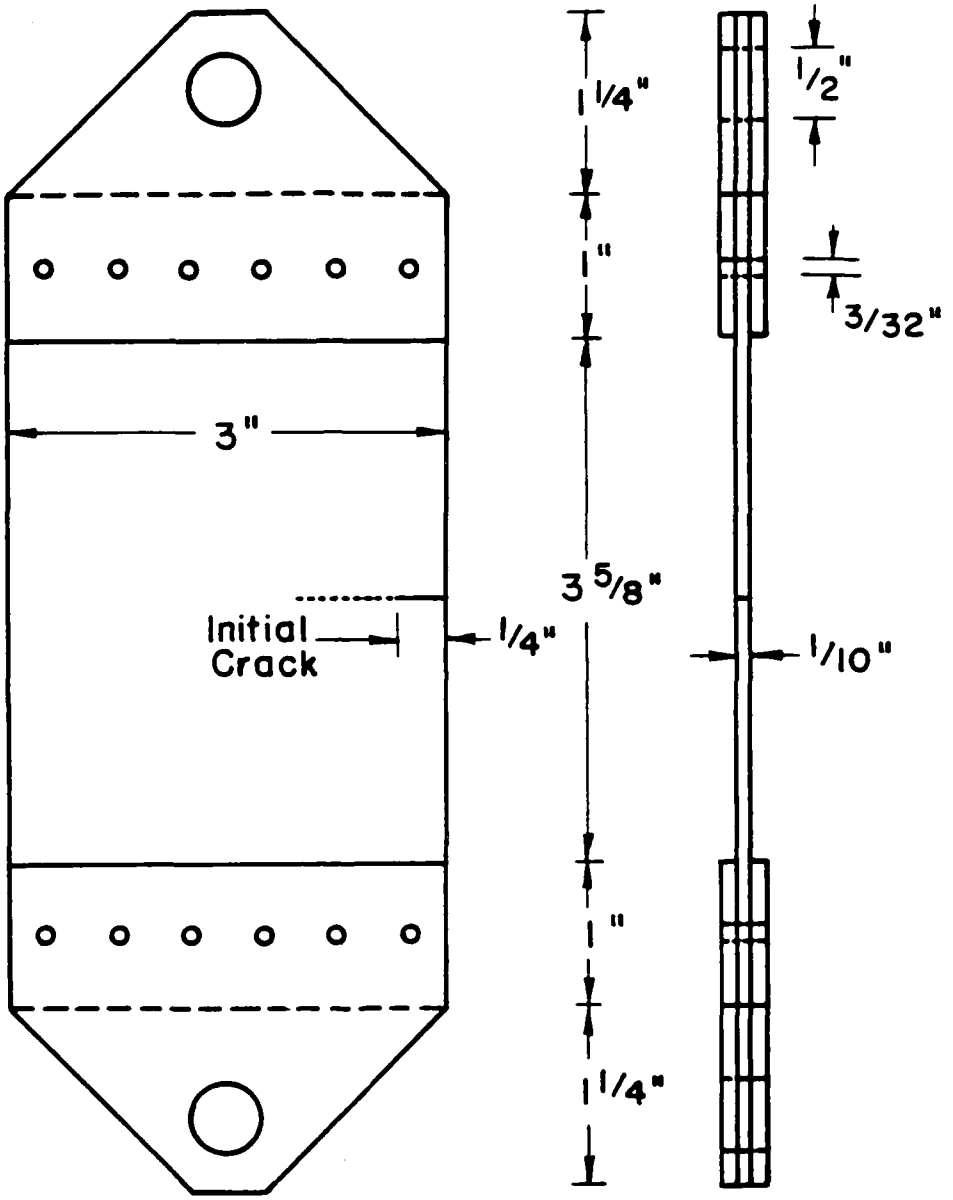

GEOMETRY CONFIGURATION OF THE TESTING SAMPLE

Figure 3.9 Geometry configuration of the testing sample.

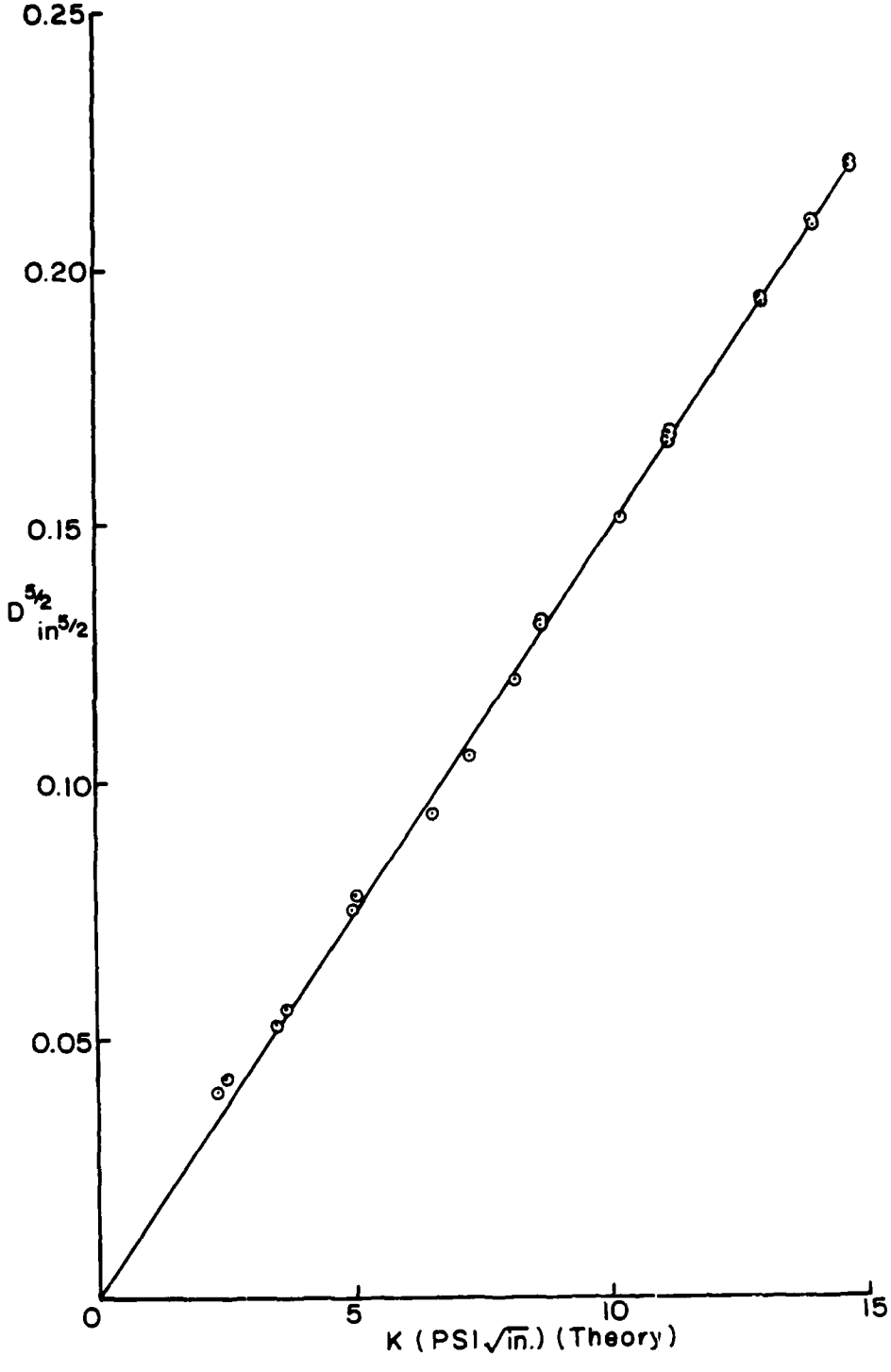

Figure 3.10 Calibration of the caustic parameter λ.

where σ is the average grip stress and (H,b) are as defined in the inset of Figure 3.11. The function $K_I / K_o = 1.1215 \cdot F(\frac{H}{b})$ is given in that figure for two end conditions that do or do not allow for rotation of the grips. In the present experiments no rotation was allowed; hence only the appropriate interpolated curve for h/b = 0.67 shown in Figure 3.11 was used.

Before proceeding to evaluate the fatigue data it is worth while to mention why the photoelastic method was not used. It turns out that with a specimen thickness of 2.5 mm (0.1 inch) the photoelastic method was no more sensitive or accurate than the caustic method. In this situation the caustic method is easier to use because only a single parameter must be measured (D) while in the photoelastic method field data needs to be analyzed for a best fit of the crack-tip stress field to existing photo-elastic figures [9].

3.6 Data Scatter

A brief note is in order regarding data scatter. It will be noted that there is very little data scatter present in all the subsequent measurements. This fact is a direct consequence of the care with which the maximum stress intensity was determined in each cycle as well as the how the crack length was determined. The latter was measured under conditions when the crack was almost closed (lowest stress in any cycle). These simple rules produced very consistent data subject only to variations in material properties along the crack path, which variations could give rise to data scatter measurements of the crack propagation rate. That this did not happen to any sizable degree testifies only to the uniformity of test material.

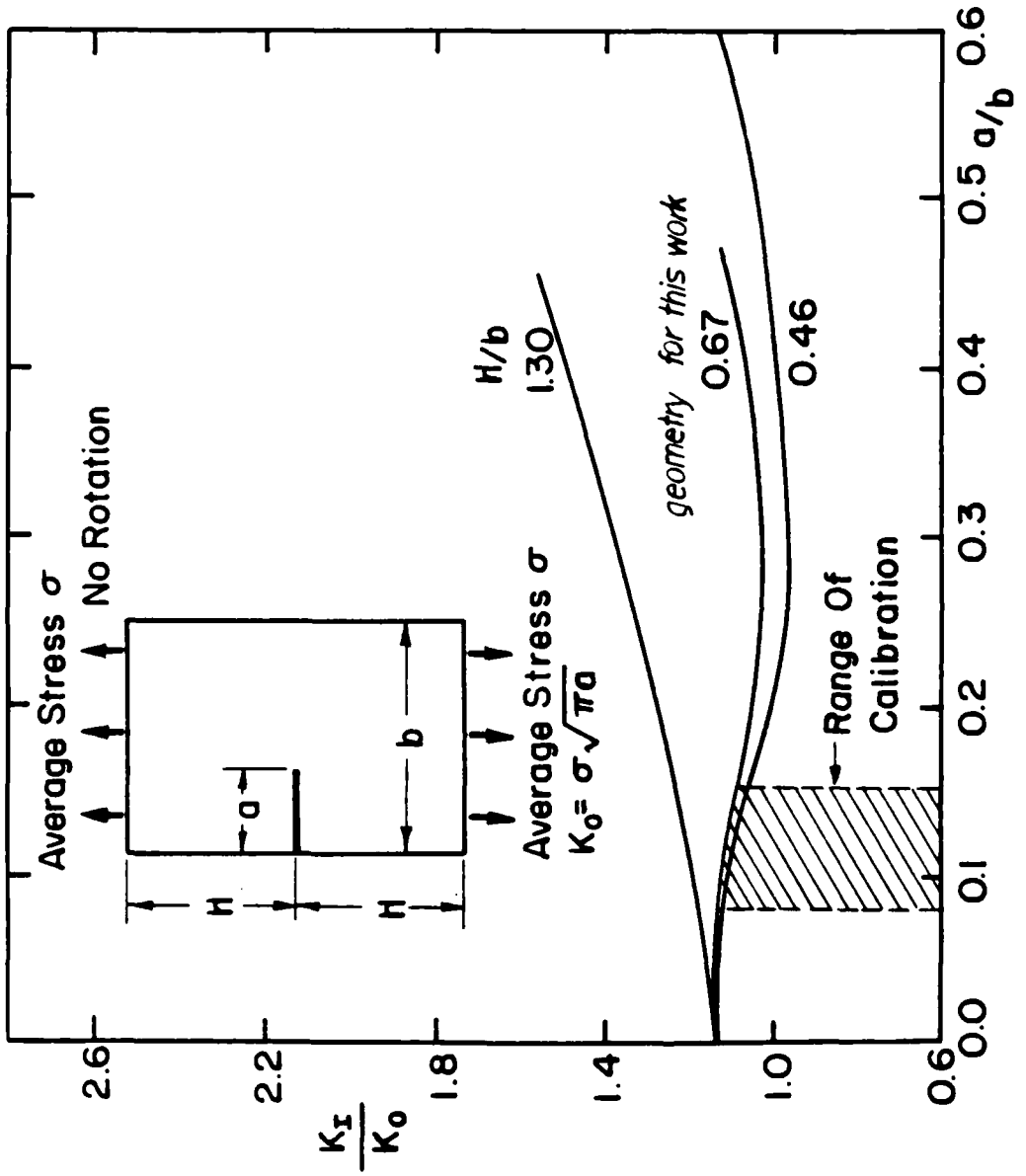

Figure 3.11 Computed stress intensity factor for test geometry (Ref. 8).

4. RESULTS

In order to explore the applicability of the crack propagation equation (1) it is necessary to perform tests over a matrix of frequencies and temperature. If the material behaves in a thermorheologically simple manner, it would be sufficient to perform these tests at only one frequency and several temperatures, or at one temperature and several frequencies. Although in previous, steady-state test the crack propagation behavior followed essentially thermorheologically simple behavior we do not know for certain what the effect of cycle frequency is on generating heat at the crack tip and thus influence the crack growth rate in this secondary manner. For this reason two sets of data were taken: in one - let us call it Set I - the temperature varied but the frequency was always 1 Hz while in the second set - for discussion purposes denoted by Set II - the frequency varied and the temperature remained constant at 20°C. These test points are shown graphically in the plot of the viscoelastical caustic boundary (cf. Figure 3.6).

For any of these tests one records the length of the crack as a function of the number of cycles as well as the corresponding instantaneous stress intensity factor. For Set I (varied temperature at 1 Hz) the data are recorded in Figure 4.1 and 4.2, while for Set II (varied frequency at 20°) they are shown in Figures 4.3 and 4.4. Note the relatively small amount of data scatter. The crack length data in Figures 4.1 and 4.3 are then differentiated numerically by the five-point Lagrange method [10,11]. Differentiation is accomplished with respect to the number of cycles (as a continuous variable), though Set I leads directly to the time derivative because the frequency is one Hz; the results of this differentiation are given in Figures 4.5 and 4.6.

Upon cross-plotting the data from Figures 4.2 and 4.5 one eliminates the

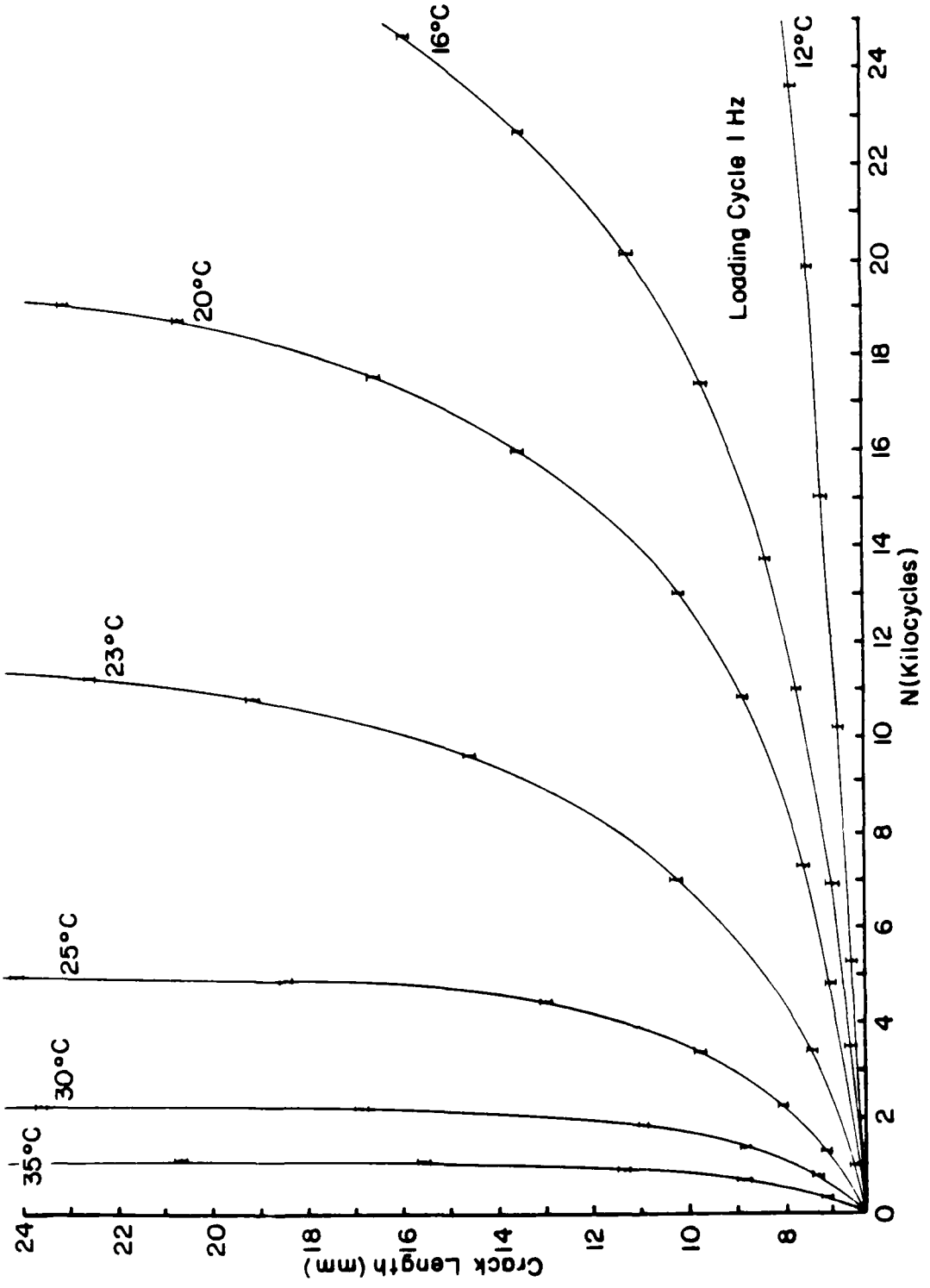

Figure 4.1 Crack length recorded as a function of the number of cycles in different temperatures.

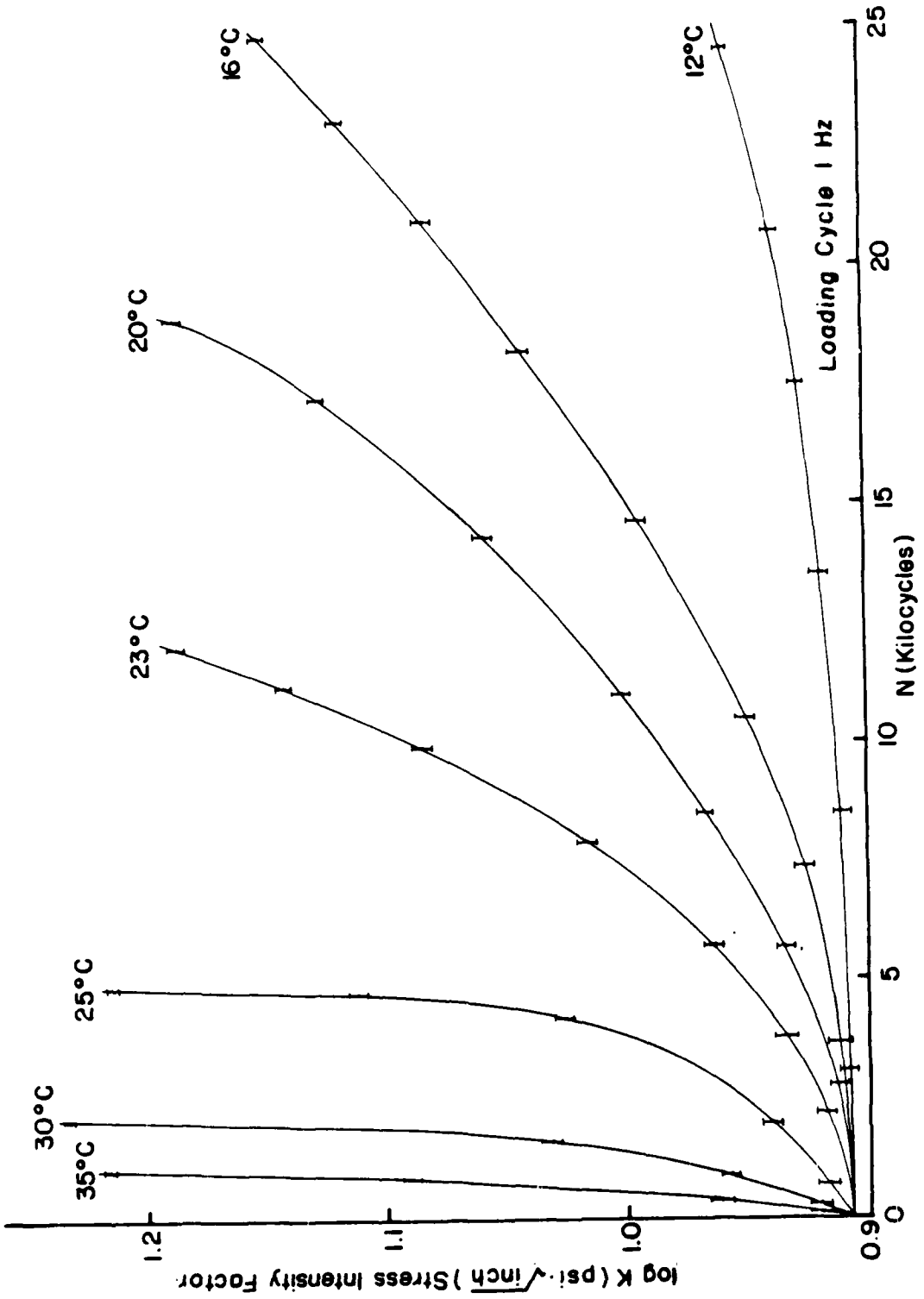

Figure 4.2 The log values of stress intensity factors K_I recorded as a function of the number of cycles in different temperatures.

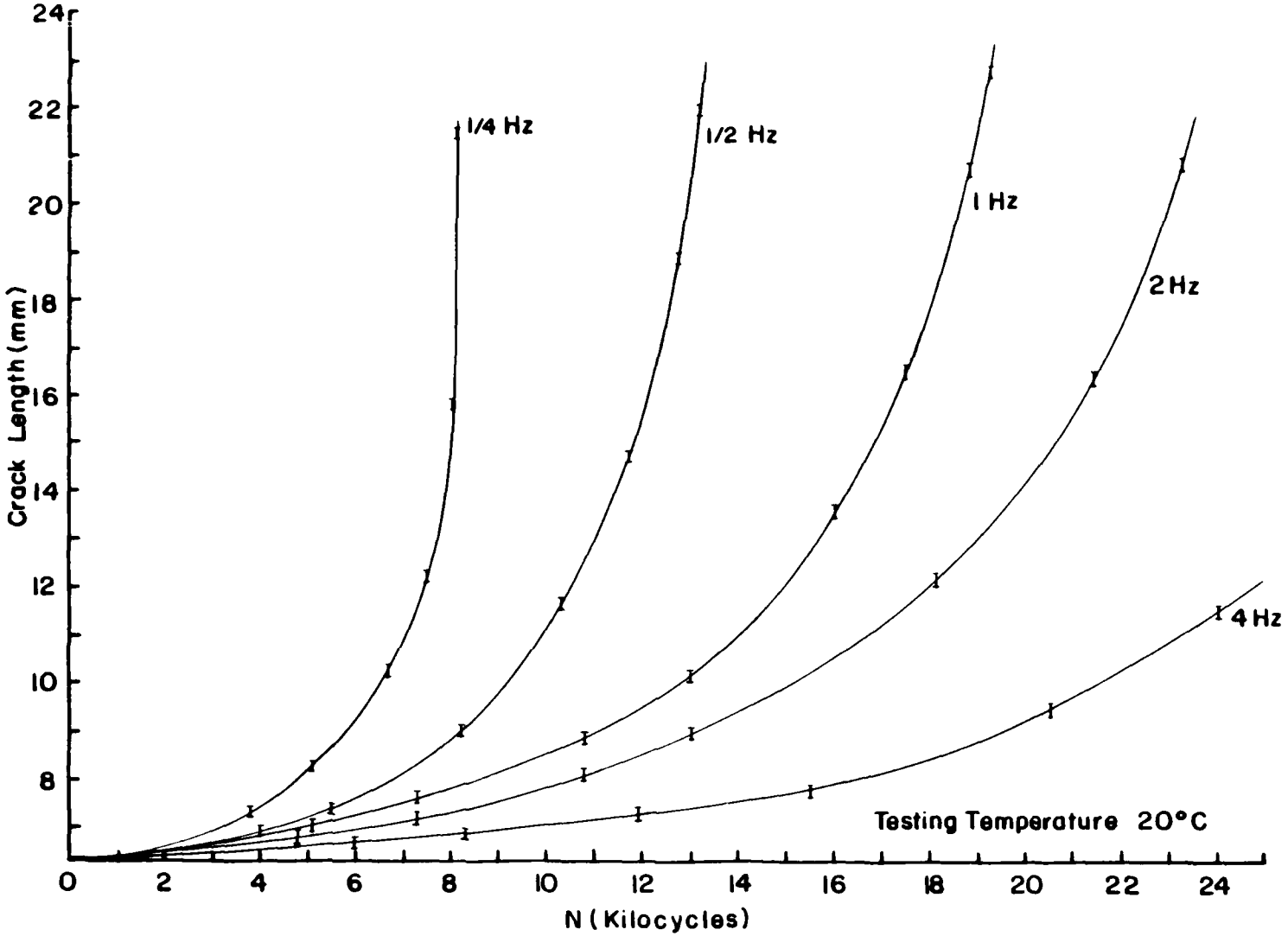

Figure 4.3 Crack length recorded as a function of the number of cycles under different loading frequencies.

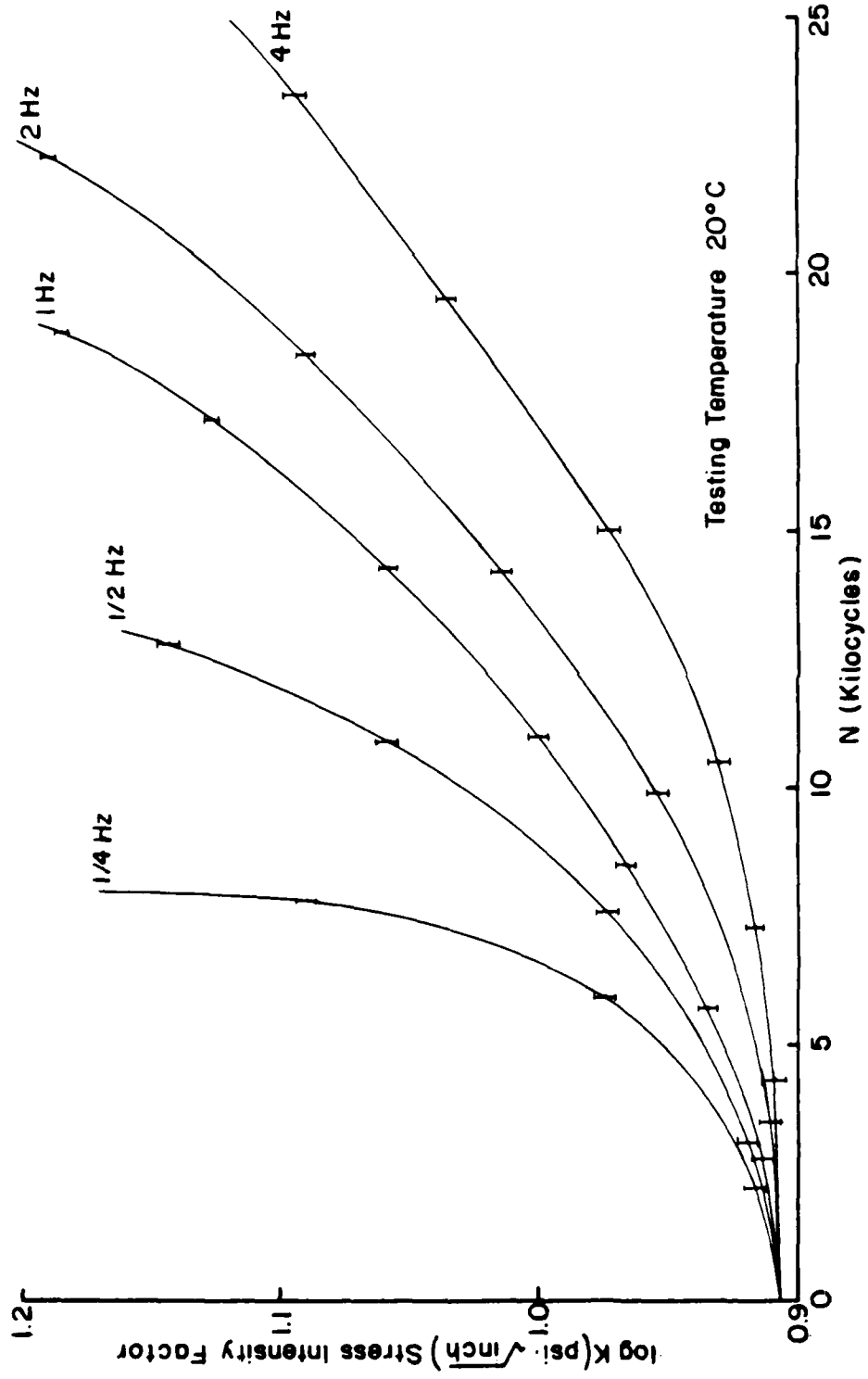

Figure 4.4 The log values of stress intensity factor K_I recorded as a function of the number of cycles under different loading frequencies.

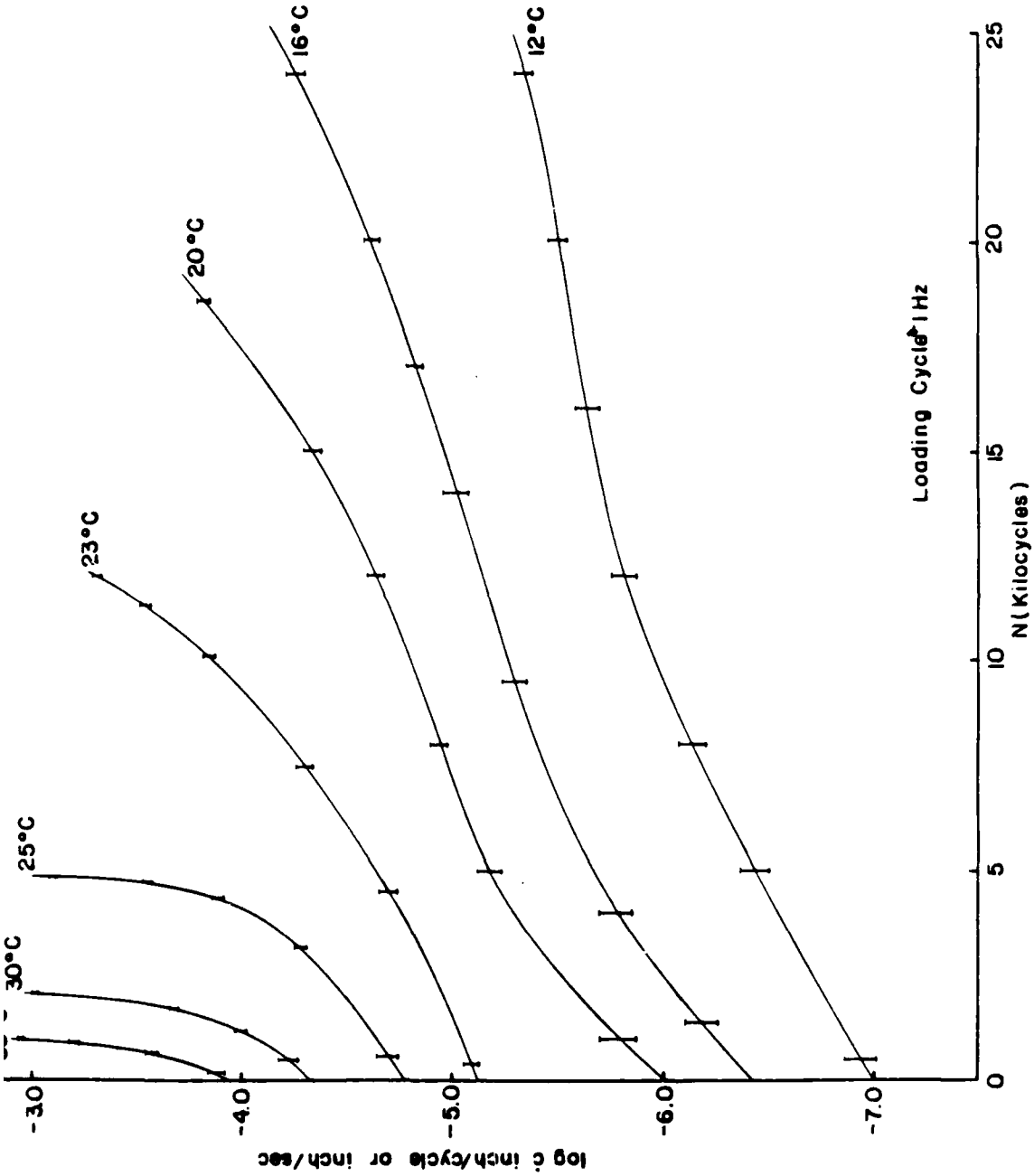

Figure 4.5 The crack propagation speed due to change of the temperature.

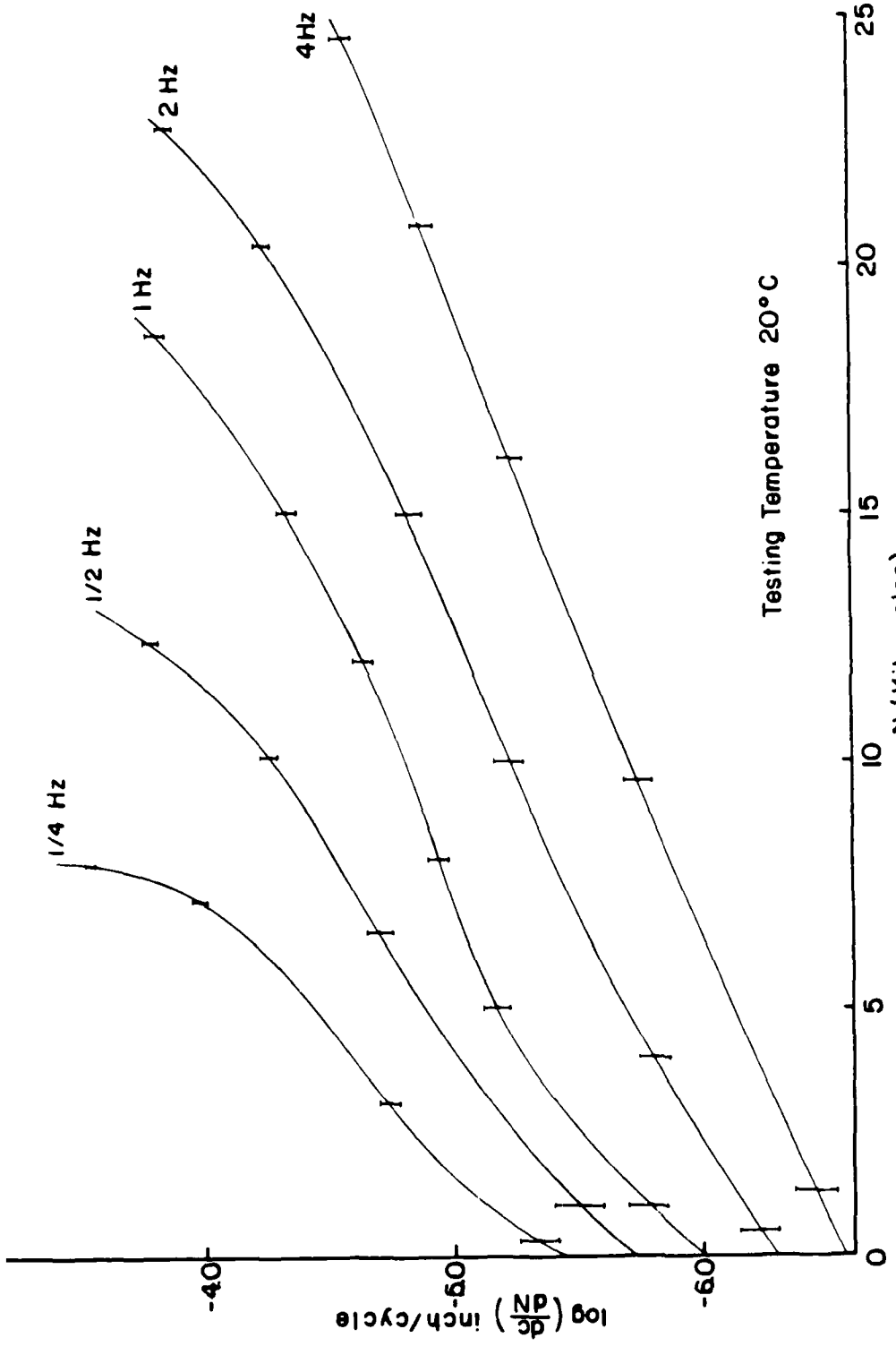

Figure 4.6 Crack propagation speed due to change of loading frequencies.

cycle number and derives a plot of crack growth rate as a function of the maximal stress intensity factor in each cycle (K_{max}/K_{min} ranges between 3.0 and 3.6 during these tests); this is shown for Set I in Figure 4.7. Similarly, if one cross plots Figures 4.4 and 4.6 one arrives at the data in Figure 4.8 for Set II. Thus Figures 4.7 and 4.8 constitute the starting data for examining the possible effect of viscoelasticity on crack propagation under transient loading.

5. ANALYSIS OF EXPERIMENTAL RESULTS

We notice first, with respect to Figure 4.7, that the overall behavoir of crack growth as a function of temperature is as expected from the time-temperature superposition behavior. However two deviations are rather obvious: If the data behaved strictly according to the time-temperaure superposition principle, the curves in Figure 4.7 should all have the same shape. That is clearly not the case at low (maximal) stress intensity and progressively less true as the temperature increases.

In this connection it must be remembered that stress cycling occurred between some minimum and maximum value in each cycle. In these tests the minimum value (2.5 psi) was large enough so that during most of the cycle crack propagation became possible at the higher temperature. This "anomaly" of the data in the low-K, high-T region is thus due to an effectively superposed steady stress intensity factor which makes a significant contribution only when K_{max} is small ($K_{max}/K_{min} \rightarrow 3.0$) and when the temperature is such as to allow significant crack growth under this low stress condition.

The second "anomaly" becomes apparent when one time-temperature shifts the curves in Figure 4.7 or cross plots them at difference values of the stress intensity factor against temperature. This plotting is done in Figures 4.9 and 4.10. In accordance with the time-temperature behavior indicated by the dotted

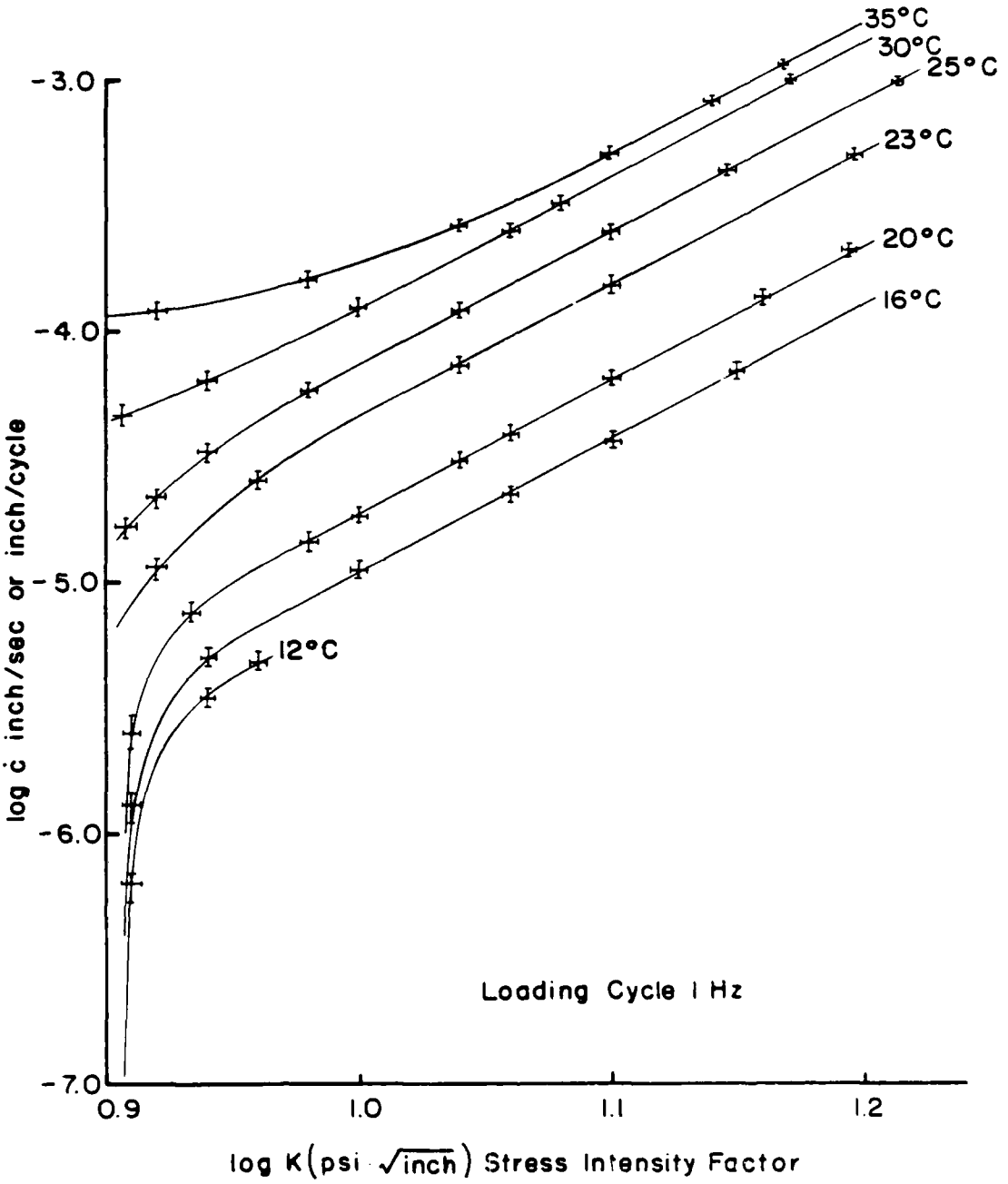

Figure 4.7 Crack propagation rate due to change of temperature.

AD-A152 064 A STUDY OF THE TIME DEPENDENCE IN FRACTURE PROCESSES RELATING TO SERVICE..(U) CALIFORNIA INST OF TECH PASADENA GRADUATE AERONAUTICAL LABS W G KNAUSS

UNCLASSIFIED 30 JUN 84 GALCIT-SM-84-10 AFOSR-TR-85-0239 F/G 11/4 NL

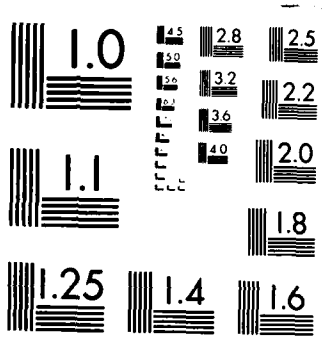

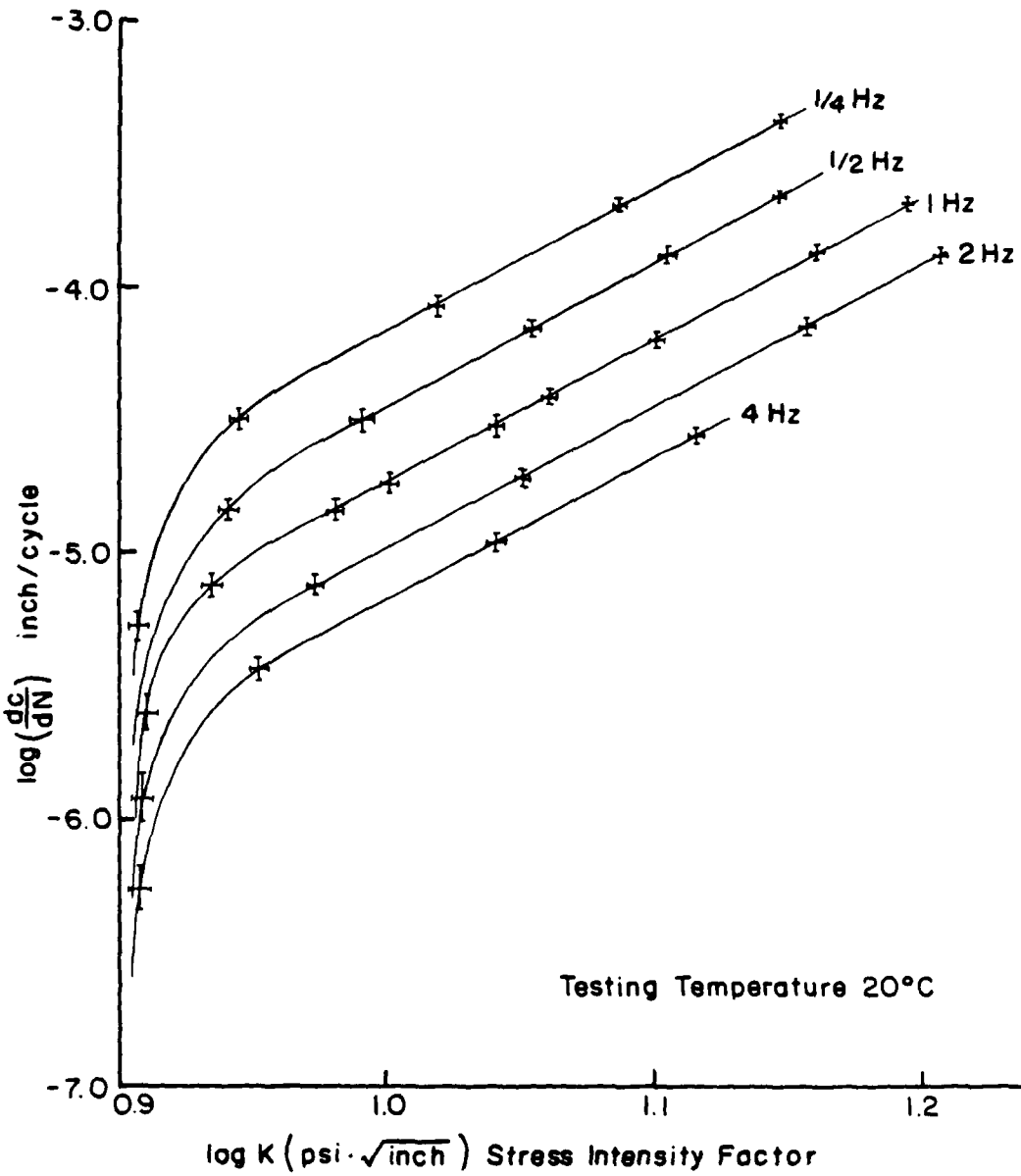

Figure 4.8 Crack propagation rate due to change of loading frequencies.

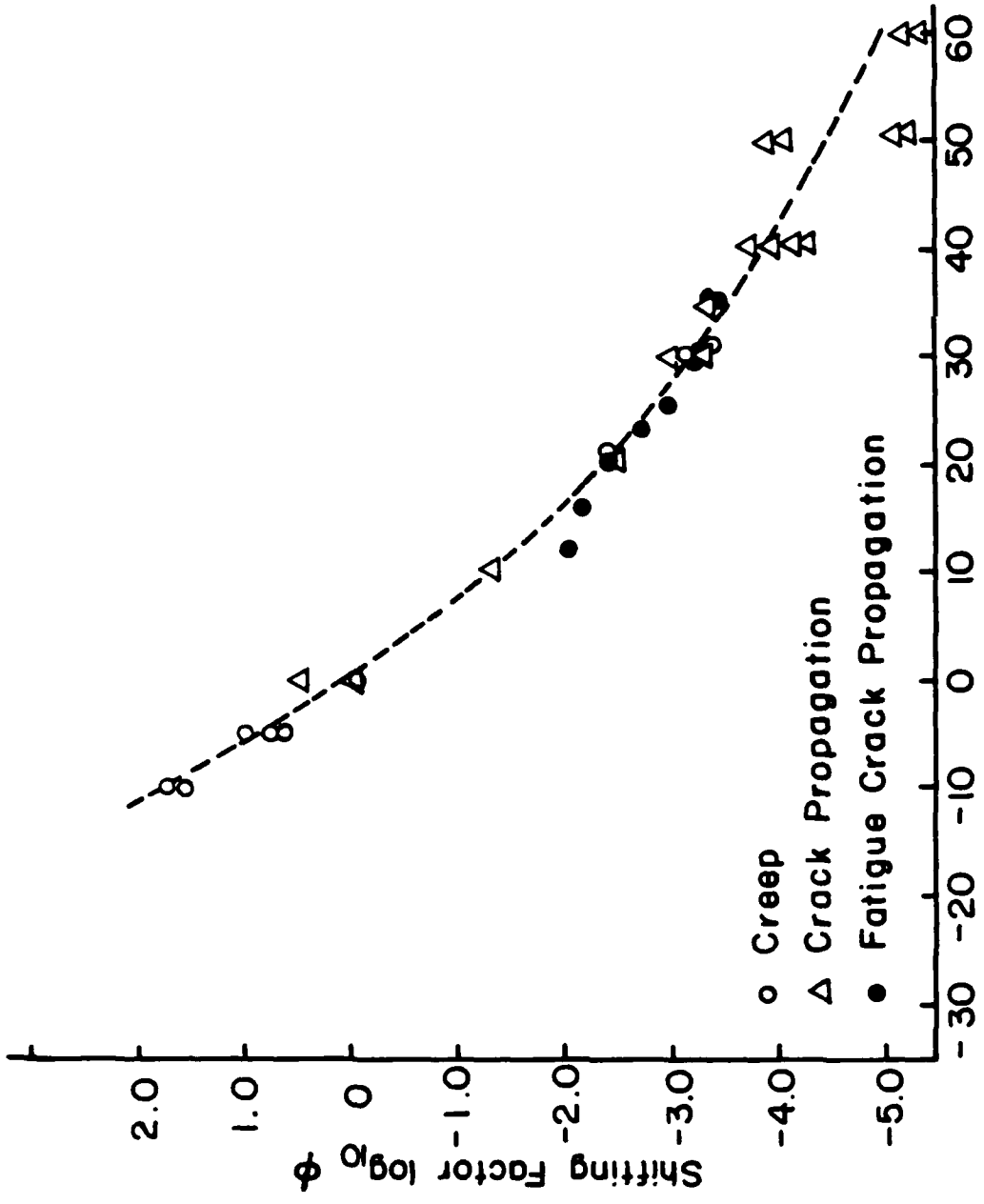

Figure 4.9 Master curve of shifting factors.

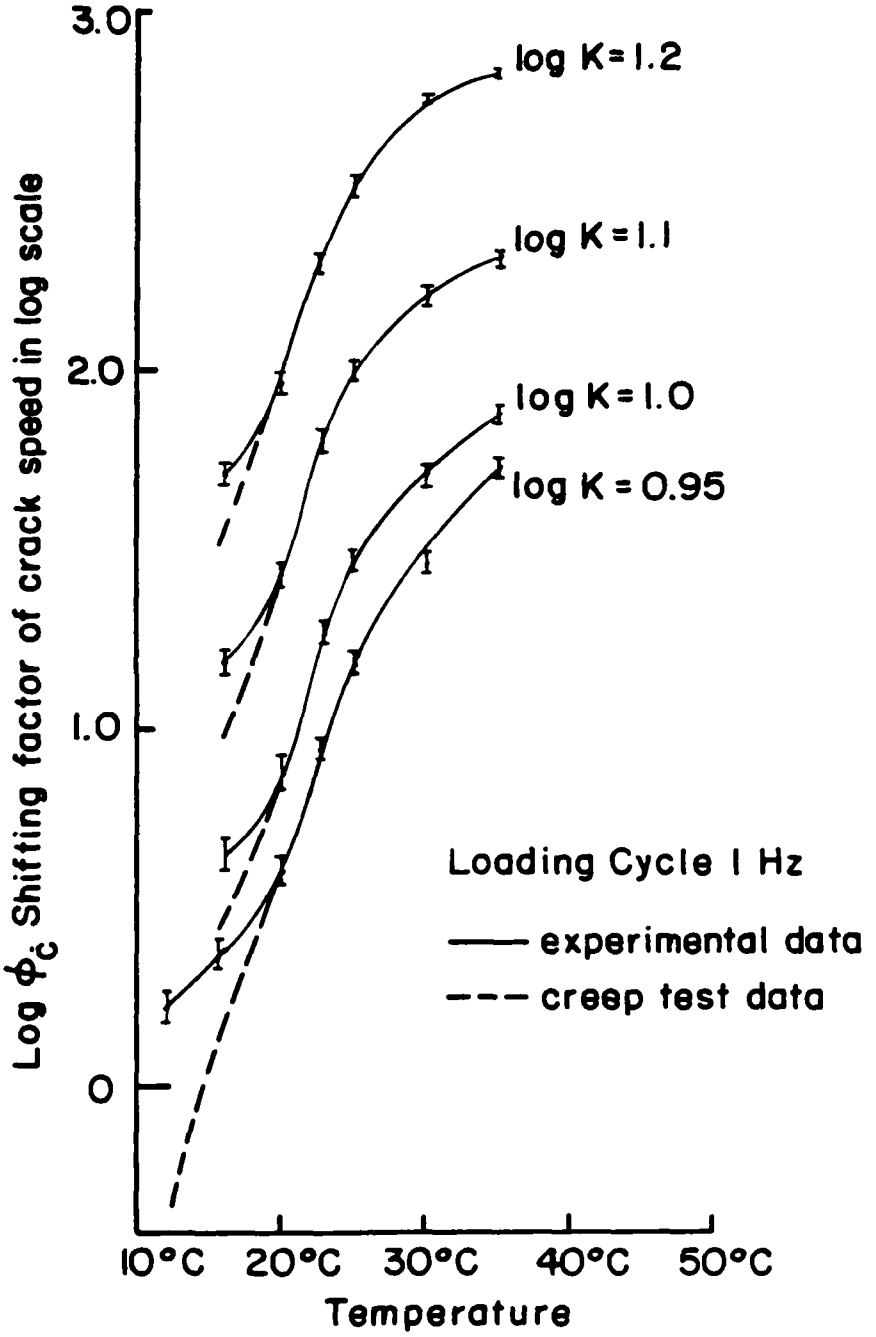

Figure 4.10 Shifting factor of crack speed due to change of temperature.

curve[1] in Figure 4.9 the plots in Figure 3.10 should exhibit a monotonic curvature behavior as a function of temperature. The fact that this does not occur but significant deviation occurs *consistently* at the lower temperatures indicates a systematic variation of the fatigue crack growth from standard time-temperature superposition behavior. In fact the deviation is such (the dashed curves in Figure 4.9 correspond to the dotted one in Figure 4.10) that *crack propagation is higher at these low temperatures than normal* time-temperature superposition would predict. We are aware of the normal data scatter in measurements of this type, but believe that the behavior in Figure 4.10 is systematic at all stress intensities.

If one neglects these finer points, one finds that, grossly speaking the time-temperature behavior is well obeyed in these fatigue tests as long as the temperature remains above 20°C at a frequency of 1 Hz. This, more rough comparison is illustrated in Figure 4.11 which shows comparison of the K-$\dot{c}$ relation computed from equation (1) assuming quasisteady behavior (equation (1) valid instantaneously; dashed curve for 0°C, see Ref. 6). The experimental data for the present study (solid curve) agrees rather well with the computed data at 20°C (dotted curve).

Let us now examine the behavior at 20°C when the cycle frequency is changed. It is clear from Figure 4.8 that a standard plot of dc/dN against K makes the cyclic growth rate strongly dependent on frequency. It is natural to ask, therefore, whether the characterization on a "per-cycle" basis is more appropriate than on a "per-unit-time" basis.[2] After all, we have seen in Section 2 that the crack growth should, at least approximately, be predictable by a time-differential equation. Thus, if one converts the ordinate in Figure 3.8 from

1. This figure is an accumulation of data from different tests on the same material [2-4].
2. Standard fatigue data is presented on a "per cycle" basis.

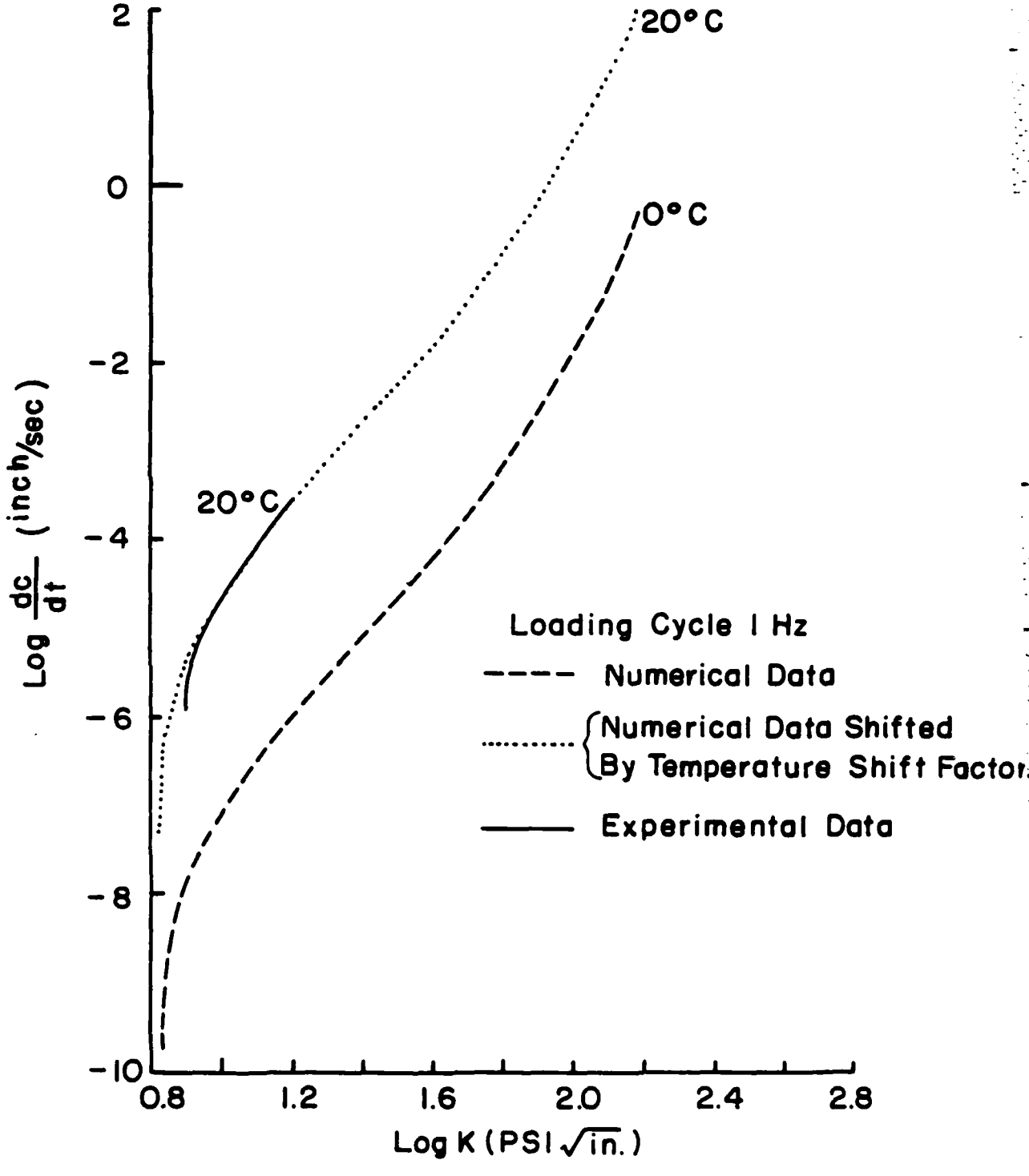

Figure 4.11 Comparison of computed and measured crack propagation rate.

dc/dN to dc/dt one finds in Figure 4.12 a much closer agreement, although, due primarily to the low data scatter in Figures 4.3 and 4.4, one can distinguish a systematic separation of the curves with increasing frequency. Specifically we note that ***higher frequencies lead to faster crack propagation rates*** than lower frequencies. For 'low" frequencies the curves all seem to collapse into a simple master curve which should be equal to that computed from the quasi-static and monotonically-based crack propagation equation (1).

With reference to the previous test series 'Set I" were low temperature produced crack growth rates that were higher than those predicted by the quasi-static theory the same is true here for higher frequency. Since higher frequency has the same effect on viscoelastic behavior as lower temperature, we conclude that ***under increased viscoelastic material response in the near-relaxed range of material behavior crack propagation is accelerated by a cyclic load history. This behavior is commensurate with the concept of fatigue.***

That the curves in Figure 4.13 do not all collapse onto a single master curve - thus attributing the separation of the curves possibly to data scatter - is evident when one cross plots the data in Figure 4.13 for constant frequencies as in Figure 4.12. If all the curves where essentially statistical variants of each other the dotted curves in Figure 4.13 should have all zero slope. It is evident that that would hardly be an appropriate interpretation and that the systematic and pronounced slope is significant, thus demonstrating the systematic variation of the crack growth rate with frequency.

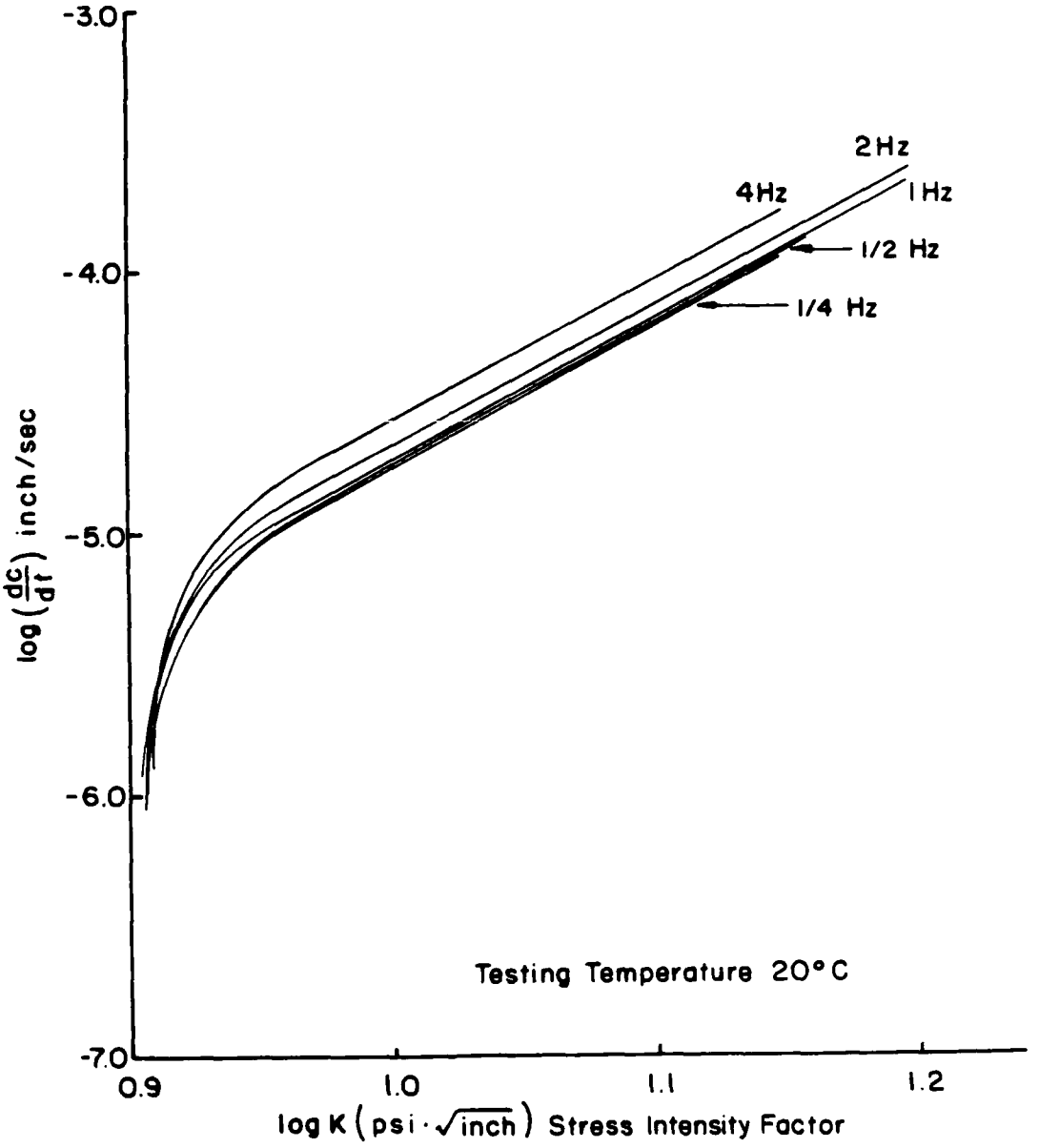

Figure 4.12 Crack propagation rate due to change of loading frequencies.

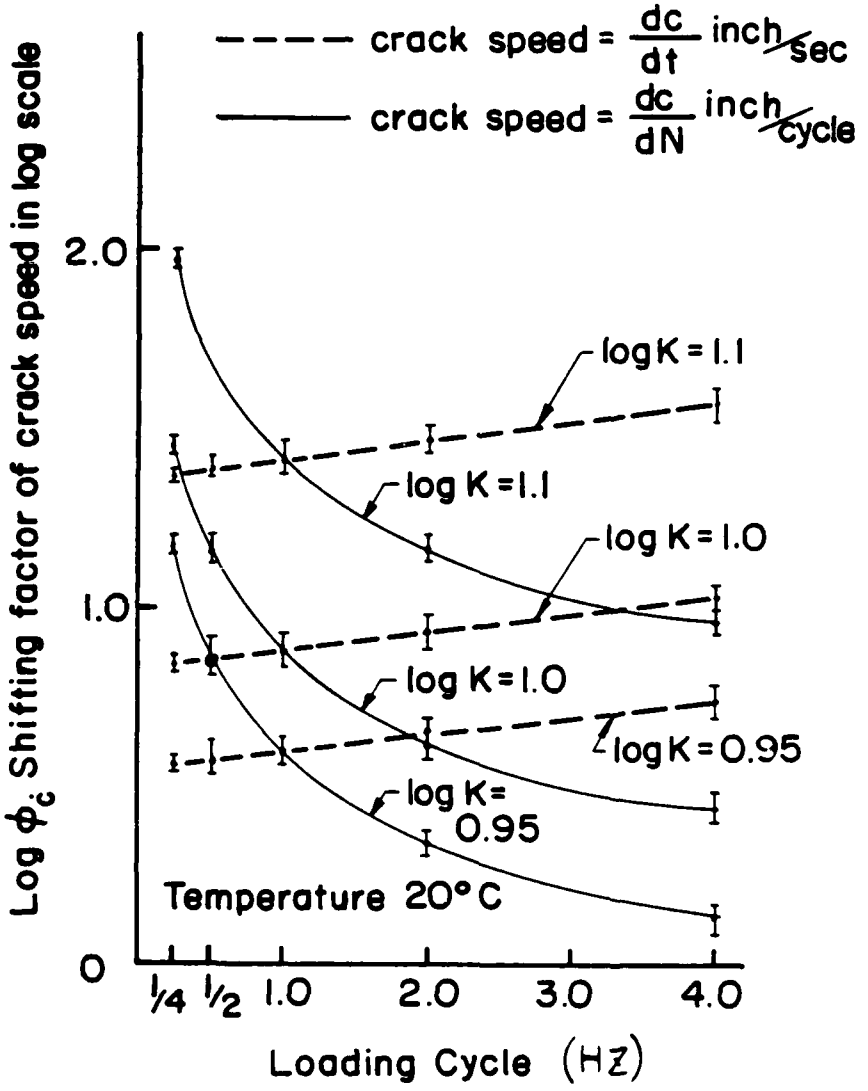

Figure 4.13 Shifting factor of crack speed due to change of loading frequency.

REFERENCES

1. Knauss, W.G., and Dietmann, H. "Crack Propagation Under Variable Load Histories in Linearly Viscoelastic Solids," *Int. J. Eng. Sci.*, Vol. 8 (1970) pp. 643-656.

2. Knauss, W.G., "On the Steady Propagation of a Crack in a Viscoelastic Sheet: Experiments and Analysis." *Deformation and Fracture of High Polymers*, H.H. Kausch, J.A. Hassell and R.I. Jaffee (eds.), Plenum Press (1973).

3. Schapery, R.H., "A Theory of Crack Initiation and Growth in Viscoelastic Media; I. Theoretical Development," *Int. J. Fracture*, 11 (1975) pp. 141-159.

4. Schapery, R.H., "A Theory of Crack Initiation and Growth in Viscoelastic Media; II. Approximate Methods of Analysis," *Int. J. Fracture*, 11 (1975) pp. 369-388.

5. Knauss, W.G., "Fracture of Solids Possessing Deformation Rate Sensitive Material Properties." *The Mechanics of Fracture*, F. Erdogan (ed.) AMD-Vol. 19, Amer. Soc. of Mech. Eng. (1976)

6. von Bernstorff, Bernd-Steffen Graf, "Crack Growth in Viscoelastic Materials Under Varying Load Histories," Thesis, California Institute of Technology, 1980.

7. Kim, K.S., and Knauss, W.G., "Dynamic Fracture in Viscoelastic Solids," GALCIT SM Report 81-7 (1981).

8. Rooke, D.P., and Cartwright, D.J., "Compendium of Stress Intensity Factors," Her Majesty's Stationery Office (HMSO), London (1976).

9. Kobayashi, A.S., "Photoelasticity Techniques." *Experimental Techniques in Fracture Mechanics*, SESA No. 1 (1973).

10. Dahlquist, G., and Björck, A., "Numerical Methods." Prentice-Hall (1974).

11. Hildebrand, F.B., "Introduction to Numerical Analysis." McGraw-Hill (1956).

APPENDICES

APPENDIX A: ENVIRONMENTAL CONTROL

In this Appendix we describe briefly the experimental set-up with regard to temperature and frequency control. This is appropriate because relatively small changes in temperature may affect the crack propagation rate measurably and singificantly. The schematic of the interacting components are shown in Figure A-1.

THE LOADING SYSTEM

The servo-hydraulic loading device is home built but essentially from component that normally makes up MTS equipment employing an MTS frame ratio at 22 klb. However, the maximum load applied was always less than 10 lbs., so the frame can be treated as rigid body.

A hydraulic power system with servo controler monitors and controls the loading history through a function generator with a DC offsetting sine wave of fixed frequency and maximum amplitude. Thus the loading system provided essentially amplitude (sinusoidal) displacement control to the ends of the specimen. Because of the limitations on the available cooling system the whole loading system can run continuously for up to 16 hours with steady put. The environmental chamber (Figure A-2) is a double-wall wooden container with dimensions that just fit between the MTS' frame. The testing sample, Solithane 113 strip, is located in the chamber in a steady temperature environment. With the help of a fan air circulates from a conditioning chamber into the environmental chamber (Figure A-2) which by itself is an adjustable temperature chamber. The temperature capability of this facility is in the range 100°C to 150°C (in the low temperature range cooling is accomplished with the aid of

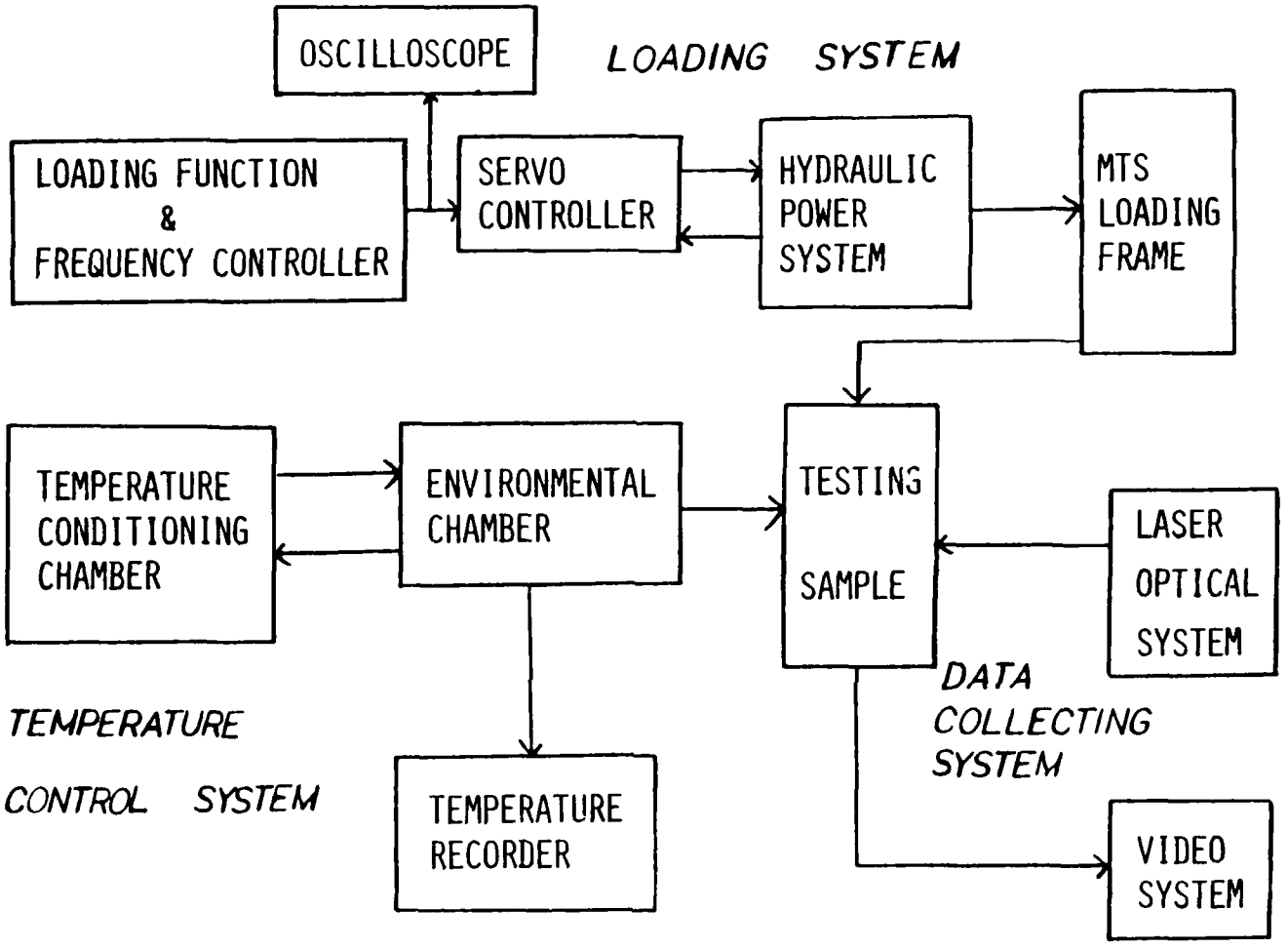

Figure A-1 Experimental set-up.

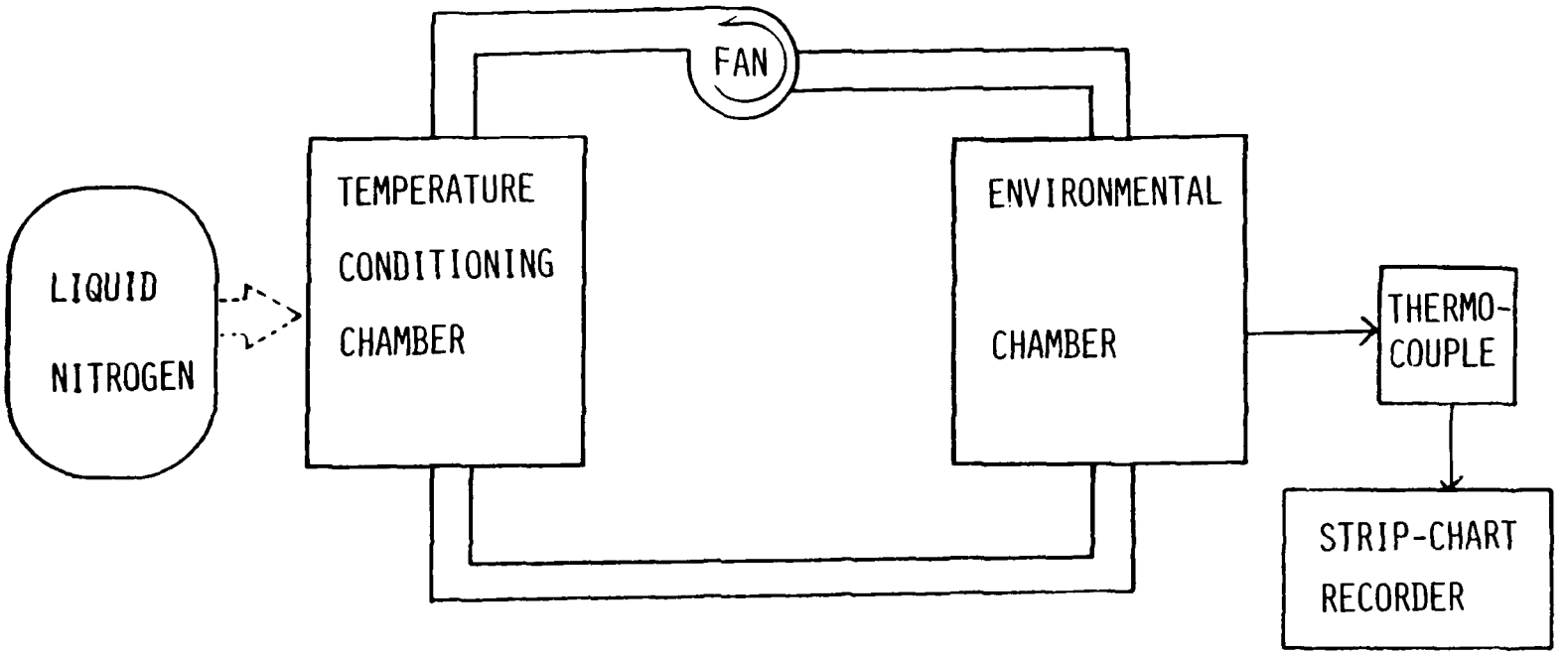

Figure A-2 Temperature control system.

liquid Nitrogen).

Two Nickel-Chromium vs. Copper-Nickel thermo couples are placed on the surfaces of the Solithane 113 specimen and the temperature, as the output voltages from the thermo-couples, is recorded continuously on HP 7200B, a strip-chart recorder. For the range of test temperatures, $12°C \leq T \leq 35°C$, the temperature control system can maintain temperature fluctuations on the specimen surfaces to within $\pm$ 0.02 mV of the thermocouple voltage, i.e. average temperature error is $\pm$ 0.3 $\sim$ 0.5°C. This range corresponds to approximately a variation in temperature of $\pm$ 0.4°C.

APPENDIX B: CRACK TIP LOCATION RELATIVE TO THE CAUSTICS

On the image plane, the caustic curve is:

$$x' = r_s(\cos\varphi + \frac{2}{3}\cos(\frac{3}{2}\varphi))$$

$$y' = r_s(\sin\varphi + \frac{2}{3}\sin(\frac{3}{2}\varphi))$$

$$D = 2y'_{max}$$

$$\frac{dy'}{d\varphi} = r_s(\cos\varphi + \cos(\frac{3}{2}\varphi)) \qquad (A.1)$$

$$\frac{d^2y'}{d\varphi^2} = -r_s(\sin\varphi + \frac{3}{2}\sin(\frac{3}{2}\varphi)) \qquad (A.2)$$

let $\frac{dy'}{d\varphi} = 0$ from (A.1) it is:

$$\frac{3}{2}\varphi = 180^\circ - \varphi \qquad \text{for } 0 \le \varphi \le 180^\circ$$

$$\varphi = 72^\circ$$

$$\frac{d^2y'}{d\varphi^2}\Big|_{\varphi=72^\circ} = -2.378\, r_o < 0$$

So it is proved that at $\varphi = 72^\circ$ $y' = y'_{max}$

$$x'\Big|_{\varphi=72^\circ} = 0.103\, r_s$$

finding $y' = 0$, i.e.,

$$\sin\varphi + \frac{2}{3}\sin(\frac{3}{2}\varphi) = 0 \qquad \varphi = 0^\circ \text{ or } 151.05^\circ$$

$$x'\Big|_{\varphi=0^\circ} = \frac{5}{3}r_s$$

$$x'\Big|_{\varphi=151.05^\circ} = -1.3333113\, r_s$$

$$\cong -\frac{4}{3}r_s$$

$$L = \left| -\frac{4}{3}r_s \right| + \left| \frac{5}{3}r_s \right| = 3r_s$$

$$\frac{\left| -\frac{4}{3}r_s \right|}{3r_s} = \frac{4}{9}$$

the position of crack tip is at $\frac{4}{9}L$. And the position of the maximal distance of the caustic from the x-axis, i.e. $Y' = \frac{D}{2}$ occurs at a distance $\bar{x}$ from the left of the caustics (see Figure 3.8).

$$\frac{\bar{x}}{L} = \frac{\frac{4}{3}r_s + 0.103r_s}{3r_s} = 0.479$$

END

FILMED

5-85

DTIC